Nine Mile Point Unit 1 210 Degree Pressure Vessel Surveillance Capsule Report

March, 1998

Report Number MPM-398675

Final Report

entitled

Nine Mile Point Unit 1 210 Degree Surveillance Capsule Report

prepared for

Niagara Mohawk Power Corporation
Nine Mile Point Unit 1
Lake Road
Lycoming, NY 13093

by

MPM Technologies, Inc.
2161 Sandy Drive
State College, PA 16803-2283

March, 1998

Executive Summary

Capsule B, located at the 210 degree azimuthal angle, was irradiated from reactor start-up to the end of fuel cycle 12 (March, 1997) for a total of 16.81 effective full power years at 1850 MWt. The capsule contained a total of 36 Charpy impact specimens, 10 tensile specimens, and 9 dosimeter wires. Prior to performing the mechanical property tests, chemical measurements were made on several Charpy and tensile specimens to verify the plate material used to fabricate the specimens. It was verified that the base metal specimens were fabricated from plate G-8-1 material and the weld and heat-affected-zone (HAZ) specimens were fabricated from welded prolongations cut from beltline plate G-8-3 during vessel fabrication.

A fluence of 9.34×10^{17} n/cm^2 has been estimated for the Capsule B exposure using the capsule copper dosimetry data and the 300 degree capsule neutron transport analysis results. An evaluation of all of the Capsule B dosimetry data and evaluation of the changes in fuel cycle core designs indicates that fuel cycle effects have affected the accuracy of the previous neutron transport results. The results reported here for the capsule, as judged by the consistency of the dosimetry data sets and the reasonable uncertainty estimates, are considered appropriate for the purpose of assigning a mean flux to the capsule measured shift. However, a transport analysis will be completed and incorporated into the next P-T curve Technical Specification amendment to reduce the uncertainty associated with calculating the peak flux in the vessel wall. The data indicate that the fuel loading changes which have been implemented over the past few cycles have resulted in a fast flux reduction to the vessel. Based on analysis of the copper dosimetry data, the best estimate average flux for Capsule B is 1.76×10^9 n/cm^2/s. The recommended value from the 300 degree capsule was 1.90×10^9 n/cm^2/s, which is about 8% higher than the Capsule B value.

The Charpy and tensile data trends show that the neutron induced embrittlement of plate G-8-1 is moderate. The Capsule B plate G-8-1 Charpy shift is within the expected range. At a fluence of $\sim 9.34 \times 10^{17}$ n/cm^2, the Capsule B measured shift in the 30 ft-lb transition temperature is only 77.7 F. The measured USE drop was only 0.8 ft-lb, which is not statistically significant. Therefore, it has been concluded that there was no measurable drop in USE and this result is in agreement with the 300 degree capsule data. The G-8-1 tensile data showed $\sim$ 14 ksi room temperature yield strength increase, and these data are in agreement with the moderate Charpy shifts observed. Similarly, moderate surveillance weld embrittlement data trends were observed.

Contents

1.0 Introduction

1.1 Neutron Embrittlement

Ferritic reactor pressure vessel (RPV) materials undergo a transition in fracture behavior from brittle to ductile as the test temperature of the material is increased. Charpy V-notch tests are conducted in the nuclear industry to monitor changes in the fracture behavior during irradiation. Neutron irradiation to fluences above about 5×10^{16} n/cm^2 causes an upward shift in the ductile-to-brittle transition temperature (DBTT) and a drop in the upper shelf energy (USE). The nuclear industry indexes the DBTT at 30 ft-lbs of absorbed energy and the shift in the DBTT is referred to in the literature as the ΔRT_{NDT} or the ΔT_{30}. This behavior is illustrated schematically in Figure 1-1. The initial nil-ductility reference temperature (RT_{NDT}) is measured in accordance with Section III of the American Society of Mechanical Engineers (ASME) Boiler & Pressure Vessel Code (the Code) and involves measurement of drop weight data and Charpy data at discrete test temperatures.

In order to ensure safe operation of a nuclear power plant during heatup, cooldown, and leakage/hydro test conditions, it is necessary to conservatively calculate allowable stress loadings for the ferritic RPV materials. These allowable loadings can be conveniently presented as a plot of measured coolant pressure versus measured coolant temperature (P-T curves). Appendix G to Title 10 of the Code of Federal Regulations (CFR) Part 50 (10CFR50) [1-1] and Appendix G to Section III of the American Society of Mechanical Engineers (ASME) Boiler and Pressure Vessel Code [1-2] presents a procedure for obtaining the allowable loadings for ferritic pressure-retaining materials in Class 1 components using linear elastic fracture mechanics (LEFM). Although the Code suggests that the lower bound toughness should be measured for the vessel materials of interest, Regulatory Guide 1.99, Revision 2 (RG 1.99(2)) [1-3] allows the use of the ASME reference stress intensity factor (K_{IR}) and requires that this curve be shifted by the Charpy shift to account for radiation effects. In particular, neutron damage within the RPV during plant operation is accounted for in the allowable pressure loading by calculating an adjusted nil-ductility reference temperature (ART_{NDT}). RG 1.99(2) defines the ART_{NDT} as the sum of the initial unirradiated nil-ductility reference temperature (RT_{NDT}), plus the RT_{NDT} irradiation induced shift (ΔRT_{NDT}), plus a margin term. Within the nuclear industry, the ΔRT_{NDT} is determined from the Charpy transition curve shift indexed at 30 ft-lbs of absorbed energy.

The requirement to conduct an RPV surveillance program is given in 10CFR50 Appendix H, and the detailed implementation is described in American Society for Testing and Materials (ASTM) standard E 185. For most boiling water reactor (BWR) plants in the US, three surveillance capsules were placed in the downcomer near the vessel inner diameter (ID) surface prior to initial startup. These capsules contain neutron dosimeters and tensile specimens in addition to Charpy specimens. Some capsules contain Charpy and tensile specimens which were machined from an ASTM reference plate (referred to as correlation monitor material) and these specimens were included so that utilities could compare data from their surveillance program

with a large industry data set to confirm the validity of their program. This could be accomplished by plotting the data on a graph of ΔT_{30} versus fluence. However, because of data traceability problems, ASTM has been slow to standardize a procedure and the correlation monitor data have not been widely used. However, it is prudent to test and report these data and thereby contribute to the national data base.

1.2 Surveillance Program Description

1.2.1 Original Program

Three surveillance capsules were installed within the NMP-1 downcomer region in 1969 prior to initial operation. Three capsules have been removed to date and tested, including the present Capsule B. The results of the capsule testing are given in References [1-4, 1-5]. The number and type of mechanical behavior specimens included in the original surveillance program as specified by GE, as well as the capsule identification and location within the vessel, are summarized in Table 1-1.

During the time period over which the A and C capsules were tested, it was not known that a material mixup had occurred in the NMP-1 surveillance program. The results for the C capsule seemed to indicate a ΔT_{30} of 114°F for plate G-8-3, which was larger than the shift predicted by the regulatory guide model. The A capsule, which had been lost in the spent fuel pool, was found and sent to Battelle for testing to confirm the large apparent shift. The results of the A capsule testing seemed to confirm the C capsule results, and these conclusions were based on the surveillance program documentation which incorrectly indicated that all of the base metal Charpy and tensile specimens were fabricated from a prolongation from plate G-8-3.

1.2.2 Surveillance Program Revision

As a result of the large measured Charpy shifts, the NMP-1 surveillance program was revised and NMPC committed to performing a plant-specific surveillance program because the industry data did not adequately represent the NMP-1 data trend. As described in detail in Reference [1-6], two reinsertion capsules were designed, fabricated, and reinstalled with the NMP-1 vessel. This was the first set of reinsertion capsules ever reinstalled in a commercial nuclear power plant for the purpose of generating plant-specific surveillance data. The summary of the mechanical property specimens which are currently being irradiated at NMP-1 is given in Table 1-2.

1.2.3 Material Mixup Resolution

After the capsule reinsertion was completed, NMPC turned attention to finding the cause for the apparent large Charpy shift. A contract was placed with GE to locate the G-8-3 archive plate material and GE found a large piece of the plate. A contract was placed with Battelle to

analyze the plate to ensure its authenticity and to measure baseline mechanical properties. The measurements which were made by Battelle are fully documented in [1-6] and included: chemical composition; tensile properties; Charpy data; hardness measurements; and drop weight measurements. In addition to the Battelle efforts, NMPC performed an extensive records search and found as-built records. After extensive study and data analysis, it was definitively concluded that a material mixup had occurred. The base metal Charpy specimens were actually fabricated from a plate G-8-1 nozzle dropout, and not from plate G-8-3, as indicated in the plant documentation. However, the base metal portion of Charpy weld and heat-affected-zone (HAZ) specimens are composed of plate G-8-3 material as indicated in the records. As a result, the plate G-8-3 ΔT_{30}, originally thought to 114°F, was correctly established to be 11°F at a fast fluence of 4.78×10^{17} n/cm^2. Since the surveillance program is irradiating two plate materials (G-8-3 and G-8-1), the Charpy ΔT_{30} can be determined for both materials each time a capsule is withdrawn. These data are summarized in [1-6].

As a result of the discovery of a material mixup, the earlier plant documentation contains errors and misleading data. Therefore, a new baseline materials data report, Reference [1-6], was written and this report supersedes all previous materials property data reports. This report also contains an in-depth description of the revised surveillance program.

1.3 210 Degree Capsule

This report documents the testing and analysis of the 210 degree capsule. Throughout the report the capsule is referred to by its azimuthal position in the reactor or as "Capsule B". The capsule was removed from the reactor during the March, 1997 refueling outage. The specimens were removed from the capsule and tested by MPM. Chemical composition measurements were made to verify the material used to fabricate the mechanical behavior specimens. The capsule dosimeters have been counted and weighed to determine the specific activity for use in flux determination. The tensile and Charpy specimens have been tested and the embrittlement has been quantified in terms of Charpy shift, shelf drop, and elevation of yield stress. The results are described in detail in the chapters which follow.

1.4 Chapter 1 References

[1-1] Code of Federal Regulations, Title 10, Part 50, Appendix G

[1-2] ASME Boiler and Pressure Vessel Code, Section III, Appendix G for Nuclear Power Plant Components, Division 1, "Protection Against Nonductile Failure"

[1-3] U.S. NRC Regulatory Guide 1.99, "Radiation Embrittlement of Reactor Vessel Materials," Revision 2, May 1988

[1-4] Stahl, D., Manahan, M.P., Failey, M.P., Landow, M.P., Jung, R.G., and Lowry, L.M., "300 Degree Capsule Examination, Testing and Evaluation of Irradiated Pressure Vessel Surveillance Specimens From the Nine Mile Point Nuclear Power Station", Niagara Mohawk Power Corporation, July 18, 1984

[1-5] Manahan, M.P., Failey, M.P., and Landow, M.P., "Examination and Evaluation of the Nine Mile Point-Unit 1 30 Degree Azimuthal Surveillance Capsule, Final Report from Battelle to Niagara Mohawk Power Corporation, April 3, 1985

[1-6] Manahan, M.P., "Nine Mile Point Unit 1 Surveillance Capsule Program", NMEL-90001, dated January 4, 1991

Table 1-1 Original NMP-1 Surveillance Program Mechanical Behavior Specimen Inventory

Capsule Identification	Azimuthal Location	Year Withdrawn	Exposure (EFPY)	Charpy Specimens	Tensile Specimens
A	30°	1979	5.8	12 Base 12 Weld 12 HAZ	3 Base 3 Weld 3 HAZ
B	210°	1997	16.81	9 Base 9 Weld 9 HAZ 9 APED	3 Base 3 Weld 2 HAZ 2 APED
C	300°	1982	7.98	8 Base 8 Weld 8 HAZ	2 Base 2 Weld 2 HAZ

Note: APED refers to correlation monitor material installed by GE
The NMP-1 surveillance weld is heat/flux lot 5214/5G13F
Previous NRC submittals indicated Capsule B to have been located at 120°. This table has been updated, along with revised number of specimens, to indicate the actual Capsule B location and contents.

Table 1-2 Current NMP-1 Surveillance Program Mechanical Behavior Specimen Inventory

Capsule Identification	Azimuthal Location	Charpy Specimens	Tensile Specimens
A'	30°	6 Base -O 6 Base - R 12 Weld - O 12 HAZ - O	2 Base - O 2 Base - M 2 Weld - O 3 HAZ - O
C'	300°	12 Base - R 12 Weld - R 12 Base - U	4 Base - M 4 Weld - M 3 Base - U

Note: O = original irradiated and untested specimen
M = miniature tensile specimen machined from the broken halves of a previously tested specimen
R = weld reconstituted Charpy specimen
U = previously unirradiated specimen

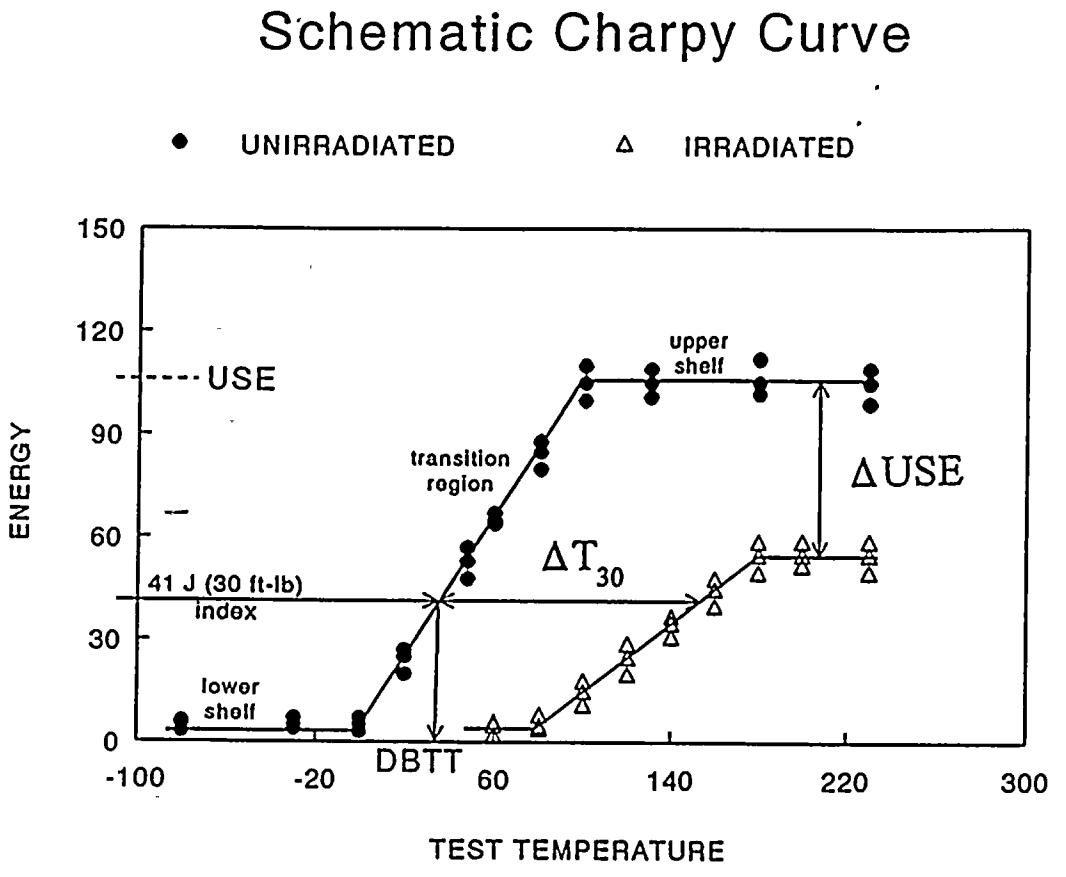

NOT ACTUAL DATA

Figure 1-1 **Schematic Illustration of Typical Charpy Curve and the Effect of Neutron Irradiation on the Curve**

2.0 Neutron Dosimeter Measurements

This section of the report describes the measurements made to determine the specific radionuclide activity contained in the dosimeter materials. Information on the dosimeter materials, the measurement techniques, and the instruments and procedures used to make the measurements are described. The results are summarized in tabular form.

2.1 Dosimeter Material Description

The Capsule B dosimeter materials are pure metal wires which were located within the Charpy packets in the surveillance capsule. The three wires types provided by GE are copper, iron, and nickel. Each wire is about three inches long. Upon receipt at the radiometric lab, the wires were removed from their plastic containers and visually inspected. Each group of three wires were then photographed prior to preparation for counting and weighing.

2.2 Dosimeter Mass Measurement

After photographing, the dosimeter wires were cleaned with a lab wipe soaked in pure ethanol. Each wire was then sectioned into pieces about 0.75" long for subsequent coiling into an approximate point source geometry. The sectioned segments were then soaked in a bath of pure ethanol for at least 30 minutes. The cleaning was performed to remove any loose material and other removable deposits from the dosimeter wires prior to mass determination. The wire segments were allowed to completely dry in air at room temperature. Since there was no evidence of oxidation or surface contamination, no further cleaning was required. The total mass of each wire was measured using a Mettler HL-52 digital balance. Table 2-1 lists the results of these measurements, as well as the identification assigned to each dosimeter wire.

2.3 Radiometric Analysis

Radiometric analysis was performed using high resolution gamma emission spectroscopy, often simply called gamma spectroscopy. In this method, gamma emissions from the dosimeter materials are detected and quantified using solid-state gamma ray detectors and computer-based signal processing and spectrum analysis. The specifications of the gamma ray spectrometer system (GRSS) are listed in Table 2-2. As shown in this table, there are two separate detectors in this system, one an older-style germanium-lithium, or Ge(Li) detector, and the other a newer, hyperpure germanium (HPGe) unit. Each detector is housed in a lead-copper shield (cave) to reduce background count rates.

System calibration was performed using a NIST-traceable quasi-point source supplied by Amersham Corporation. The analysis software was procured from Aptec Nuclear, Inc., and provides the capability for energy, resolution, and efficiency calibration using specified standard source information. Calibration information is stored on magnetic disk for use by the spectrographic

analysis software package.

Since detector efficiency depends on the source-detector geometry, a fixed, reproducible geometry/distance must be selected for the gamma spectrographic analysis of the dosimeter materials. For this work, the counting geometry was that of a quasi-point source (coiled 0.75 inch long wire) placed five inches vertically away from the top surface of the detector shell. In this way, extended sources up to 0.5" can be analyzed with a reasonable approximation to a point source. The coiled wires were well within the area needed to approximate a point source geometry. Both the Ge(Li) and HPGe detectors were calibrated for efficiency using the NIST traceable source.

The accuracy of the efficiency calibration was tested using a gamma spectrographic analysis of a traceable gamma source, separate from that used to perform the efficiency calibration, and supplied by a separate vendor. The isotope contained in this check source emits gamma rays which span the energy response of the detector for the dosimeter wires. The results are summarized below in Tables 2-3 and 2-4. They show that the efficiency calibration is providing a valid estimate of source activity. The acceptance criteria for these measurements is that the software must yield a valid isotopic identification, and that the quantified activity of each correctly identified isotope be within the uncertainty specified in the source certification.

Table 2-5 shows the counting schedule established for this work. The shorter-lived radionuclides were analyzed first to avoid further decay of the activity. These turned out to be the iron dosimeter wires. After these, the nickel wires were analyzed, and then the copper materials. The Ni-2 wire listed in Table 2-5 was recounted later to improve the counting statistics. Neutrons interact with the constituent nuclei of the dosimeter materials, producing radionuclides in varying amounts depending on total neutron fluence and its energy spectrum, and the nuclear properties of the dosimeter materials. Table 2-6 below lists the reactions of interest and their resultant radionuclide products for each element contained in the wire dosimeters. Many of these are threshold reactions involving and n-p or n-α interaction.

Finally, Table 2-7 presents the primary results of interest for flux determination. The activity units are in dps/mg, which normalizes the activity to dosimeter mass. The activities are specified for both the time of the analysis, and a "Reference Date/Time", which in this case is the NMP-1 shutdown date and time. This was specified as March 3, 1997, at 23:02 EST.

Table 2-1 Dosimeter Wire Descriptions

Charpy Packet No.	Wire Composition	Wire Mass (milligrams)	Wire ID
1	Copper	342.70	Cu-1
	Iron	130.00	Fe-1
	Nickel	233.44	Ni-1
2	Copper	328.65	Cu-2
	Iron	127.45	Fe-2
	Nickel	162.25	Ni-2
3	Copper	342.77	Cu-3
	Iron	146.69	Fe-3
	Nickel	211.90	Ni-3

Table 2-2 GRSS Specifications

System Component	Description and/or Specifications
Detectors	One Ge(Li), PGT Model LGC14, One HPGe, Canberra Model GC1420
Energy Resolution	Ge(Li): 1.78 @ 1332.5 KeV HPGe: 1.77 @ 1332.5 KeV
Detector Efficiency (Relative to 3"x3" NaI)	Ge(Li): 12.9% @ 1332.5 KeV HPGe: 14.0% @ 1332.5 KeV
Amplifiers	Two Aptec Nuclear Inc. Model 6300 Low-Noise Spectroscopy Amplifiers
ADC	Two Aptec Nuclear Inc. Model S4008 PC-ISA Cards, 8192 Channels, 6 µsec. fixed conversion time, successive approximation conversion method
Computer System	120 MHZ Pentium-Based PC, 16 MB Main Memory, 1.1 GB Hard Disk, 17" Monitor, Laserjet 4M Printer
Software	Aptec Nuclear, Inc. OSQ/Professional, Version 6.10
Bias Supplies	Two Mech-Tronics Model 258 HV Supplies

Table 2-3 Performance Check of the Ge(Li) Detector and OSQ Software

Isotope ID	Specified Activity in (μCi)	Specified Uncertainty (%)	Measured Activity in (μCi)	Measured Uncertainty (%)	Acceptance Criteria Met?
^{57}Co	0.4778	3.1	0.4788	0.4	Yes
^{60}Co	0.5063	3.6	0.5009	0.7	Yes

Table 2-4 Performance Check of the HPGe Detector and OSQ Software

Isotope ID	-- Specified Activity in (μCi)	Specified Uncertainty (%)	Measured Activity in (μCi)	Measured Uncertainty (%)	Acceptance Criteria Met?
^{57}Co	0.4778	3.1	0.4764	0.3	Yes
^{60}Co	0.5063	3.6	0.5032	0.5	Yes

Table 2-5 Dosimeter Wire Counting Schedule

Dosimeter Wire ID	Count Start Date	Count Start Time (EDT)	Count Duration (Live Time Seconds)
Cu-1	7/17/97	16:44	62705
Fe-1	7/16/97	16:27	64527
Ni-1	7/17/97	12:21	8030
Cu-2	7/22/97	15:46	54746
Fe-2	7/16/97	16:29	71055
Ni-2	9/9/97	15:14	59754
Cu-3	7/22/97	15:48	55079
Fe-3	7/17/97	10:39	87920
Ni-3	7/18/97	10:14	80000

Table 2-6 Reactions of Interest

Wire Composition	Neutron-Induced Reactions	Reaction Product Isotope
Copper	n-α	Co-60
Iron	n-p	Mn-54
	n-γ	Fe-59
Nickel	n-p	Co-58

Table 2-7 Results of the Radiometric Analysis

Wire ID	Isotope ID	Activity At Count Date/Time[a] (dps/mg)	Activity At Reference Date/Time[b] (dps/mg)	Activity Uncertainty (%)
Cu-1	^{60}Co	19.67	20.66	1.37
Fe-1	^{54}Mn	110.8	149.4	2.39
	^{59}Fe	7.552	59.89	2.76
	^{60}Co	53.46	56.11	1.41
Ni-1	^{57}Co	25.87	36.63	3.25
	^{58}Co	457.4	1725.0	2.56
	^{60}Co	406.0	426.3	1.35
Cu-2	^{60}Co	19.78	20.81	1.43
Fe-2	^{54}Mn	102.8	138.6	2.49
	^{59}Fe	6.980	55.35	2.33
	^{60}Co	50.14	52.63	1.37
Ni-2	^{57}Co	22.24	36.19	3.04
	^{58}Co	255.3	1636.0	2.55
	^{60}Co	380.3	407.2	1.33
Cu-3	^{60}Co	18.47	19.43	1.39
Fe-3	^{54}Mn	100.4	135.7	2.39
	^{59}Fe	7.823	62.76	2.42
	^{60}Co	58.02	60.92	1.38
Ni-3	^{57}Co	25.10	35.64	3.00
	^{58}Co	418.4	1592.0	2.57
	^{60}Co	470.9	494.6	1.32

[a] See Table 2-5

[b] This was specified as March 3, 1997, at 23:02 EST.

3.0 Neutron Flux Calculation

3.1 Flux Calculation Method/Assumptions

Capsule B was irradiated from reactor start-up to March 1997 for a total of 16.81 effective full power years at 1850 MWt. The power history was supplied as the thermal generation per month over this period. The use of monthly power history data is not expected to introduce any significant error in the results, even for the relatively short-lived nickel reaction.

As discussed in Chapter 2, the dosimetry from Capsule B consisted of three sets of Cu, Fe, and Ni wires. This dosimetry was counted to determine the fast neutron reactions shown in Table 3-1. This table also gives the nuclear constants used to determine the reaction rates. These data are taken from the appropriate ASTM standards [3-1,3-2,3-3,3-4].

The Capsule B flux was calculated using the 300 degree capsule neutron spectrum (see Reference [3-5]). In particular, a flux for each dosimeter was calculated by dividing the measured reaction rate by the spectral average cross section above 1 MeV, and then averaging the results by flux wire type. Inherent in this approach is the assumption that the 300 degree transport model is representative of subsequent fuel loadings through March, 1997.

The neutron transport results from earlier analyses can, in principle, be used because the NMP-1 capsules are located at octally equivalent azimuthal positions. However, it must be recognized that there can be differences in fuel cycles which can introduce differences in flux to the capsule for the same power generation. If these effects are large, then a neutron transport analysis must be done to accurately interpret the dosimetry data. As discussed below, this has been found to be the case and a neutron transport analysis will be performed and used in the next P-T curve revision calculation. However, the use of the 300 degree capsule transport data, in conjunction with the copper dosimeter data, has been shown to yield an accurate flux for the Capsule B exposure.

3.2 Flux Estimation Results

The key dosimetry results are tabulated in Table 3-2. The dosimeter measurements are presented in units of disintegrations per second per milligram (dps/mg), adjusted to the end-of-irradiation (March 3, 1997 at 23:02). Using the power history, the ratio of reaction rate to dps was calculated, and the results are also in Table 3-2. The units of reaction rate are reactions per second per target nucleus.

Using the same calculated neutron spectrum as in Reference 3-5, averaged at the center of the capsule, together with reaction cross sections in 47 groups from Reference 3-6, the flux above 1 MeV was determined. The flux is given by the measured reaction rate divided by the spectral averaged cross section above 1 MeV. The flux determined in this way for each dosimeter, and the average for each of the three dosimeter types, is given in Table 3-2. The 47 group spectrum at the

capsule center (arbitrary normalization) is given in Table 3-3.

The results in Table 3-2 indicate that a consistent difference is observed between the three monitors, while the individual monitors of the same type are in good agreement. The difference may be indicative of a significant change in flux level in the capsule at full power that would have occurred in the last cycle. Such a change could be due to a change in fuel loading from earlier patterns or other reactor change.

Comparison may be made with earlier results from the capsule at 300 degrees presented in Reference 3-5. In the earlier case, good agreement was observed among the different dosimeter reactions. Thus, the capsule B result differences are not typical. Since the time history may not accurately represent the flux at the capsule, it is recommended that only the copper reaction be used since only this reaction measures fluence from any but the last cycle or two. Therefore, the recommended average flux for Capsule B is 1.76E09 n/cm^2/s. Other recommended values for exposure for Capsule B are given in Table 3-4. It must be recognized that, if the last cycle relative flux is low as is indicated to be true by the other reactions, then the value measured by the copper will also be slightly low (~5% low). The recommended value from the 300 degree capsule was 1.90E09 n/cm^2/s which is in reasonable agreement (about 8% higher) with the Capsule B results.

3.3 Uncertainty Estimation

An uncertainty estimate was made for the capsule fluence. The main sources of uncertainty are the calculated neutron flux spectrum in the capsule, and the deviation in flux history from the power history of the reactor. Use of the copper monitor alone provides only a normalization of the calculated fluence and no check on the accuracy of the calculated neutron spectrum. Based on experience with other capsules (Reference 3-7), this uncertainty is conservatively estimated to be 12%. An estimate of the power history uncertainty effect was derived from the changes necessary to allow the copper and iron reactions to be in agreement. This change affected the copper reaction rate by 7%. The 7% value was chosen to be an estimate of the 1σ uncertainty from this source. Combining the two uncertainties in quadrature results in an overall uncertainty estimate of 14%.

Uncertainty estimates for the vessel fluence will be higher because of the additional uncertainty from extrapolation from the capsule measurement location. Because the capsule is located very close to the vessel, the major uncertainty in extrapolation is due to error in the calculation of the azimuthal flux variation. Some of this error will arise from differences in the void fraction in the various outer assemblies from that used in the calculation. An estimate of the uncertainty in the fluence extrapolation is 10%. Combining this with the capsule fluence uncertainty results in a total uncertainty of 17% for the maximum midplane vessel fluence. The neutron transport analysis for cycle 12 is expected to result in vessel fluxes with lower uncertainty. The revised uncertainty estimates will be include with the next P-T curve revision report.

3.4 Additional Analyses

The analysis of the Capsule B data has indicated that fuel cycle effects may have invalidated neutron transport results obtained for the 300 degree capsule [3-5]. Therefore, the vessel flux and fluence data are not included in this report. Accordingly, NMPC has authorized MPM to perform a neutron transport analysis which will be used in the next P-T curve revision to reduce the uncertainty associated with calculating the peak flux in the vessel wall.. The results reported here for the capsule, as judged by the consistency of the dosimetry data set and the reasonable uncertainty estimates, are considered appropriate for the purpose of assigning a mean flux to the capsule measured shift.

3.5 Chapter 3 References

3-1 ASTM Designation E263-88, *Standard Method for Determining Fast-Neutron Flux Density by Radioactivation of Iron*, in ASTM Standards, Section 12, American Society for Testing and Materials, Philadelphia, PA, 1997.

3-2 ASTM Designation E264-92, *Standard Method for Determining Fast-Neutron Flux Density by Radioactivation of Nickel*, in ASTM Standards, Section 12, American Society for Testing and Materials, Philadelphia, PA, 1997.

3-3 ASTM Designation E523-87, *Standard Method for Determining Fast-Neutron Flux Density by Radioactivation of Copper*, in ASTM Standards, Section 12, American Society for Testing and Materials, Philadelphia, PA, 1997.

3-4 ASTM Designation E1005-84, *Standard Test Method for Application and Analysis of Radiometric Monitors for Reactor Vessel Surveillance,* in ASTM Standards, Section 12, American Society for Testing and Materials, Philadelphia, PA, 1997.

3-5 D. Stahl, et. al., "Final Report on Examination, Testing and Evaluation of Irradiated Pressure Vessel Surveillance Specimens from the Nine Mile Point Nuclear Power Station", BCL-585-84-6, Battelle Memorial Institute, 505 King Avenue, Columbus, Ohio 43201, July 1984.

3-6 RSICC Data Library Collection, DLC-185, BUGLE-96, Coupled 47 Neutron, 20 Gamma Ray Group Cross Section Library Derived from ENDF/B-VI for LWR Shielding and Pressure Vessel Dosimetry Applications, available from the Radiation Safety Information Computational Center, Oak Ridge National Laboratory, Oak Ridge, TN, March 1996.

3-7 E. P. Lippincott, "Westinghouse Surveillance Capsule Neutron Fluence Reevaluation", WCAP-14044, Westinghouse Electric Corporation, PO Box 355, Pittsburgh, Pa 15230, April 1994.

Table 3-1 Nuclear Parameters Used in the Evaluation of Neutron Sensors

Monitor Material	Reaction of Interest	Target Fraction	Approx. Response Threshold	Product Half-Life
Copper	$Cu^{63}(n,\alpha)Co^{60}$	0.6917	5 MeV	5.271 yrs
Iron	$Fe^{54}(n,p)Mn^{54}$	0.0580	2 MeV	312.5 days
Nickel	$Ni^{58}(n,p)Co^{58}$	0.6827	2 MeV	70.78 days

Table 3-2 Tabulation of Dosimetry Results

Dosimeter	Measured decay (dps/mg)	Reaction Rate (react./atom/s)	Flux (E>1 MeV) ($n/cm^2/s$)
Cu-1	20.66	4.788E-18	1.789E+09
Cu-2	20.81	4.823E-18	1.802E+09
Cu-3	19.43	4.503E-18	1.683E+09
Avg Cu	20.30	4.705E-18	1.758E+09
Fe-1	149.4	2.689E-16	1.519E+09
Fe-2	138.6	2.495E-16	1.409E+09
Fe-3	135.7	2.442E-16	1.380E+09
Avg Fe	141.2	2.542E-16	1.436E+09
Ni-1	1725	2.670E-16	1.180E+09
Ni-2	1636	2.532E-16	1.119E+09
Ni-3	1592	2.464E-16	1.089E+09
Avg Ni	1651	2.555E-16	1.129E+09

Table 3-3 300 Degree Capsule Flux Spectrum Used to Evaluate Dosimetry Data

Calculated 47 Group Neutron Spectrum at Capsule Center					
Group	Energy (MeV)	Flux (n/cm²/sec)	Group	Energy (MeV)	Flux (n/cm²/sec)
1	1.733E+01	3.2877E-07	25	2.972E-01	6.2753E-05
2	1.419E+01	1.5603E-06	26	1.832E-01	5.7107E-05
3	1.221E+01	5.2415E-06	27	1.111E-01	4.6158E-05
4	1.000E+01	1.0103E-05	28	6.738E-02	3.7686E-05
5	8.607E+00	1.4384E-05	29	4.087E-02	1.4599E-05
6	7.408E+00	3.7165E-05	30	3.183E-02	6.7296E-06
7	6.065E+00	4.6127E-05	31	2.606E-02	6.6289E-06
8	4.966E+00	6.5161E-05	32	2.418E-02	6.7343E-06
9	3.679E+00	3.9357E-05	33	2.188E-02	1.9261E-05
10	3.012E+00	2.6214E-05	34	1.503E-02	3.4036E-05
11	2.725E+00	2.7706E-05	35	7.102E-03	3.2421E-05
12	2.466E+00	1.3087E-05	36	3.355E-03	2.8647E-05
13	2.365E+00	3.2264E-06	37	1.585E-03	5.0954E-05
14	2.346E+00	1.5840E-05	38	4.540E-04	2.1062E-05
15	2.231E+00	3.9865E-05	39	2.145E-04	2.8705E-05
16	1.920E+00	3.8042E-05	40	1.013E-04	3.8092E-05
17	1.653E+00	4.9990E-05	41	3.727E-05	4.6016E-05
18	1.353E+00	7.2987E-05	42	1.068E-05	2.6864E-05
19	1.003E+00	4.2339E-05	43	5.044E-06	3.4360E-05
20	8.208E-01	2.2685E-05	44	1.855E-06	2.4681E-05
21	7.427E-01	5.0727E-05	45	8.764E-07	2.3401E-05
22	6.081E-01	4.2102E-05	46	4.140E-07	7.3272E-05
23	4.979E-01	5.0983E-05	47	1.000E-07	8.7644E-04
24	3.688E-01	4.1246E-05			

Table 3-4 Exposure Values for Capsule B

Parameter	Exposure Value	Units
Flux (E> 1.0 MeV)	1.76E+09	$n/cm^2/s$
Flux (E> 0.1 MeV)	3.08E+09	$n/cm^2/s$
dpa/s	2.69E-12	/s
Fluence (E > 1.0 MeV)	9.34E+17	n/cm^2
Fluence (E > 0.1 MeV)	1.63E+18	n/cm^2
dpa	.00143	

4.0 Test Specimen Chemical Analysis

As described in Reference [4-1], a material mix-up occurred in the NMP-1 surveillance program. Reference [4-1] documents the mix-up and its resolution. Accordingly, MPM has recommended that chemical composition measurements be performed on Charpy and tensile specimens to confirm the base metal material composition. These measurements were performed using inductively coupled plasma - optical emission (ICP-OE) spectrometry.

4.1 Specimen Selection and Machining of Samples

A total of six chemistry samples were taken by NMPC from Capsule B Charpy and tensile specimens prior to testing. The samples were machined using a clean end mill to ensure that no contamination of the sample occurred. The samples were machined from the ends of the Charpy specimens and the grip ends of the tensile specimens to ensure that the mechanical behavior would not be affected during subsequent testing.

4.2 Preparation of Samples for Analysis

Chemistry samples were placed in marked plastic vials. Table 4-1 lists the sample identifications established for this work and their corresponding descriptions. Note that the sample denoted as "Plate A" was taken from archived plate G-8-3. The G-8-3 material was used as a check on the validity of the results. Prior to analysis via ICP-OE, the samples were cleaned by immersion in a bath of 100% ethyl alcohol to remove any surface contaminants.

4.3 ICP Measurements

The ICP-OE system used in this program was manufactured by Perkin-Elmer and is designated as the Optima 3000 system. It was calibrated using traceable ICP standard solutions. The specimens taken for analysis were dissolved in an acid solution in preparation for introduction to the ICP-OE system. ICP data were accumulated to show well-defined emission peaks for the elements of interest. Table 4-2 lists the elements of interest and the results obtained from the ICP-OE analysis. It should be noted that iron is assumed to be the matrix element and is not quantified.

Analysis of plate G-8-3 was performed to establish the reliability of the ICP method and to check its precision against previous results obtained for this material. The procedures followed for this work established the acceptance criterion as being that the current results must fall within two standard deviations from the average of all previous measurements. Using this, the results indicate that the acceptance criterion has been met for all cases where it can be applied.

4.4 Material Identification

Table 4-3 provides a comparison of the Charpy and tensile specimen measured chemistries with the NMP-1 beltline plates. The five elements presented in the table are the elements found useful in Reference [4-1] for resolving the material mixup. As expected, the chemistry data supports the Reference [4-1] conclusion that the base metal specimens were machined from plate G-8-1 and the weld and HAZ specimens were prepared from a welded prolongation from plate G-8-3.

4.5 Chapter 4 References

[4-1] Manahan, M. P., "Nine Mile Point Unit 1 Surveillance Capsule Program", NMEL-90001, Report to Niagara Mohawk, January 4, 1991

Table 4-1 Sample Identifications and Descriptions

Sample ID	Material Description
E21	Base Metal Charpy E21 (one end only)
JD4	Base Metal Tensile JD4 (one end only)
J2B-L	HAZ Charpy J2B, Left End
J2B-R	HAZ Charpy J2B, Right End
JU4-L	HAZ Tensile JU4, Left End
JU4-R	HAZ Tensile JU4, Right End
Plate A	Archive Plate G-8-3

Table 4-2 Results of the ICP Analysis

Element Symbol	Sample E21	Sample JD4	Sample J2B-L	Sample J2B-R	Sample JU4-L	Sample JU4-R	Archive Plate G-8-3
	(wt %)	(wt %)	(wt %)	(wt %)	(wt %)	(wt %)	(wt %)
Fe	Matrix	Matrix	Matrix	Matrix	Matrix	Matrix	Matrix
Co	0.011	0.012	0.011	0.008	0.012	0.012	0.012
P	0.030	0.026	0.034	0.039	0.01	0.019	0.022
Cu	0.236	0.238	0.160	0.172	0.163	0.174	0.177
Mo	0.433	0.440	0.473	0.499	0.445	0.478	0.475
Ni	0.508	0.501	0.603	0.106	0.541	0.590	0.597
Mn	1.357	1.377	1.141	1.685	1.094	1.181	1.163
V	<0.001	<0.001	<0.001	<0.001	<0.001	<0.001	<0.001
Cr	<0.0003	<0.0003	<0.0003	<0.0003	<0.0003	<0.0003	<0.0003
Ti	<0.0001	<0.0001	<0.0001	<0.0001	<0.0001	<0.0001	<0.0001

Table 4-3 Comparison of Charpy and Tensile Specimen Chemistry with the NMP-1 Plate Chemistry

Element	Lukens Plate G-8-1 (wt %)	Base Metal Charpy E21 (wt %)	Base Metal Tensile JD4 (wt %)	Lukens Plate G-8-3 (wt %)	HAZ Charpy J2B-L (wt %)	HAZ Tensile JU4-R (wt %)
Cu	0.23	0.236	0.238	0.18	0.160	0.174
Ni	0.51	0.508	0.501	0.56	0.603	0.590
P	0.021	0.030	0.026	0.012	0.034	0.019
Mn	1.34	1.357	1.377	1.16	1.141	1.181
Mo	0.45	0.433	0.440	0.47	0.473	0.478

5.0 Tensile Test Results

5.1 Test Procedure

Tensile tests were conducted in accordance with ASTM Standard Practice E 185-82. The 1982 version of E185 has been reviewed and approved by NRC for surveillance capsule testing applications. This standard references ASTM E8 and E21. In cases where three irradiated tensile specimens are available for testing, the standard requires testing of one specimen in the vicinity of the upper end of the Charpy energy transition region. The remaining specimens from each material are tested at the service temperature and midtransition temperature. In the case of the HAZ and APED specimens, only two tensile specimens were available and these were tested at a temperature near the upper shelf and at midtransition.

The tensile tests were conducted using an MTS servo hydraulic test machine equipped with a furnace for heating the specimens. The MTS load cell and LVDT were calibrated prior to testing by MTS corporation using NIST traceable standards. The Charpy tests, which are described in Chapter 6, were performed prior to tensile testing so that the test temperatures could be accurately defined in accordance with ASTM E185-82. The representative operating temperature in the NMP-1 downcomer was conservatively taken to be 520 F. All tests, including the room temperature tests, were conducted with thermocouples attached to the gage length of the specimen. Temperature control was maintained to ± 5 F of the desired test temperature for at least 20 minutes prior to the start of the test.

All tests were conducted at a crosshead speed of 0.1 inches/minute. Since most of the tests were conducted at a temperature which would preclude the use of an extensometer, the deflection was obtained from the LVDT in the ram, corrected for load train compliance. The data were recorded in the computer continuously at an acquisition rate of 5 Hz, averaged, and stored on disk at a rate of 1 Hz. Total elongation was determined from punch marks using calibrated calipers. The cross sectional area of the gage length before and after testing was measured using calibrated calipers. A drawing of a typical test specimen is shown in Figure 5-1.

5.2 Tensile Test Results

The Capsule B flow curves are given in Appendix A and the key tensile properties are listed in Table 5-1. This table gives the tensile properties by specimen identification, material type, and test temperature. In most cases, the material exhibited upper and lower yield point elongation. The HAZ specimens did not exhibit upper/lower yield phenomena and therefore the yield stress for these tests was determined using the 0.2 % offset method. The total elongation was determined from the punch marks on the specimen. The reduction of area was calculated from measurements of the diameter in the gage length before and after testing. The post-test measurements were made by fitting the fracture surface back together after the test and measuring the diameter with calipers.

The key tensile parameters which characterize neutron induced embrittlement are compared with unirradiated data and with data from the 30° and 300° capsules in Tables 5-2 and 5-3. Overall the data trend shows a moderate embrittlement with increasing fluence as expected. In particular, the yield and ultimate stress are increasing with neutron exposure and the measures of ductility (reduction of area and total elongation) are generally decreasing with increasing exposure. Reference [5-1] reports a correlation between Charpy shift and irradiation hardening. In particular,

$$\Delta T_{30} \sim C\, \Delta\sigma,$$

where,

ΔT_{30}	=	Charpy 30 ft-lb transition temperature shift (°C)
C	=	0.5 °C/MPa for plate materials
$\Delta\sigma$	=	irradiation induced yield strength increase (Mpa)

Applying this correlation to the Capsule B plate G-8-1 elevation in yield strength of ~ 14 ksi, and accounting for the unit conversion, the Reference [5-1] correlation would predict a Charpy 30 ft-lb shift of 86.9 °F. This prediction is consistent with the measured Charpy shift of 77.7°F. Therefore, the Charpy shift and tensile yield strength elevation show consistent data trends with neutron exposure.

5.3 Chapter 5 References

[5-1] EPRI Report NM-3319, "Physically Based Regression Correlations of Embrittlement Data From Reactor Pressure Vessel Surveillance Programs", January, 1984

Table 5-1 Tensile Data for NMP-1 210° Surveillance Capsule

Specimen Identification	Material Type	Test Temperature (F)	Upper Yield Strength[2,3] (ksi)	Lower Yield Strength[3] (ksi)	Ultimate Strength (ksi)	Engineering Fracture Stress (ksi)	Fracture Load (lbs)	True Fracture Stress (ksi)	Uniform Elongation[4] (%)	Total Elongation[4] (%)	Reduction of Area (%)
JD4	Base	134.3	80.3	80.1	98.9	66.3	3282	179.7	16.5	25.1	63.1
JD5	Base	269.6	76.6	75.9	94.7	68.6	3371	165.6	16.9	22.8	58.6
JD6	Base	519.2	71.4	71.1	94.6	70.2	3449	170.5	13.5	20.4	58.8
JLL	Weld	65.7	77.7	76.2	92.8	62.9	3060	167.5	18.7	26.3	62.4
JL5	Weld	143.7	80.3	77.6	91.7	63.0	3063	178.0	14.4	25.4	64.6
JMM	Weld	522.3	66.3	65.7	84.9	63.6	3074	161.8	13.6	20.3	60.7
JU4	HAZ	69.8	69.4	n/a	91.2	61.6	3015	181.3	14.4	22.1	66.0
JU1	HAZ	128.3	68.7	n/a	88.1	61.0	2971	182.4	12.5	21.4	66.6
APED 17	Base	57.7	78.4	75.8	97.6	62.9	3048	163.7	18.9	28.0	61.5
APED 0	Base	124.5	73.7	72.5	93.1	62.3	3049	187.2	16.4	26.9	66.7

(1) All tests were conducted at a crosshead speed of 0.1 in./min.
(2) Upper and lower yield were determined directly from the raw data.
(3) In cases where upper and lower yield behavior was not observed, the 0.2% offset method was used to determine the yield strength.
(4) Elongation is for a one inch gage length. Total elongation was determined from punch marks.

Table 5-2 Comparison of Plate G-8-1 Irradiated and Unirradiated Tensile Properties

Specimen Identification - Temperature	Yield/ Upper Yield (ksi)	Ultimate Tensile Strength (ksi)	Reduction of Area (%)	Total Elongation[a] (%)
Unirradiated				
G-8-1 - RT	66.6	87.5	66.0	27.0[b]
		30 ° Capsule	fluence = 3.60×10^{17} n/cm²/s	
JDE - RT	76.1	96.8	66.1	24.1
		300 ° Capsule	fluence = 4.78×10^{17} n/cm²/s	
JJA - RT	79.2	99.7	65.7	27.7
JDB - 550 F	69.4	92.9	58.0	19.7
		210 ° Capsule	fluence = 9.34×10^{17} n/cm²/s	
JD4 - 134 F	80.3	98.9	63.1	25.1
JD5 - 270 F	76.6	94.7	58.6	22.8
JD6 - 519 F	71.4	94.6	58.8	20.4

[a] Elongation in 1 inch unless otherwise specified
[b] Elongation in 2 inch

Table 5-3 Comparison of Surveillance Weld Irradiated and Unirradiated Tensile Properties

Specimen Identification - Temperature	Yield/ Upper Yield (ksi)	Ultimate Tensile Strength (ksi)	Reduction of Area (%)	Total Elongation[a] (%)
Unirradiated				
W5214	65.0	84.0	67.0	27.5[b]
300 ° Capsule			fluence = 4.78×10^{17} n/cm²/s	
JLB - RT	73.7	90.2	68.1	23.2
JL7 - 550 F	67.8	84.7	62.4	20.9
210 ° Capsule			fluence = 9.34×10^{17} n/cm²/s	
JLL - 66 F	77.7	92.8	62.4	26.3
JL5 - 144 F	80.3	91.7	64.6	25.4
JMM - 522 F	66.3	84.9	60.7	20.3

[a] Elongation in 1 inch unless otherwise specified
[b] Elongation in 2 inch

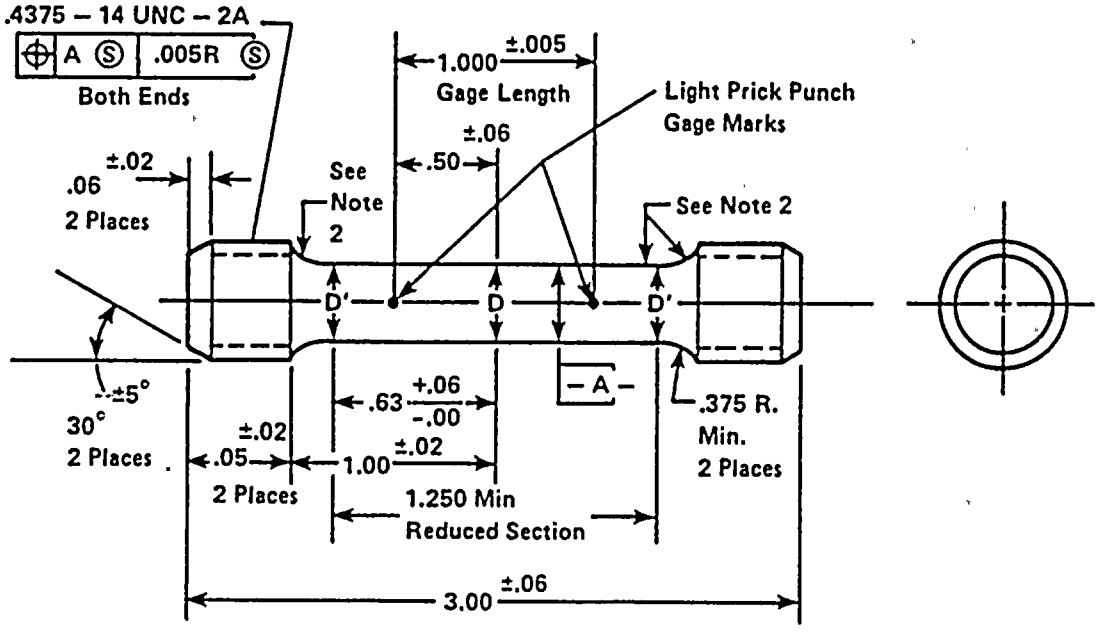

Notes:

1. D = $.250^{\pm.001}$ dia. at center of reduced section. D' = actual D dia. + .002 to .005 at ends of reduced section tapering to D at center.
2. Grind reduced section and radii to 32✓ radii to be tangent to reduced section with no circular tool marks at point of tangency or within reduced section. Point of tangency shall not lie within reduced section.

Figure 5-1 Drawing Showing a Typical Tensile Test Specimen

6.0 Charpy Test Data

6.1 Charpy Test Procedure

Charpy impact tests were conducted in accordance with ASTM Standard Practice E 185-82. A drawing showing the Charpy test specimen geometry is given in Figure 6-1. The 1982 version of E185 has been reviewed and approved by NRC for surveillance capsule testing applications. This standard references ASTM E23. The tests were conducted using a Tinius Olsen Testing Machine Company, Inc. Model 84 impact test machine with a 300 ft-lb range. The MPM Model 84 is equipped with a dial gage as well as an optical encoder for accurate absorbed energy measurement. In all cases, the optical encoder measured energy was reported as the impact energy. The impact energy was corrected for windage and friction for each test performed. The velocity of the striker at impact was 17.94 ft/s. Calibration of the machine was verified as specified in E-23 and verification specimens were provided by NIST.

Impact tests were conducted using an instrumented striker system fabricated by MPM. A standard is currently being developed by ASTM for instrumented testing but is not yet available for use in testing. The guidance provided in the draft standard was followed in the testing, however, the instrumented data provided should not be considered as nuclear quality assurance data at the present time. Figure 6-2 illustrates the raw data recorded by the instrumented system software. The voltage-time signal is converted to a force time signal through calibration of the striker as shown in Figure 6-3. The force-time curve is integrated to produce the velocity-time curve, which in turn is integrated to yield the striker displacement-time curve. Figure 6-4 shows a typical force-displacement curve along with the critical load points. This curve is the key result from instrumented testing. The instrumented data, as shown in Figure 6-4, can be used in materials embrittlement research and for development of fracture toughness correlations.

The E23 procedures for specimen temperature control using liquid baths were followed. The low temperature bath consisted of a refrigerated methanol bath with circulation. The elevated temperature bath consisted of a circulated silicon oil bath with internal electric heating. The bath liquid levels were maintained so that a minimum of one inch of liquid surrounded the specimen at all times. Each specimen was held at the desired test temperature for at least 10 minutes prior to testing and the bath temperature was held to ± 1 F. The specimens were transferred to the test machine supports and struck within 5 seconds after removal of the specimen from the bath. Precision calibrated tongs were used for specimen transfer.

Lateral expansion was determined from measurements made with a lateral expansion gage. The lateral expansion gage was calibrated using precision gage blocks which are traceable to NIST. The percentage of shear fracture area was determined by integrating the ductile and brittle fracture areas using the MPM image analysis system. The percent shear fracture area determined by integration was checked using the E23 comparison method.

The number of Charpy specimens for measurement of the transition region and upper shelf was severely limited. Therefore, the choice of test temperatures was very important. Prior to testing, the Charpy energy-temperature curve was predicted using MPM models and previous data. The first test was then conducted near the middle of the transition region and test temperature decisions were then made based on the test results. Overall, the goal was to perform three tests on the upper shelf and to use the remaining six specimens to characterize the 30 ft-lb index. This approach was successful as illustrated in the next chapter.

6.2 Charpy Test Data

Nine irradiated base metal, weld, HAZ, and APED specimens were tested over the transition region temperature range and on the upper shelf. The data are summarized in Tables 6-1 through 6-4. The G-8-1 base metal surveillance specimens have an L-T orientation. In addition to the energy absorbed by the specimen during impact, the measured lateral expansion values and the percentage shear fracture area for each test specimen are listed in the tables. The Charpy energy was read from the Tinius Olsen optical encoder and has been corrected for windage and friction in accordance with ASTM E23. The impact energy is the energy required to initiate and propagate a crack. The optical encoder and the dial cannot correct for tossing energy and therefore this small amount of additional energy may be included in the data for some tests. The instrumented striker data is provided in Appendix B. As discussed earlier, these data were not obtained under the quality assurance program because there is not yet an ASTM test procedure available. However, since research is currently being conducted to extract fracture toughness from instrumented Charpy data, it was considered prudent to perform the tests with an instrumented test system. The instrumented integrated energy is typically different from the dial measured energy because a windage/friction correction is not needed for the instrumented striker and the tossing energy can be quantified and removed from the energy. However, since the dial/optical encoder is the method used to establish the US embrittlement database, the instrumented striker data has been normalized to agree with the encoder energy.

The lateral expansion is a measure of the transverse plastic deformation produced by the striking edge of the striker during the impact event. Lateral expansion is determined by measuring the maximum change of specimen thickness along the sides of the specimen. Lateral expansion is a measure of the ductility of the specimen. The nuclear industry tracks the embrittlement shift using the 35 mil lateral expansion index.

The percentage of shear fracture area is a direct quantification of the transition in the fracture modes as the temperature increases. All metals with a body centered cubic lattice structure, such as ferritic pressure vessel materials, undergo a transition in fracture modes. At low test temperatures, a crack propagates in a brittle manner and cleaves across the grains. As the temperature increases, the percentage of shear (or ductile) fracture increases. This temperature range is referred to as the transition region and the fracture process is mixed mode. As the temperature increases further, the fracture process is eventually completely ductile (ie., no brittle component) and this temperature range is referred to as the upper shelf region.

Preparation of pressure-temperature (P-T) operating curves requires the determination of the Charpy 30 ft-lb transition temperature shift. This index is determined by fitting the energy-temperature data to find the mean curve. It is also necessary to estimate the upper shelf energy to ensure that the shelf has not dropped below the 10CFR50, Append G, 50 ft-lb screening criterion. The Charpy data analysis results are provided in Chapter 7.

Table 6-1 Charpy V-Notch L-T Impact Test Results for Irradiated G-8-1 Base Metal Specimens from the Nine Mile Point Unit 1 210-Degree Surveillance Capsule

Specimen Identification	Test Temperature (°F)	Impact Energy (ft-lb)	Fracture Appearance (% Shear Area)	Lateral Expansion (mils)
E3P	10.0	9.4	5.0	8.5
E3L	66.5	24.6	12.0	22.0
E3B	91.0	32.0	22.5	31.0
E2A	116.0	41.6	30.3	37.9
E21	165.0	56.7	59.1	54.5
E3K	225.0	91.6	83.6	85.5
E3D	275.0	90.4	100.0	78.3
EAM	300.0	75.9	100.0	73.0
E25	325.0	85.2	100.0	79.7

Table 6-2 Charpy V-Notch Impact Test Results for Irradiated Weld Metal Specimens from the Nine Mile Point Unit 1 210-Degree Surveillance Capsule

Specimen Identification	Test Temperature (°F)	Impact Energy (ft-lb)	Fracture Appearance (% Shear Area)	Lateral Expansion (mils)
EEA	-60.0	16.7	9.9	17.0
EE5	-30.0	18.1	14.3	16.2
EEB	5.0	47.2	34.3	63.0
EE4	35.0	57.2	40.7	53.5
EE7	66.5	58.2	53.7	49.0
EDP	114.5	84.8	74.0	78.0
EE2	165.0	93.4	91.1	87.3
EE1	215.0	101.1	100.0	93.0
EE6	260.0	97.1	100.0	90.0

Table 6-3 Charpy V-Notch Impact Test Results for Irradiated HAZ Metal Specimens from the Nine Mile Point Unit 1 210-Degree Surveillance Capsule

Specimen Identification	Test Temperature (°F)	Impact Energy (ft-lb)	Fracture Appearance (% Shear Area)	Lateral Expansion (mils)
J21	-50.0	13.4	12.9	11.0
J27	-25.0	17.8	19.8	17.0
J2B	0.0	24.5	34.7	23.5
J2A	35.5	21.5	36.2	23.8
J24	50.5	50.7	59.0	45.0
J26	65.1	52.8	52.8	43.0
J23	94.5	72.3	100.0	60.5
J25	122.0	79.5	100.0	71.0
J22	160.0	81.0	100.0	72.5

Table 6-4 Charpy V-Notch Impact Test Results for Irradiated APED Metal Specimens from the Nine Mile Point Unit 1 210-Degree Surveillance Capsule

Specimen Identification	Test Temperature (°F)	Impact Energy (ft-lb)	Fracture Appearance (% Shear Area)	Lateral Expansion (mils)
APED-001	-27.0	10.4	11.8	12.0
APED-002	0.0	15.1	12.5	14.3
APED-007	40.0	24.9	24.4	25.5
APED-008	65.5	33.7	30.2	29.5
APED-006	84.2	50.2	44.8	48.5
APED-005	100.2	52.5	45.8	45.5
APED-009	122.9	100.2	100.0	84.0
APED-004	150.0	84.5	100.0	64.0
APED-003	200.0	101.9	100.0	70.0

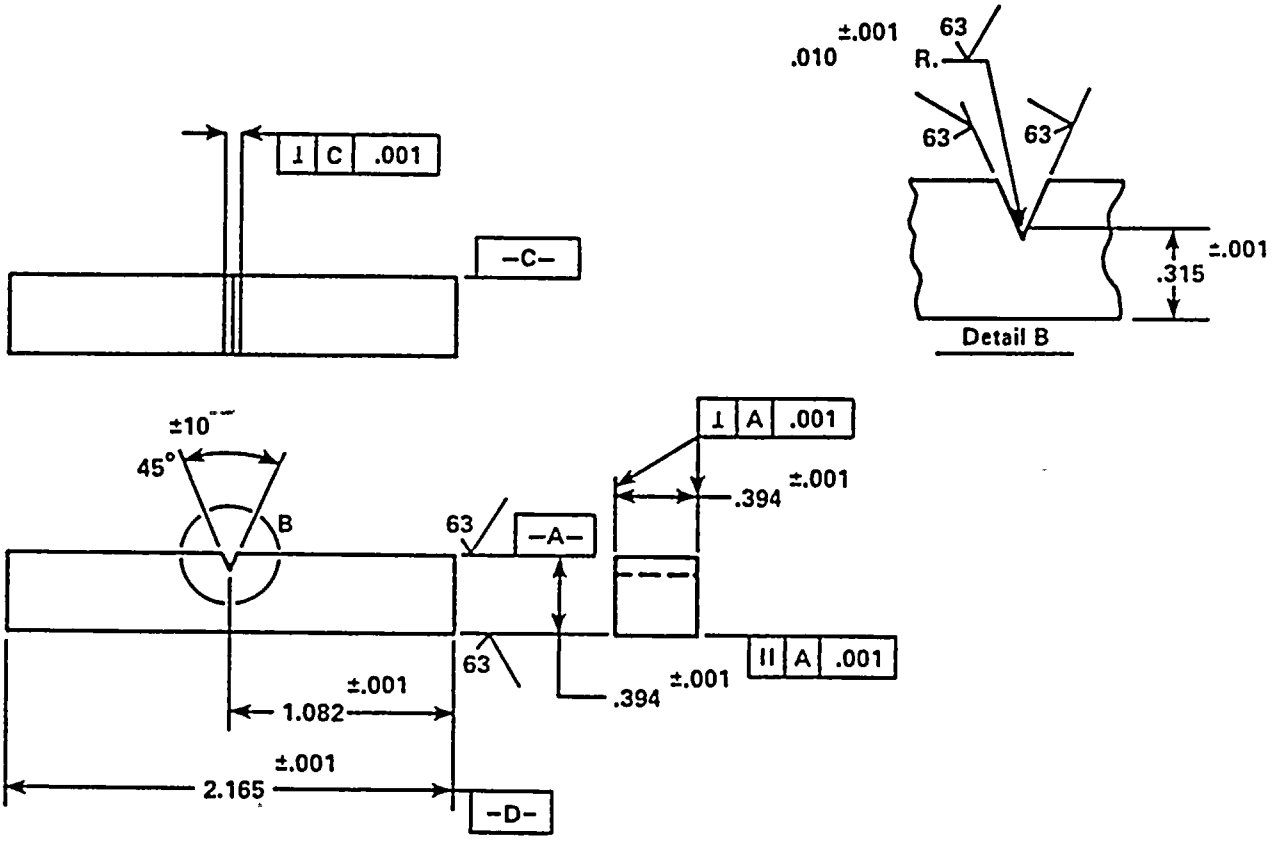

Figure 6-1 Drawing Showing Charpy Test Specimen Geometry

Impact V2.0

Summary Report

Sample ID

E21

Material Description

Base Metal

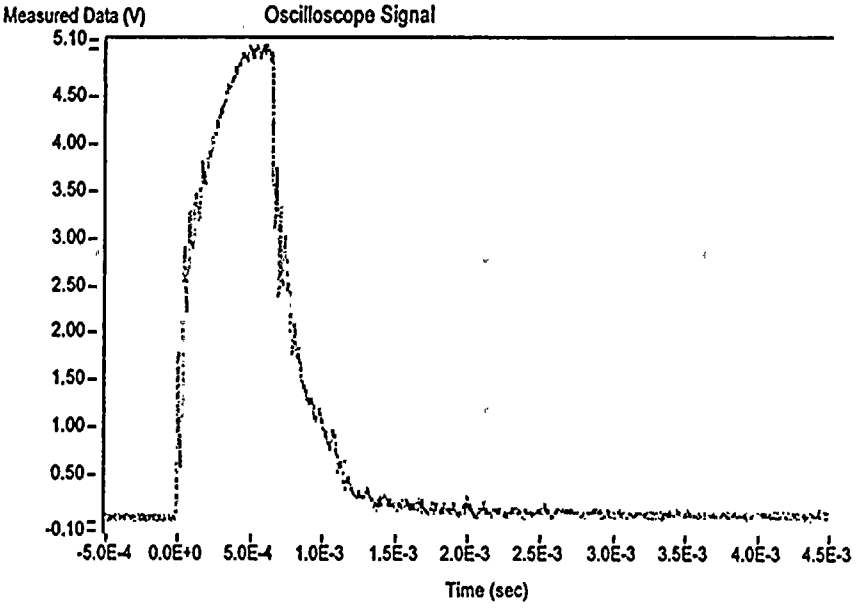

Test Parameter	Value
Operator	Dr. Michael P. Manahan, Sr.
Date Tested	2/3/98 10:58 AM
Temperature	73.90 °C
Striker Name	8 mm RadTest
Interpolation Method	Point-Point Linear
Sample Type	Metal
Sample Size	Type A
Orientation	L-T
Notch Type	V Notch, no Side-Groove
Length	2.1654 in
Width	0.3937 in
Thickness	0.3937 in
Span	1.5748 in
Uncracked Ligament	0.3150 in
Notch Radius	0.0098 in
Velocity Determination	Potential Energy & Losses
Velocity	17.94 ft/s
Shear	59.10 %
Lateral Expansion	0.0545 in

Result	Value
Optical Encoder Energy	5.672E+1 ft lbf
Dial Gage Energy	5.75E+1 ft lbf
Instrumented Striker Energy	5.706E+1 ft lbf

Figure 6-2 Typical Instrumented Striker Raw Data Signal

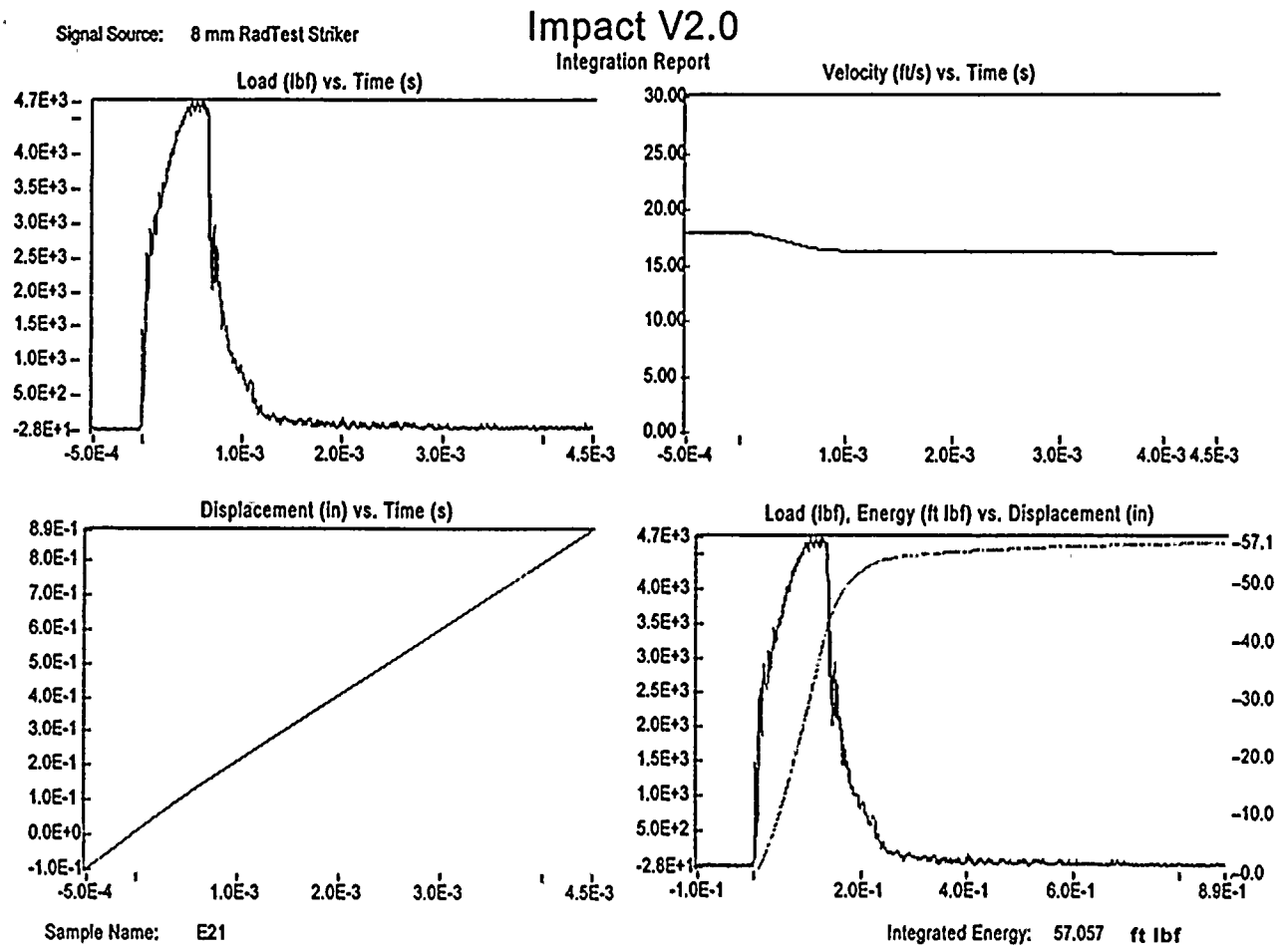

Figure 6-3 Example Plots Showing Integrations Performed to Obtain Load-Deflection Curve

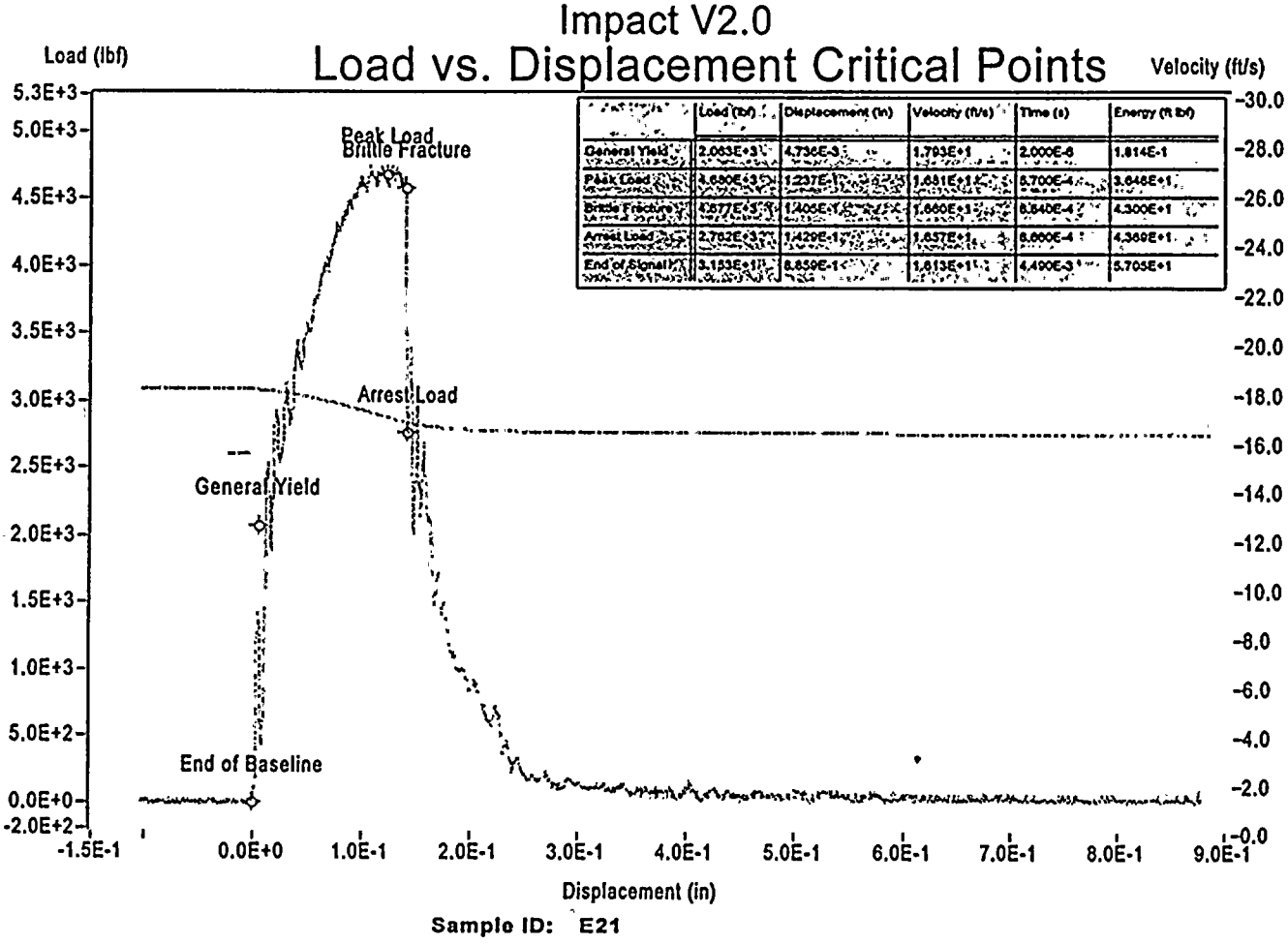

Figure 6-4 Typical Load-Deflection Curve Showing Critical Load Points

7.0 Charpy Curve Fitting

Charpy curve fitting for pressure vessel surveillance applications is a challenging task because for most capsules there are relatively few data points. In the current capsule analysis, there are only nine data points available to characterize the entire transition region and upper shelf. MPM has addressed this challenge by developing an advanced Charpy curve fitting software package (Reference [7-1]). The Charpy Fit 1.0 software has been QA validated and verified. The curve fitting results are given in terms of plots of Charpy energy, lateral expansion, and fracture appearance (percent shear) as functions of temperature. These plots show the data points as well as the best fit trends. Data from prior testing has also been fit and plotted for comparison.

Four definitions of transition temperature are applied to the fitted data and the results are summarized in tabular form. The four transition temperature definitions, referred to as the Charpy indices, are:

- 30 ft-lb Charpy energy
- 50 ft-lb Charpy energy
- 35 mil lateral expansion
- fracture appearance (50% shear)

Upper shelf Charpy energy and upper shelf lateral expansion are also tabulated.

7.1 Fitting Procedure

The Charpy Fit software allows data to be fit as a function of temperature using either of two functions. One function is the hyperbolic tangent function. The other is a second order polynomial. For each function, the user has the option of fitting a median trend for the data or fitting both a median trend and a statistical distribution trend. The statistical distribution is a three parameter Weibull type distribution for both functions. If a Weibull statistical fit is specified, then the variance from the Weibull fit is used as a weight function in the least squares fitting of the median trend. If a "median only" fit is specified the least squares weighting of the data points assumes that the variance is proportional to the magnitude of the median at that temperature. This default weighting for a "median only" fit can be circumvented by doing a "median and Weibull" fit but then fully (or partially) specifying the Weibull distribution parameters. The accuracy of the fitting algorithm was verified for each of the two fitting functions. Also, each fitting function was verified in both the "median only" and the "median and Weibull" modes.

The fitting done in the current calculation used only the hyperbolic tangent function. The "median and Weibull" mode was used in all cases with two out of the three Weibull parameters (b_1, b_2, and b_3) preselected and one Weibull parameter determined by fitting the highly populated G-8-3 unirradiated data set. The first preselected Weibull parameter, denoted b_1, sets the lower bound of the fitted parameter and this was assigned a value of 0 in all cases. The parameter b_1 has the physical

meaning of the asymptotic absolute lower bound of variable being fit in the lower shelf regime. The other preselected parameter, denoted b_3, is the temperature dependent Weibull distribution shape parameter. The parameter b_2, which was determined by the fit algorithm, has the physical meaning of the asymptotic absolute lower bound of the variable being fit in the upper shelf regime.

A study was undertaken to determine if the b_3 that results from the current fitting algorithm can be expected to converge to the actual b_3. In this study, random data sets were generated based on selected sets of median and Weibull parameters. The random data sets were then fit to see if the parameters resulting from the fits were equal to the parameters used to generate the random data. Ideally, as the number of generated data points increases toward infinity, the parameters from the fit should approach the parameters used to generate the data. The approach was to generate ten different random data sets with each set having 1000 data points. Each set was fit using the Charpy Fit software and then the mean and standard deviation of the resulting fit b_3 values were computed. This process was repeated for four values of b_3. The chosen values of b_3 were 2.0, 3.25, 3.7, and 5. This range was expected to bound the range of values to be found in real Charpy data. Recall that the Weibull distribution becomes nearly symmetric in the range of 3.25 to 3.75. A bias was found to exist in the fit b_3 values. When the b_3 used to generate the data was less than about 3.3, the fit b_3 was found to be larger than the actual b_3. When the actual b_3 was larger than about 3.3, the fit b_3 was smaller than the actual value. It was concluded that the Charpy Fit software algorithm tends to find best fit values of b_3 that result in a more normal (i.e., symmetrical) variation than was used to generate the data. The b_3 bias is essentially zero at a b_3 of about 3.3. The bias increases as the actual value of b_3 becomes increasing different from 3.3. The amount of bias that was found is not considered to be excessive, but is significant.

Reliably obtaining b_3 by fitting requires many data points (on the order of 50 to 100). The data points must also be well distributed over the entire brittle to ductile transition region. In the current calculation, there are not enough data points per data set , typically 9, to reliably fit b_3. Therefore b_3 was set to a selected value based on a fit to Charpy energy data of a similar material (unirradiated plate G-8-3 and G-8-4 which were determined to be two pieces from the same plate [7-2]) for which a large number of data points (97) were available. Figure 7-1 shows the results of fitting the 97 unirradiated data points. The top plot shows all of the 97 data points and the resulting fit when all of the data points were used in the fitting. The value of b_3 from the fitting procedure was in this case 2.5. It is concluded that after correcting for bias, the actual best fit b_3 would be about 2.2. For the 1000 point data sets used to generate the bias correction, the uncertainty in the 0.3 correction is about $\pm$ 0.1. The uncertainty for a 97 point set would be larger and could perhaps be as great or even greater than the 0.3 bias correction. The bottom plot of Figure 7-1 shows the result when only the data points between -80 F and +60 F were fit. Comparing with the top plot, it can be seen that the median trend is closer to the 1% probability trend in the bottom plot. This is consistent with the fact that the transition region data of the lower plot produced a smaller b_3. When most of the upper shelf data was eliminated from the fit, the b_3 that resulted from the fitting was 1.8. After correcting for bias, the best estimate of b_3 became 1.5. Based on the two results of Figure 7-1, an intermediate value of b_3 equal to 1.8 was selected for use in all fitting of the Capsule B data.

7.2 Surveillance Capsule Fitting Results

Since the reason for testing irradiated material is to determine the extent to which the irradiation has embrittled the material, it is necessary to compare the irradiated material test results to the test results of the same material in the unirradiated condition. Since previous tests and the resulting curve fitting efforts predated the current Charpy Fit software, it was judged appropriate that the previous data be subjected to the same fitting procedures as the Capsule B data. Therefore all previous data was reviewed and fit as a part of the current Capsule B analysis. Where possible, plots for various fluence levels of a given material were combined so that the effect of irradiation could be seen graphically.

7.2.1 Charpy Energy Data Fitting

The procedures for fitting the energy data were as follows. The Weibull b_3 parameter was set to 1.8 based on the analyses described previously. The Weibull b_1 parameter was set to zero. The b_2 parameter was left to be determined by the fit. The Weibull parameters define the statistical variation in the data as a function of temperature. The Weibull parameters affected the best fit median behavior only in terms of the weight factors that were applied to the data points in the least squares fitting algorithm. The weighting procedure used the Weibull variation to give more weight to data points at temperatures that produce less data variation (generally lower temperatures) and less weight to data points at temperatures that produce greater variation (generally higher temperatures).

Since the lower shelf temperature regime had few if any data points, the asymptotic lower shelf median trend energy parameter a_1 was set to 6 ft-lb for all fitting of energy data. The asymptotic upper shelf median trend energy parameter a_2 was calculated for each data set prior to fitting and then input to the fitting procedure. This upper shelf energy (USE) value was calculated by averaging the energies of all data points considered to be representative of upper shelf behavior. The approach to defining a data point as representing upper shelf behavior primarily considered fracture appearance. However, in some instances, consideration was also given to energy level. If a data point had a fracture appearance that was considered to be 100% shear then it was always used in calculating the a_2 parameter. If the energy for a data point was in the range of the energies for the 100% shear data points it was also used in computing an average USE even if its fracture appearance was somewhat less than 100% shear.

7.2.1.1 Charpy Energy Data and Curve Fitting for G-8-1 Base Metal

The above fitting procedures were applied to the irradiated G-8-1 base metal from Capsule B as well as the previous G-8-1 base metal data compiled in [7-2]. This previous data included unirradiated metal as well as metal at two lower irradiation levels. The data points and the resulting best fit trends are shown in Figure 7-2. The results of the data fitting are also summarized in Table 7-1.

Figure 7-2 shows a shift of the transition region to higher temperatures due to irradiation as expected. Although the Capsule B shift is a little smaller than that calculated for the 300 degree capsule, this indicated shift is within the scatter of the data and the conclusion to be drawn is that little additional shift has occurred during the most recent increment in exposure. Also, the data appear to show that the USE has not been significantly affected by irradiation.

The 30 and 50 ft-lb transition temperatures and the USE are summarized in Table 7-1. The numbers in parentheses are the values from previous curve fitting [7-2]. It can be seen that there is some effect of the curve fitting procedure but that the size of the effect is well within data scatter for Charpy testing.

7.2.1.2 Charpy Energy Data and Curve Fitting for Weld Metal

The above fitting procedures were applied to the irradiated weld metal from Capsule B as well as the previous weld metal data compiled in [7-2]. This previous data included three unirradiated data points at 10 F plus 12 data points for an intermediate irradiation level. The data points and the resulting best fit trends are shown in Figure 7-3. The unirradiated data points were not sufficient for doing a curve fit since only three points at one temperature were available. The results of the data fitting are summarized in Table 7-2.

Figure 7-3 shows that the unirradiated data points are consistent with the best fit trend of the lower irradiation level data. This suggests that the initial exposure had little effect on the transition behavior. The Capsule B data curve fit (higher fluence data) seems to show a small to moderate shift of the transition region due to the additional exposure. While this shift appears to be well supported by the data, a statistical analysis is required to determine the significance of this apparent shift. It is worth noting that the transition shift behavior of the weld data, wherein the most recent increment in fluence appears to have the greater effect, is opposite to that noted above for the base metal.

The 30 and 50 ft-lb transition temperatures and the USE are summarized in Table 7-2. Although a statistical analysis has not been done, the relatively few data points on the upper shelf and the large statistical variation of upper shelf data may make the apparent decrease in USE statistically insignificant.

7.2.1.3 Charpy Energy Data and Curve Fitting for HAZ Metal

The above fitting procedures were applied to the irradiated HAZ metal from Capsule B as well as the previous HAZ metal data compiled in [7-2]. These previous data were for a single lower irradiation level. No unirradiated data is available. The data points and the resulting best fit trends are shown in Figure 7-4. The results of the data fitting are summarized in Table 7-3.

Figure 7-4 shows the data and best fit trends for the two fluence levels The Capsule B data curve fit (higher fluence data) seems to show a small to moderate shift of the transition region due to the additional exposure. The statistical significance of this shift appears to be less than that noted

above for the weld data due to the apparently larger variance in the data demonstrated by the low energy data points at about 40 F. This transition shift behavior of the HAZ data, wherein the most recent increment in fluence appears to have an effect, is again different from that noted above for the base metal.

The 30 and 50 ft-lb transition temperatures and the USE are summarized in Table 7-3. Although a statistical analysis has not been done, the relatively few data points on the upper shelf and the large statistical variation of upper shelf data may again make the apparent decrease in USE statistically insignificant.

7.2.1.4 Charpy Energy Data and Curve Fitting for APED Metal

The above fitting procedures were applied to the irradiated APED metal from Capsule B. The material type and unirradiated database has not yet been found, therefore, no unirradiated data fits could be performed. The data points and the resulting best fit trend are shown in Figure 7-5. The results of the data fitting are summarized in Table 7-4.

7.2.1.5 Charpy Energy Data and Curve Fitting for G-8-3/G-8-4 Base Metal

The above fitting procedures were applied to the unirradiated and irradiated G-8-3/G-8-4 base metal data compiled in [7-2]. None of this material was tested in the current work. The data was fit in this study for the sake of completeness and consistency. The data points and the resulting best fit trends are shown in Figure 7-6. The results of the data fitting are also summarized in Table 7-5.

Figure 7-6 shows a small shift of the transition region to higher temperatures. A statistical analysis is needed to determine if the relatively few irradiated data points (6) are sufficient to make this apparent shift statistically significant.

The 30 and 50 ft-lb transition temperatures and the USE are summarized in Table 7-5. The numbers in parentheses are the values from previous curve fitting [7-2]. It can be seen that there is again some effect of the curve fitting procedure but that the size of the effect is reasonable when compared to the variance in the data.

7.2.2 Lateral Expansion Data Fitting

The procedures for fitting the lateral expansion data were as follows. The Weibull b_3 parameter was set to 1.8. By using this value, it was inherently assumed that the statistical behavior of lateral expansion data is the same as for the Charpy energy data. This was deemed the most reasonable assumption since a large data set of lateral expansion data, similar to that used to establish b_3 for the Charpy energy data, was not available. The Weibull b_1 parameter was set to zero. The b_2 parameter was left to be determined by the fitting algorithm.

7.2.2.1 Lateral Expansion Data and Curve Fitting for G-8-1 Base Metal

The above lateral expansion fitting procedures were applied to the irradiated G-8-1 base metal from Capsule B as well as the previous G-8-1 base metal data compiled in [7-2]. The data points and the resulting best fit trends are shown in Figure 7-7. The results of the data fitting are also summarized in Table 7-6.

Figure 7-7 shows a transition region behavior that is very similar to that for the irradiated energy data of Figure 7-2. The relatively small shift compared to the variation in the data makes the statistical significance of the apparent shift uncertain. The data appear to show that the upper shelf lateral expansion has not been significantly affected by irradiation as was the case for the absorbed energy.

7.2.2.2 Lateral Expansion Data and Curve Fitting for Weld Metal

The above lateral expansion fitting procedures were applied to the irradiated weld metal from Capsule B as well as the previous weld metal data compiled in [7-2]. This previous data consisted of irradiated metal for one lower irradiation level. The data points and the resulting best fit trends are shown in Figure 7-8. The results of the data fitting are also summarized in Table 7-7.

Figure 7-8 shows a small shift in the transition region behavior with the increase in fluence. This shift and the increase in the upper shelf lateral expansion are relatively small compared to the variation in the data and therefore it seems possible that a statistical analysis would conclude that the apparent fluence effect of Figure 7-8 is not statistically significant. The temperature shift based on the energy data of Figure 7-3 is similar but slightly greater than that of the lateral expansion data. The effect of fluence on the upper shelf energy behavior is, however, reversed from that of the lateral expansion behavior.

7.2.2.3 Lateral Expansion Data and Curve Fitting for HAZ Metal

The above lateral expansion fitting procedures were applied to the irradiated HAZ metal from Capsule B as well as the previous weld metal data compiled in [7-2]. This previous data consisted of irradiated metal for one lower irradiation level. The data points and the resulting best fit trends are shown in Figure 7-9. The results of the data fitting are also summarized in Table 7-8.

Figure 7-9 shows a small shift in the mid to upper transition region with the increase in fluence. This shift and the decrease in the upper shelf lateral expansion are relatively small compared to the variation in the data and therefore it seems possible that a statistical analysis would conclude that the apparent fluence effect of Figure 7-9 is not statistically significant. The temperature shift based on the energy data of Figure 7-4 is similar but slightly greater than that of the lateral expansion data of Figure 7-9. The effect of fluence on the upper shelf lateral expansion behavior is the opposite of that seen in Figure 7-8 for the weld material but the same as seen in Figure 7-4 for the energy data.

7.2.2.4 Lateral Expansion Data and Curve Fitting for APED Metal

The above lateral expansion fitting procedures were applied to the irradiated APED metal from Capsule B. As mentioned before, no previous unirradiated or irradiated data was available for this material. The data points and the resulting best fit trend are shown in Figure 7-10. The 35 mil lateral expansion transition temperature and upper shelf values are summarized in Table 7-9.

7.2.2.5 Lateral Expansion Data and Curve Fitting for G-8-3/G-8-4 Base Metal

The above lateral expansion fitting procedures were applied to the unirradiated and irradiated G-8-3/G-8-4 base metal data compiled in [7-2]. None of this material was tested in the current work. The data was fit in this study for the sake of completeness and consistency. The data points and the resulting best fit trends are shown in Figure 7-11. The results of the data fitting are also summarized in Table 7-10.

Figure 7-11 shows a small to moderate shift of the transition region to higher temperatures with an increase in fluence. A statistical analysis is needed to determine if the relatively few irradiated data points (6) are sufficient to make this apparent shift statistically significant.

7.2.3 Fracture Appearance Data Fitting

The procedures for fitting the fracture appearance (percent shear) data were as follows. The Weibull b_3 parameter was set to 1.8. By using this value, it was inherently assumed that the statistical behavior of fracture appearance data is the same as Charpy energy data. This was deemed the most reasonable assumption since a large data set of fracture appearance data, similar to that used to establish b_3 for the Charpy energy data, was not available. The Weibull b_1 parameter was set to zero. The b_2 parameter was left to be determined by the fit.

7.2.3.1 Fracture Appearance Data and Curve Fitting for G-8-1 Base Metal

The above fracture appearance fitting procedures were applied to the irradiated G-8-1 base metal from Capsule B as well as the previous G-8-1 base metal data compiled in [7-2]. This previous data included irradiated metal for two lower irradiation levels than that of the Capsule B material. The data points and the resulting best fit trends are shown in Figure 7-12. The results of the data fitting are also summarized in Table 7-11.

Figure 7-12 shows a shift in transition region behavior between the two lower fluence levels. The magnitude of the temperature shift, compared to the variation within the data sets, makes it seem likely that the shift is statistically significant. Similar, but somewhat smaller shifts were found for the energy and lateral expansion data. The shift between the trends of the two higher fluence data sets is smaller than for the shift between the two lower fluence data sets. This is again consistent with the lateral expansion and energy data behavior.

7.2.3.2 Fracture Appearance Data and Curve Fitting for Weld Metal

The above fracture appearance fitting procedures were applied to the irradiated weld metal from Capsule B as well as the previous weld metal data compiled in [7-2]. This previous data included irradiated metal for one lower irradiation level. The data points and the resulting best fit trends are shown in Figure 7-13. The results of the data fitting are also summarized in Table 7-12.

Figure 7-13 shows a shift in transition region behavior between the two fluence levels. The magnitude of the temperature shift, compared to the variation within the data sets, makes it seem likely that the shift is statistically significant. Similar, but somewhat smaller shifts were found for the energy and lateral expansion data. The variance in the lateral expansion and energy data appear larger than for the percent shear data. This larger variance made the apparent shifts of the lateral expansion and Charpy energy appear less statistically defensible than the shift in fracture appearance.

7.2.3.3 Fracture Appearance Data and Curve Fitting for HAZ Metal

The above fracture appearance fitting procedures were applied to the irradiated HAZ metal from Capsule B as well as the previous HAZ metal data compiled in [7-2]. This previous data included irradiated metal for one lower irradiation level. The data points and the resulting best fit trends are shown in Figure 7-14. The results of the data fitting are also summarized in Table 7-13.

Figure 7-14 shows a small shift in transition region behavior between the two fluence levels. The magnitude of the temperature shift, compared to the variation within the data sets, is fairly small thus making it seem likely that the shift may not be statistically significant. Similar and somewhat larger shifts were found for the lateral expansion data and energy data, respectively. However, these shifts were also relatively small compared to the variation in the lateral expansion data and energy data.

7.2.3.4 Fracture Appearance Data and Curve Fitting for APED Metal

The above fracture appearance fitting procedures were applied to the irradiated APED metal from Capsule B. No previous unirradiated or irradiated fracture appearance data were available for this material. The data points and the resulting best fit trend is shown in Figure 7-15. The 50% shear transition temperature is summarized in Table 7-14.

7.2.3.5 Fracture Appearance Data and Curve Fitting for G-8-3/G-8-4 Base Metal

The above fracture appearance fitting procedures were applied to the unirradiated and irradiated G-8-3/G-8-4 base metal fracture appearance data compiled in [7-2]. None of this material was tested in the current work. The previous data was fit in this study for the sake of completeness and consistency. The data points and the resulting best fit trends are shown in Figure 7-16. The results of the data fitting are also summarized in Table 7-15.

Figure 7-16 shows a small shift of the transition region to higher temperatures due to an increase in fluence. Based on the relatively large variation in the upper transition range unirradiated data and the relatively few irradiated data points (6), a statistical analysis is needed to determine if this apparent shift is statistically significant. Similar shifts were also found for the energy and lateral expansion data.

7.3 Chapter 7 References

[7-1] MPM Technologies, Inc., "Charpy Fit Version 1.0 Software", February, 1998

[7-2] Manahan, M.P., "Nine Mile Point Unit 1 Surveillance Capsule Program", NMEL-90001, dated January 4, 1991

Table 7-1 G-8-1 Base Metal L-T Charpy Impact Properties

Fluence (E>1.0 Mev) (n/cm^2)	30 ft-lb Transition Temperature (F)	50 ft-lb Transition Temperature (F)	Upper Shelf Energy (ft-lb)
0	10.4 (7.9)[1]	52.0 (49.9)	86.7[2] (86.7)
3.60×10^{17}	64.4 (63)	99.5 (100)	---[3] (---)
4.78×10^{17}	94.8 (87.2)	148.9 (132.8)	93.7[2] (94.6)
9.34×10^{17}	88.1	132.5	85.8[4]

[1]Numbers in () are from curve fitting of previous studies.
[2]Based on the average of three upper shelf data points.
[3]No upper shelf data points were generated (fitting assumed an upper shelf of 88.4 ft-lbs based on averaging all upper shelf data for all fluences).
[4]Based on the average of four upper shelf data points.

Table 7-2 Weld Metal Charpy Impact Properties

Fluence (E>1.0 Mev) (n/cm^2)	30 ft-lb Transition Temperature (F)	50 ft-lb Transition Temperature (F)	Upper Shelf Energy (ft-lb)
4.78×10^{17}	-39.1 (-43)[1]	1.8 (4)	109.6[2] (116)
9.34×10^{17}	-15.2	28.4	97.2[3]

[1]Numbers in () are from curve fitting of previous studies.
[2]Based on the average of four upper shelf data points.
[3]Based on the average of three upper shelf data points.

Table 7-3 HAZ Metal Charpy Impact Properties

Fluence (E>1.0 Mev) (n/cm^2)	30 ft-lb Transition Temperature (F)	50 ft-lb Transition Temperature (F)	Upper Shelf Energy (ft-lb)
4.78×10^{17}	-9.3 (-10)[1]	35.8 (37)	91.5[2] (96)
9.34×10^{17}	17.6	61.3	77.6[2]

[1]Numbers in () are from curve fitting of previous studies.
[2]Based on the average of three upper shelf data points.

Table 7-4 APED Metal Charpy Impact Properties

Fluence (E>1.0 Mev) (n/cm^2)	30 ft-lb Transition Temperature (F)	50 ft-lb Transition Temperature (F)	Upper Shelf Energy (ft-lb)
9.34×10^{17}	51.7	82.0	95.5[1]

[1]Based on the average of three upper shelf data points.

Table 7-5 G-8-3/G-8-4 Base Metal L-T Charpy Impact Properties

Fluence (E>1.0 Mev) (n/cm^2)	30 ft-lb Transition Temperature (F)	50 ft-lb Transition Temperature (F)	Upper Shelf Energy (ft-lb)
0	-22.5 (-26.5)[1]	6.9 (14.4)	100.8[2] (99.5)
4.78×10^{17}	-11.5 (-15.3)	21.1 (22.0)	---[3] (~100)

[1]Numbers in () are from curve fitting of previous studies.
[2]Based on the average of 18 upper shelf data points.
[3]Only one data point was generated on the upper shelf (114.3 ft-lbs) so fitting assumed an unchanged median upper shelf energy of 100.8 ft-lbs.

Table 7-6 G-8-1 Base Metal L-T Charpy Test Lateral Expansion Behavior

Fluence (E>1.0 Mev) (n/cm^2)	35 mil Lateral Expansion Transition Temperature (F)	Upper Shelf Lateral Expansion (mils)
3.60×10^{17}	79.1	---[1]
4.78×10^{17}	113.5	70.7[2]
9.34×10^{17}	103.4	79.1[3]

[1]No upper shelf data points were generated (fitting assumed an upper shelf of 74.9 mils based on averaging upper shelf data for all fluences).
[2]Based on the average of three upper shelf data points.
[3]Based on the average of four upper shelf data points.

Table 7-7 Weld Metal Charpy Test Lateral Expansion Behavior

Fluence (E>1.0 Mev) (n/cm²)	35 mil Lateral Expansion Transition Temperature (F)	Upper Shelf Lateral Expansion (mils)
4.78×10^{17}	-27.2	78.4[1]
9.34×10^{17}	-8.3	90.1[2]

[1]Based on the average of four upper shelf data points.
[2]Based on the average of three upper shelf data points.

Table 7-8 HAZ Metal Charpy Test Lateral Expansion Behavior

Fluence (E>1.0 Mev) (n/cm²)	35 mil Lateral Expansion Transition Temperature (F)	Upper Shelf Lateral Expansion (mils)
4.78×10^{17}	19.4	71.6[1]
9.34×10^{17}	34.3	68.0[1]

[1]Based on the average of three upper shelf data points.

Table 7-9 APED Metal Charpy Test Lateral Expansion Behavior

Fluence (E>1.0 Mev) (n/cm²)	35 mil Lateral Expansion Transition Temperature (F)	Upper Shelf Lateral Expansion (mils)
9.34×10^{17}	58.0	72.7[1]

[1]Based on the average of three upper shelf data points.

Table 7-10 G-8-3 Base Metal L-T Charpy Test Lateral Expansion Behavior

Fluence (E>1.0 Mev) (n/cm²)	35 mil Lateral Expansion Transition Temperature (F)	Upper Shelf Lateral Expansion (mils)
0	-17.0	79.7[1]
4.78×10^{17}	13.1	85.8[2]

[1]Based on the average of 6 data points.
[2]Based on a single upper shelf data point.

Table 7-11 G-8-1 Base Metal L-T Charpy Test Fracture Appearance

Fluence (E>1.0 Mev) (n/cm^2)	50% Shear Transition Temperature (F)
3.60×10^{17}	130.4
4.78×10^{17}	161.8
9.34×10^{17}	149.3

Table 7-12 Weld Metal Charpy Test Fracture Appearance

Fluence (E>1.0 Mev) (n/cm^2)	50% Shear Transition Temperature (F)
4.78×10^{17}	15.4
9.34×10^{17}	52.2

Table 7-13 HAZ Metal Charpy Test Fracture Appearance

Fluence (E>1.0 Mev) (n/cm^2)	50% Shear Transition Temperature (F)
4.78×10^{17}	26.2
9.34×10^{17}	37.5

Table 7-14 APED Metal Charpy Test Fracture Appearance

Fluence (E>1.0 Mev) (n/cm^2)	50% Shear Transition Temperature (F)
9.34×10^{17}	86.8

Table 7-15 G-8-3 Base Metal L-T Charpy Test Fracture Appearance

Fluence (E>1.0 Mev) (n/cm^2)	50% Shear Transition Temperature (F)
0	25.4
4.78×10^{17}	42.6

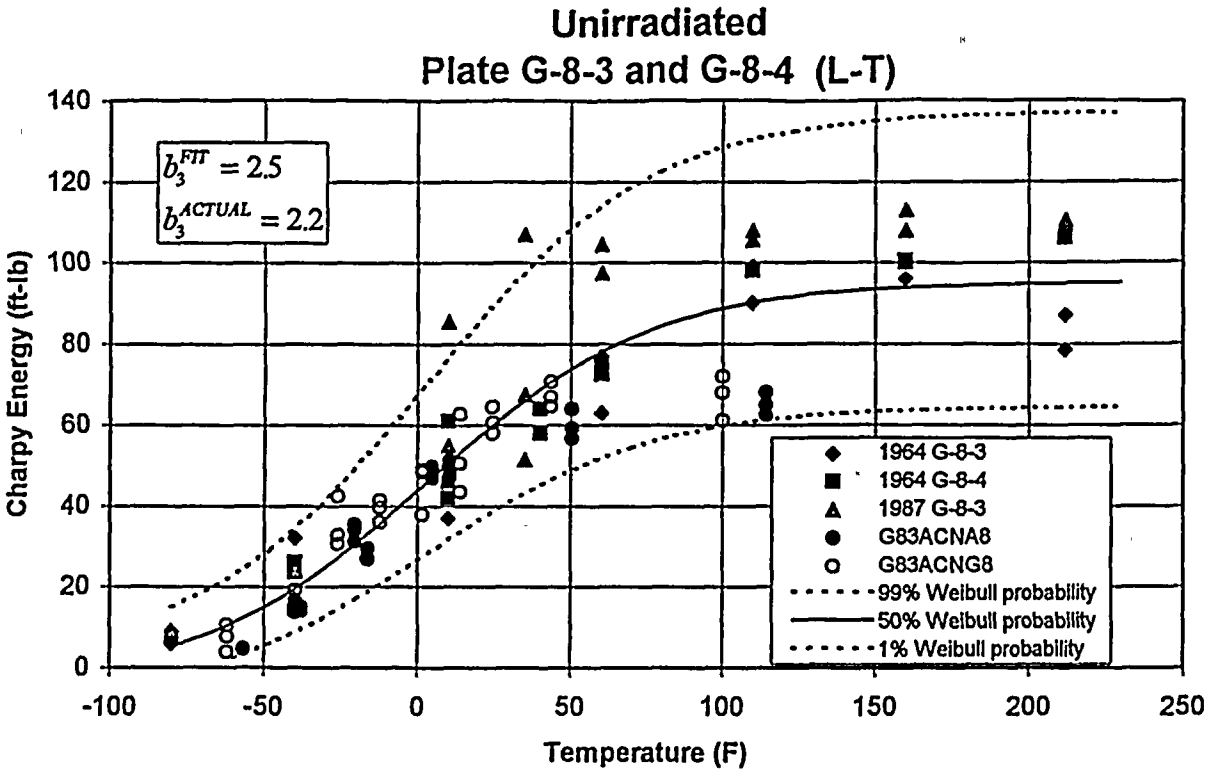

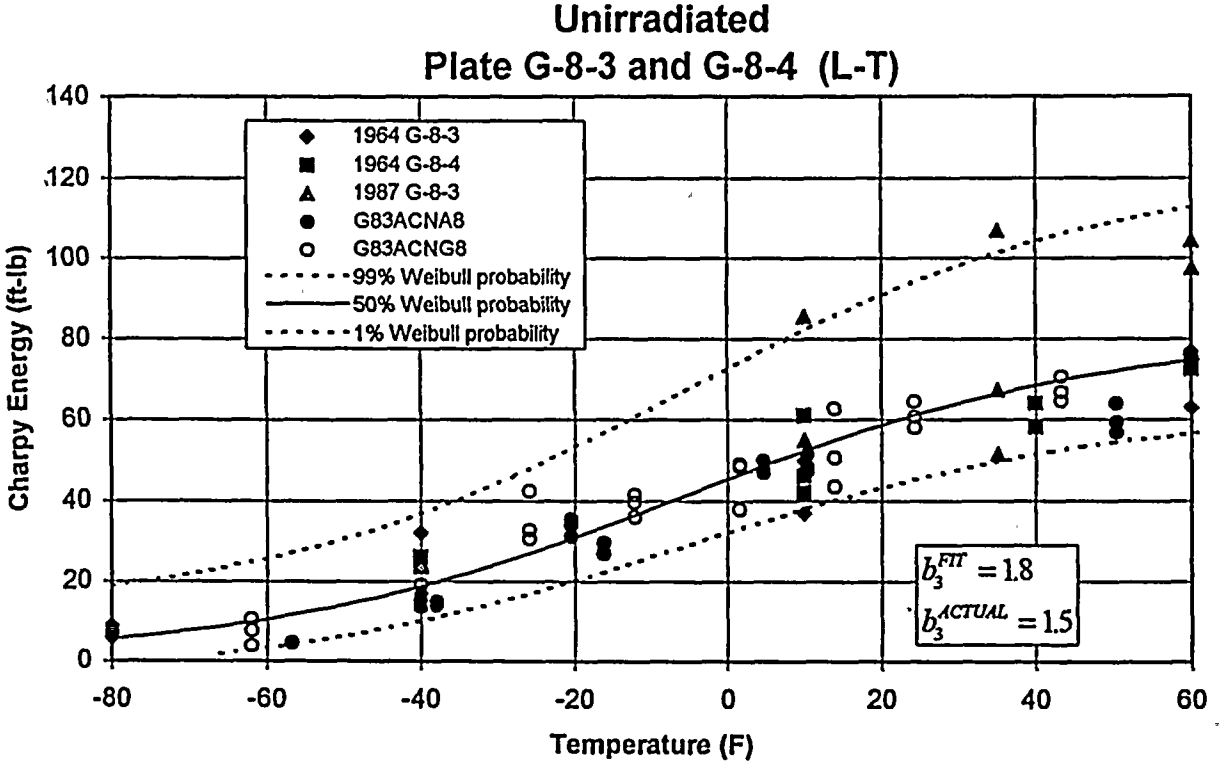

Figure 7-1 Determination of b_3 by Fitting of a Large Data Set for Unirradiated Material

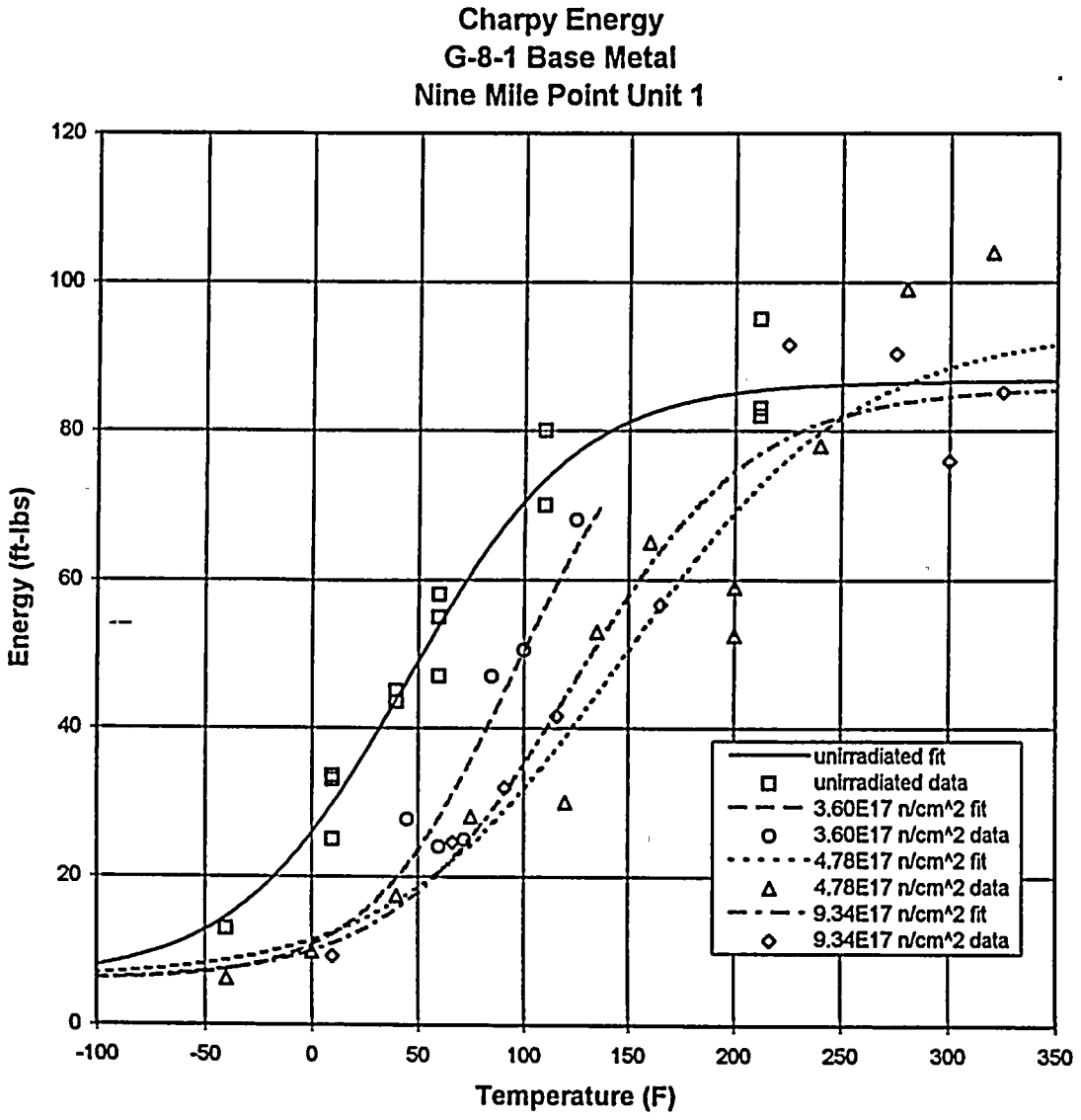

Figure 7-2 Charpy L-T Energy Data and Curve Fits for G-8-1 Base Metal

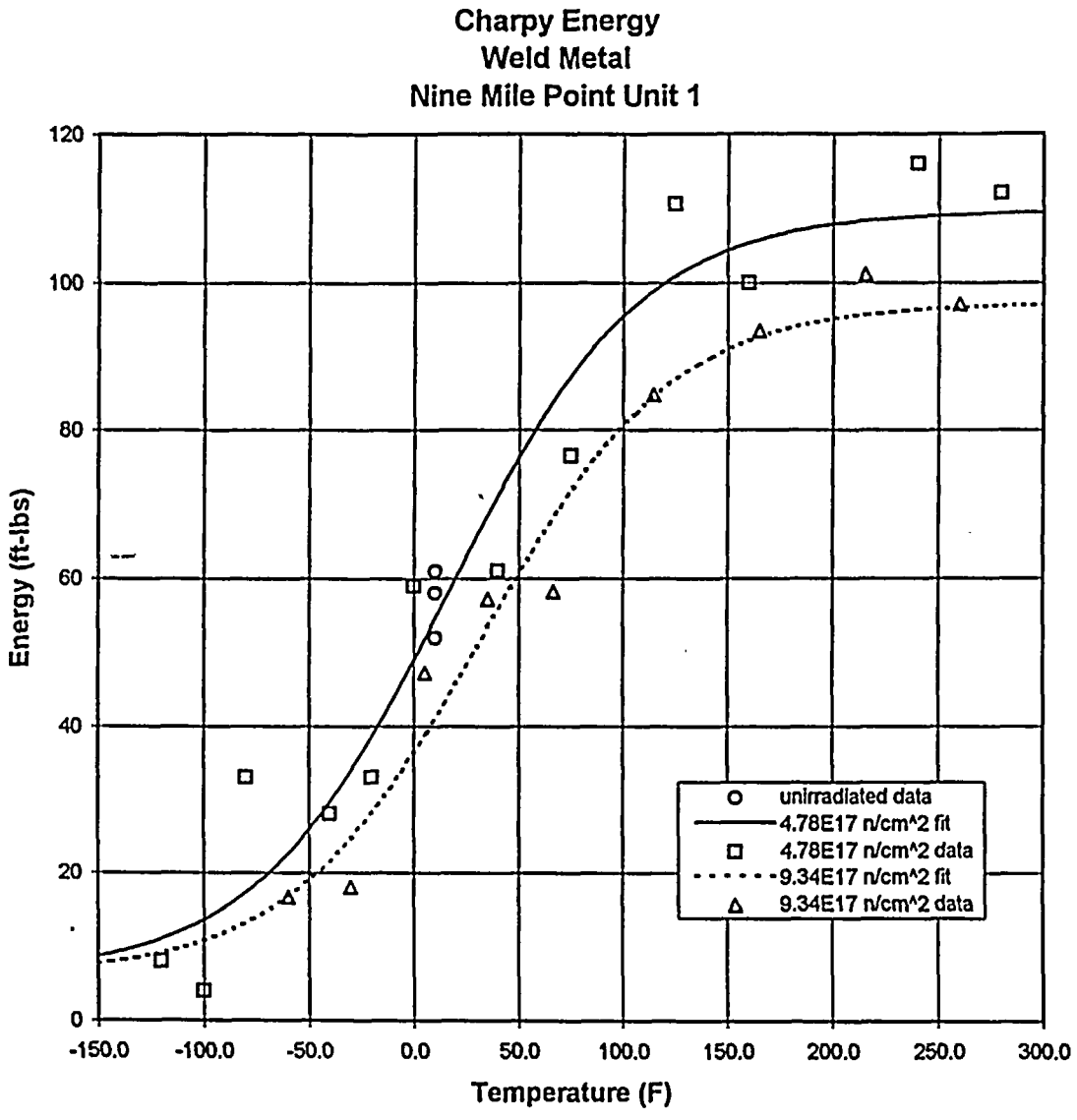

Figure 7-3 Charpy Energy Data and Curve Fits for Weld Metal

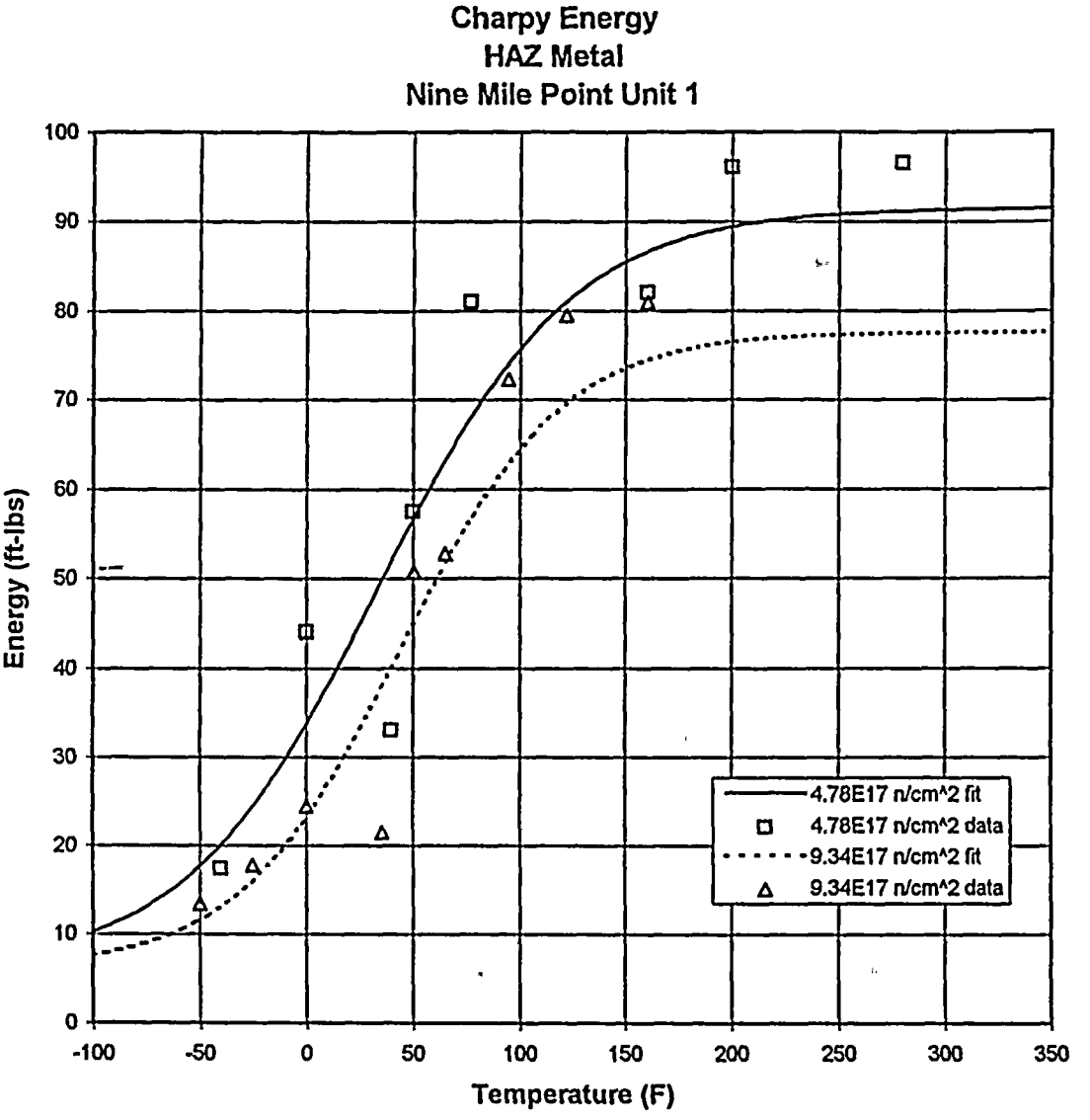

Figure 7-4 Charpy Energy Data and Curve Fits for HAZ Metal

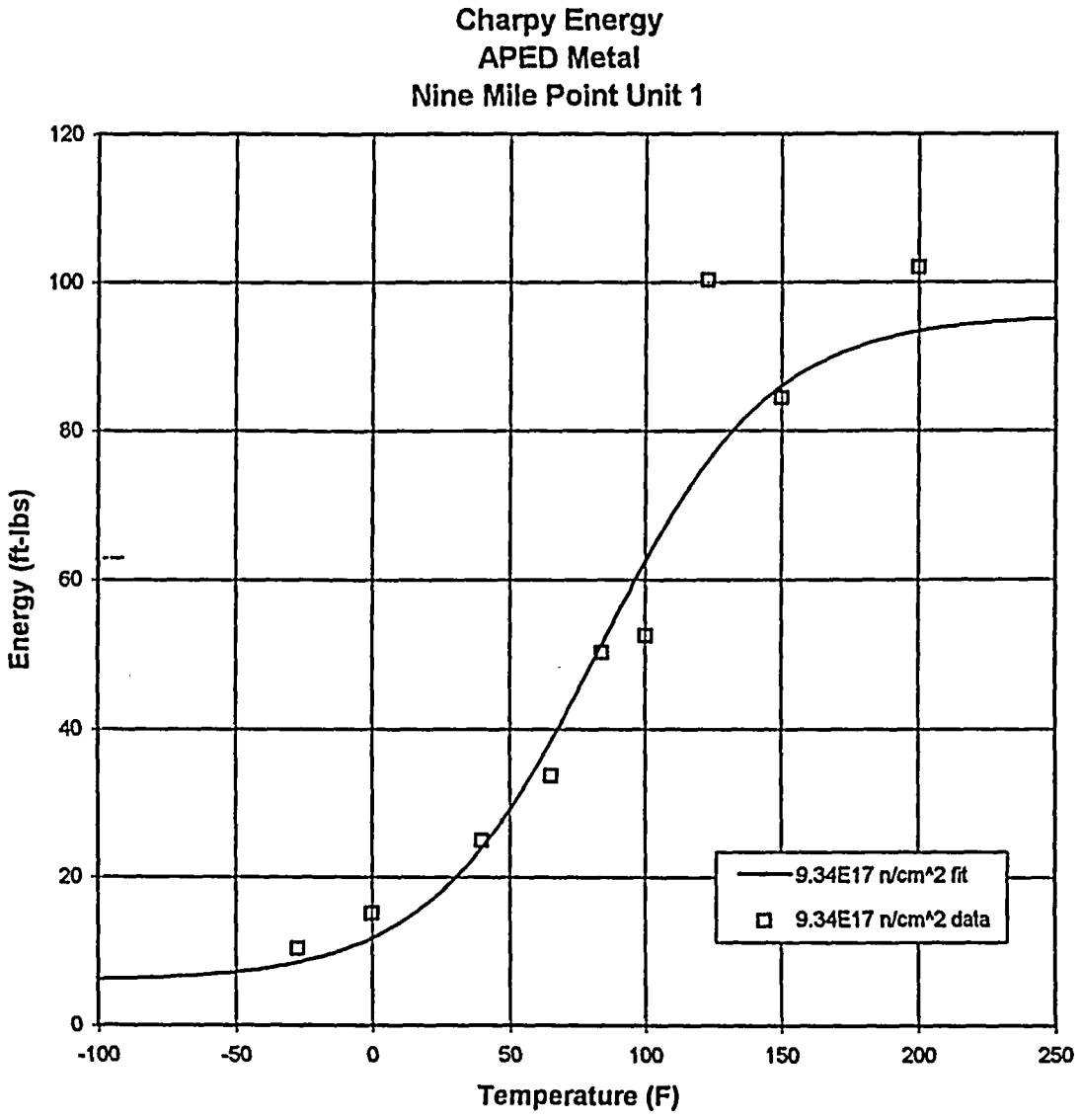

Figure 7-5 Charpy Energy Data and Curve Fits for APED Metal

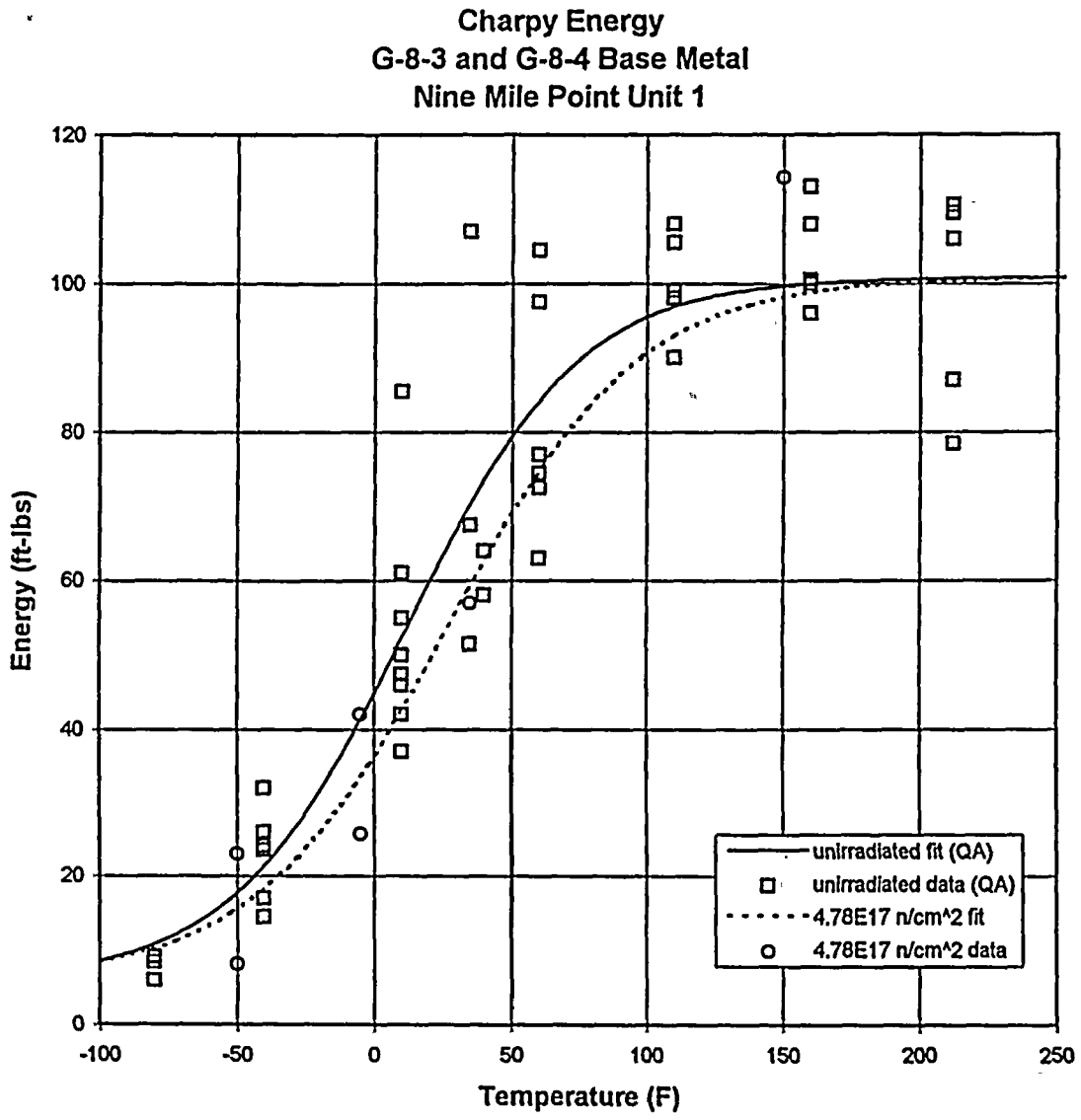

Figure 7-6 Charpy Energy Data and Curve Fits for G-8-3/G-8-4 Base Metal

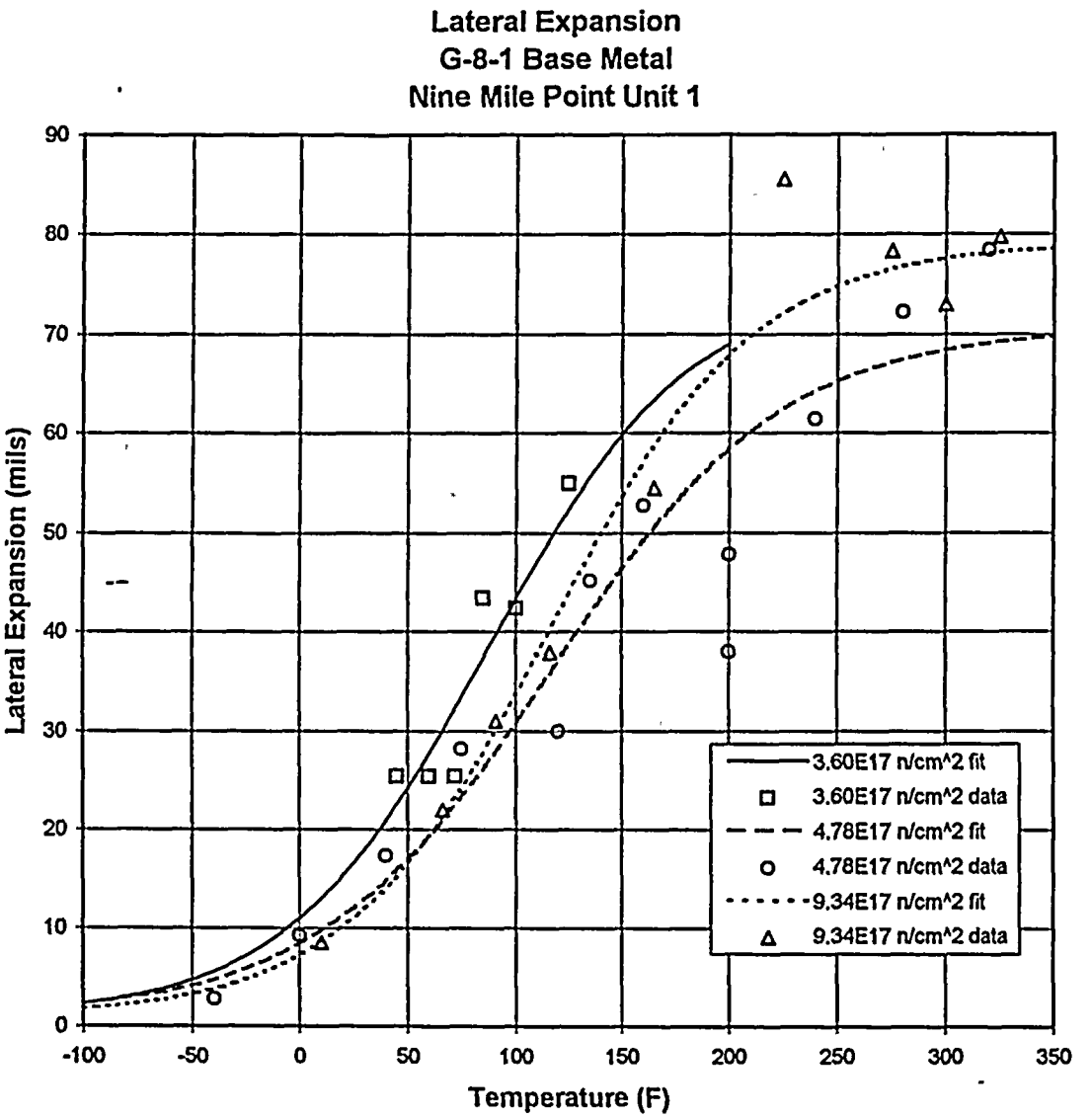

Figure 7-7 Lateral Expansion Data and Curve Fits for G-8-1 Base Metal

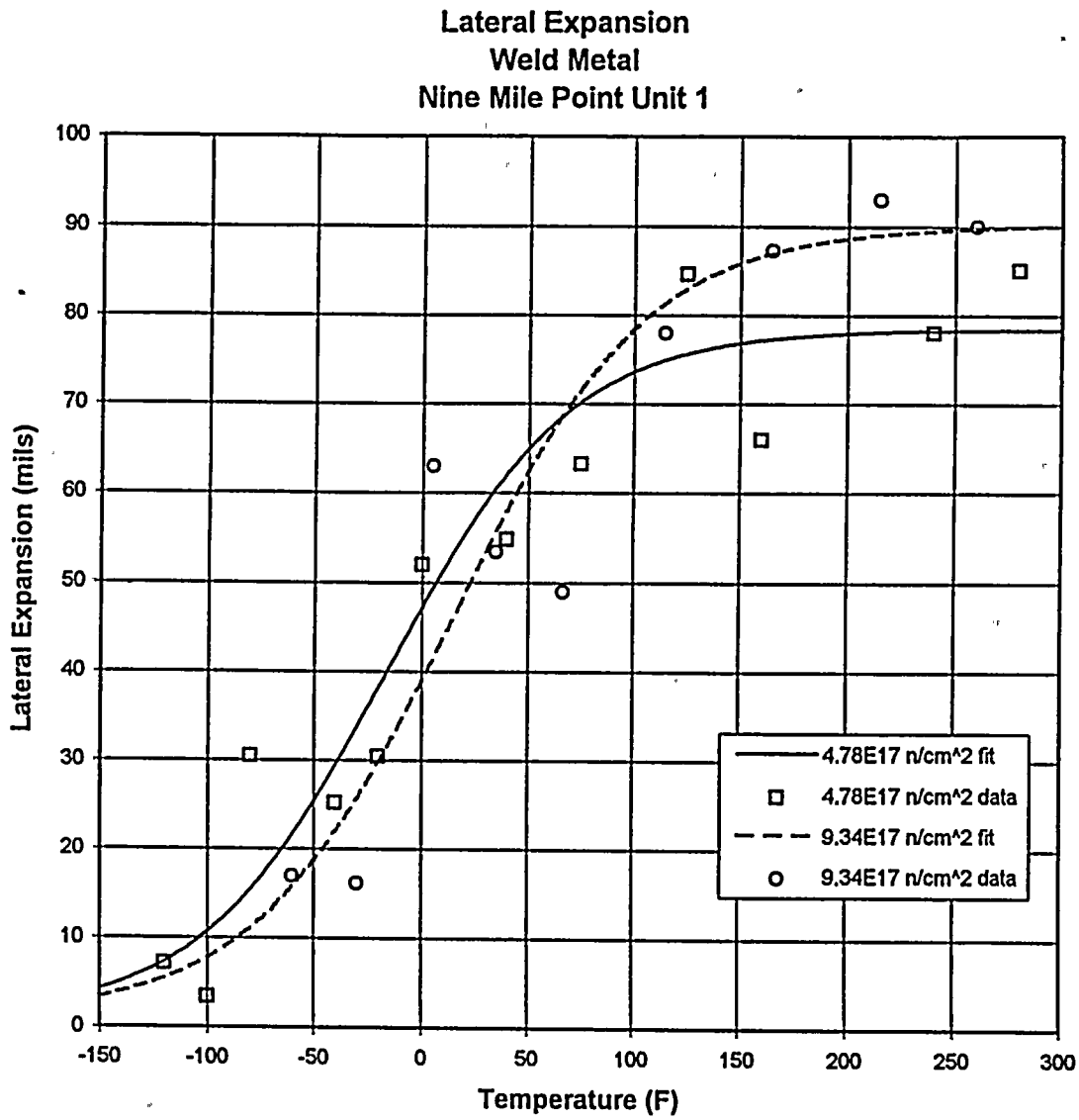

Figure 7-8 Lateral Expansion Data and Curve Fits for Weld Metal

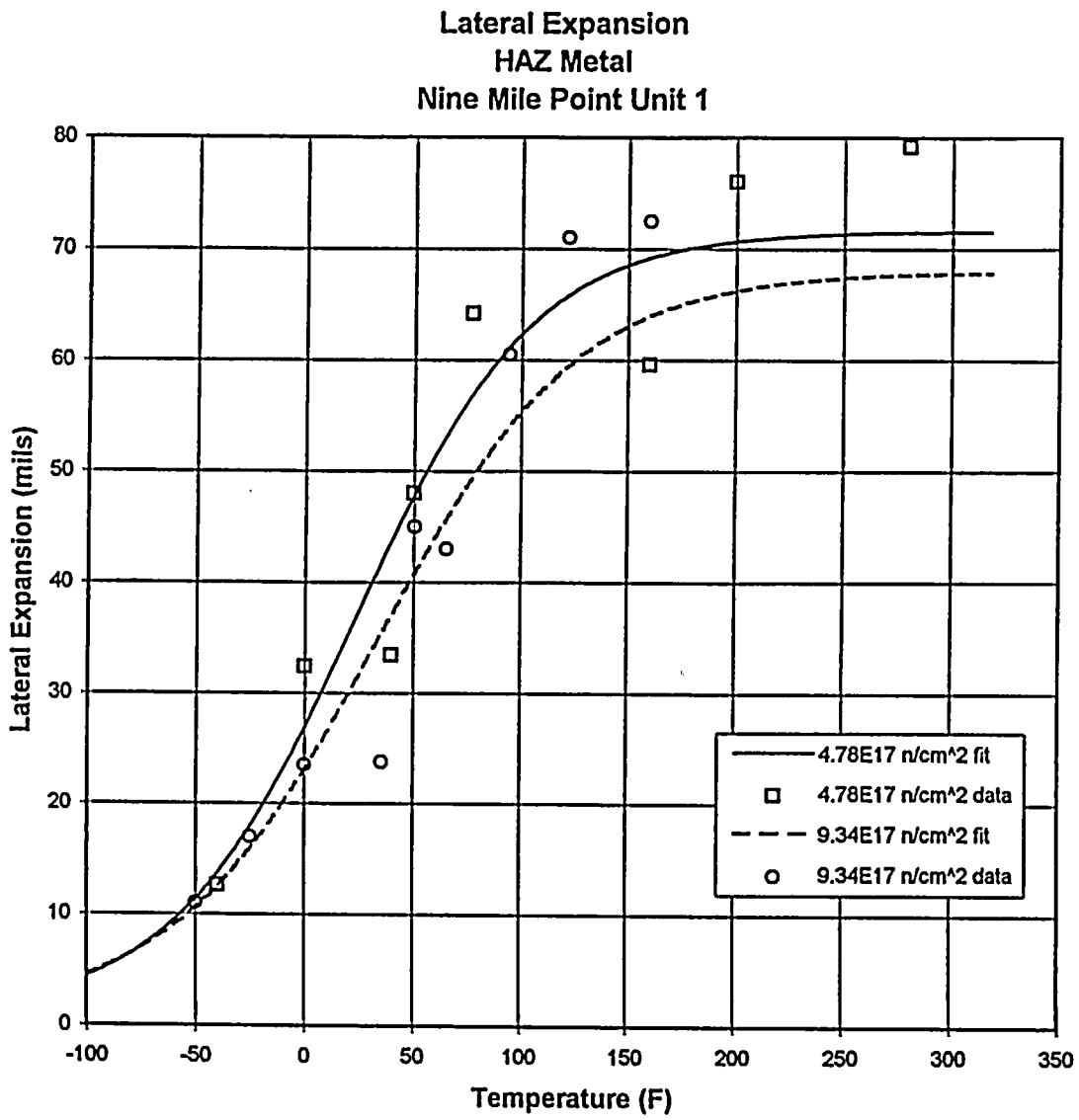

Figure 7-9 Lateral Expansion Data and Curve Fits for HAZ Metal

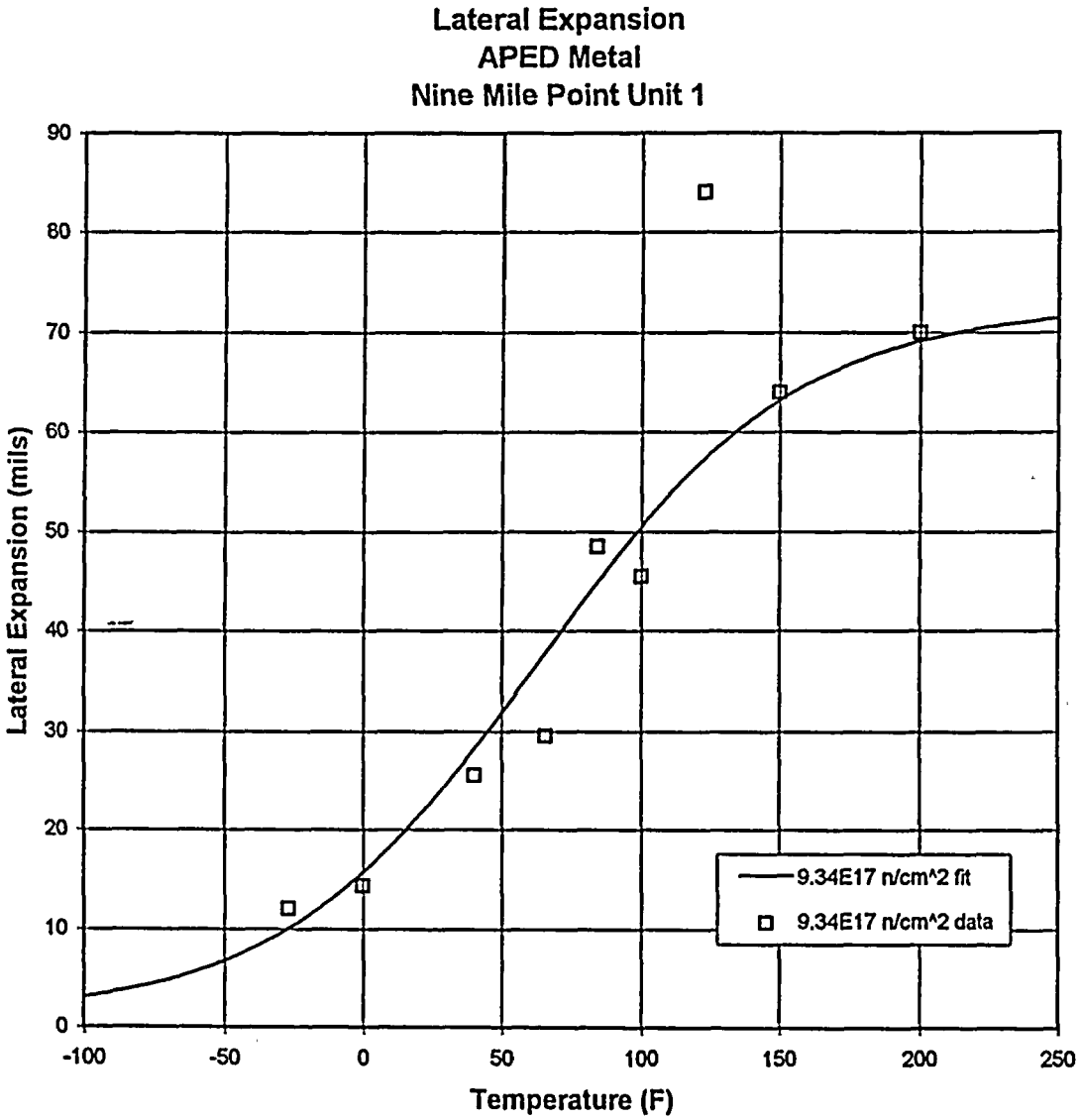

Figure 7-10 Lateral Expansion Data and Curve Fits for APED Metal

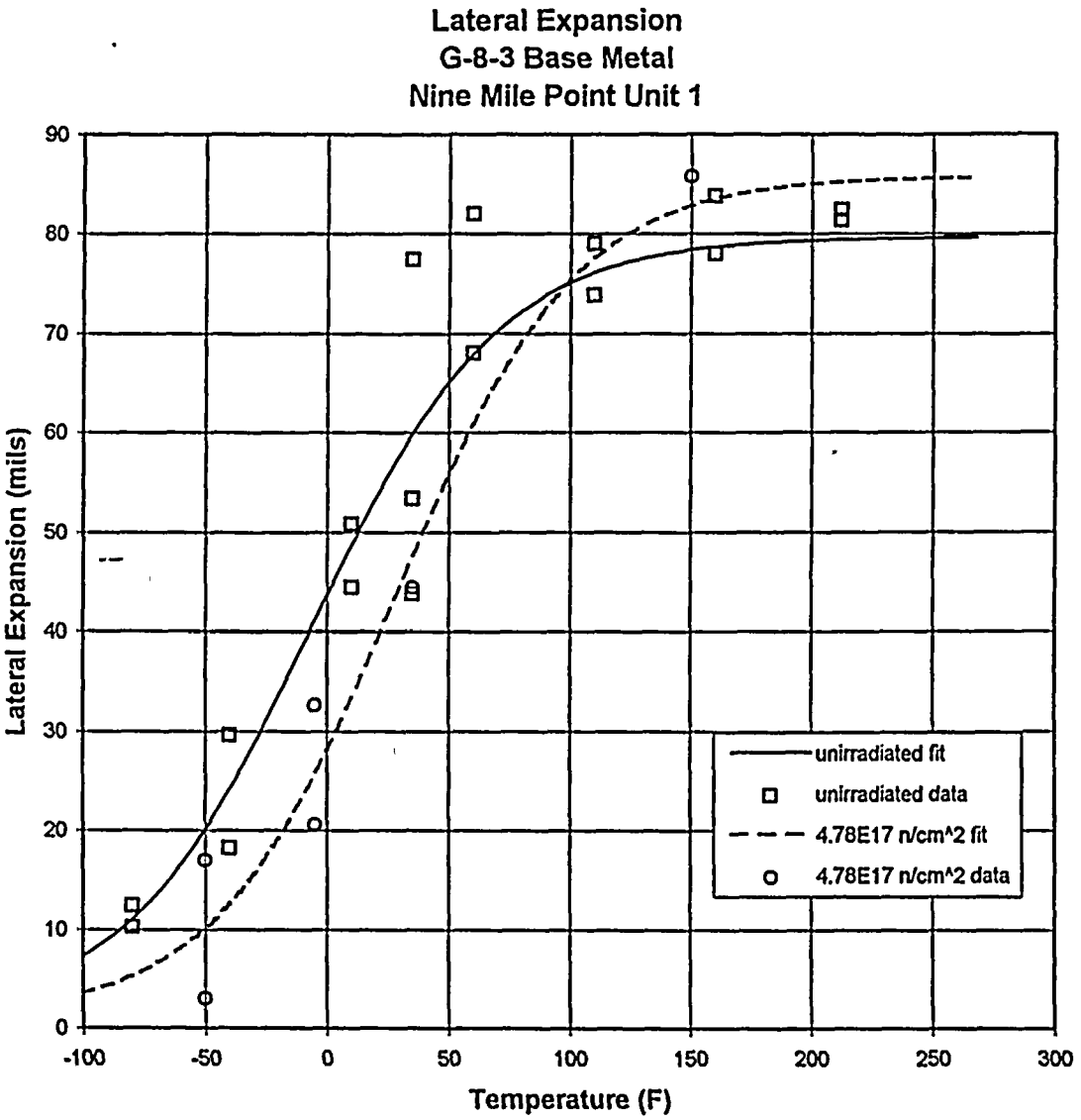

Figure 7-11 Lateral Expansion Data and Curve Fits for G-8-3/G-8-4 Base Metal

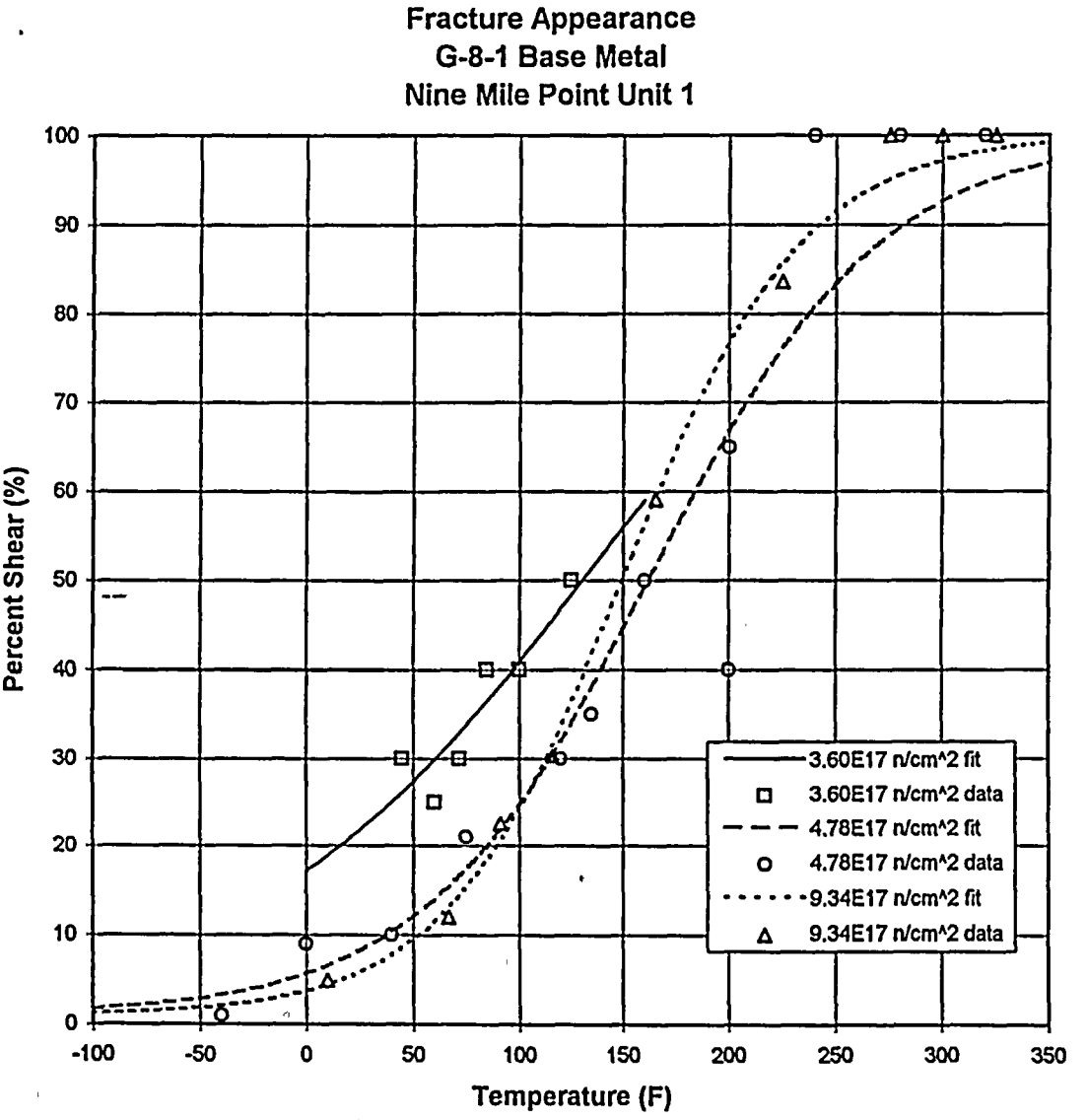

Figure 7-12 Fracture Appearance Data and Curve Fits for G-8-1 Base Metal

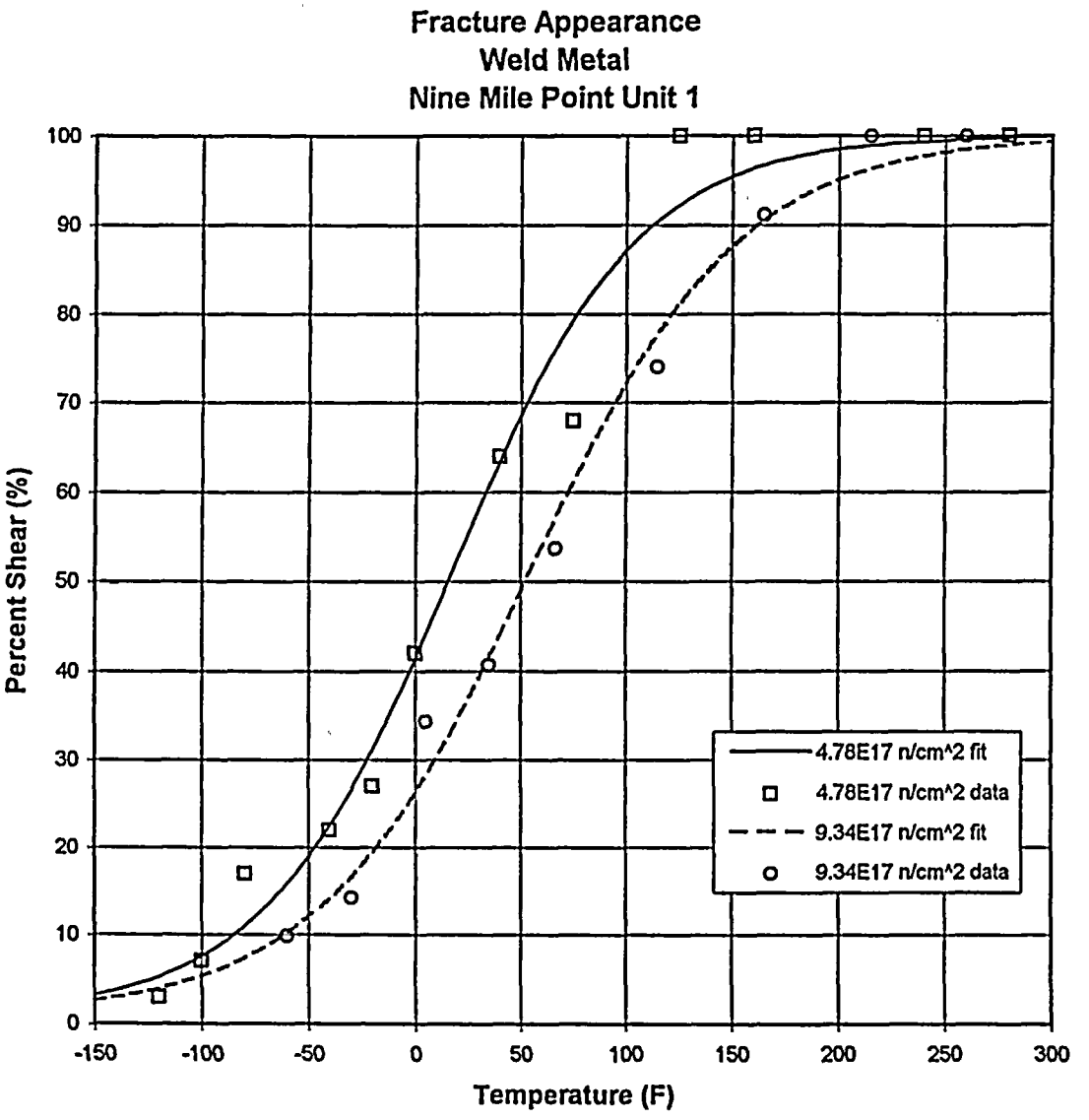

Figure 7-13 Fracture Appearance Data and Curve Fits for Weld Metal

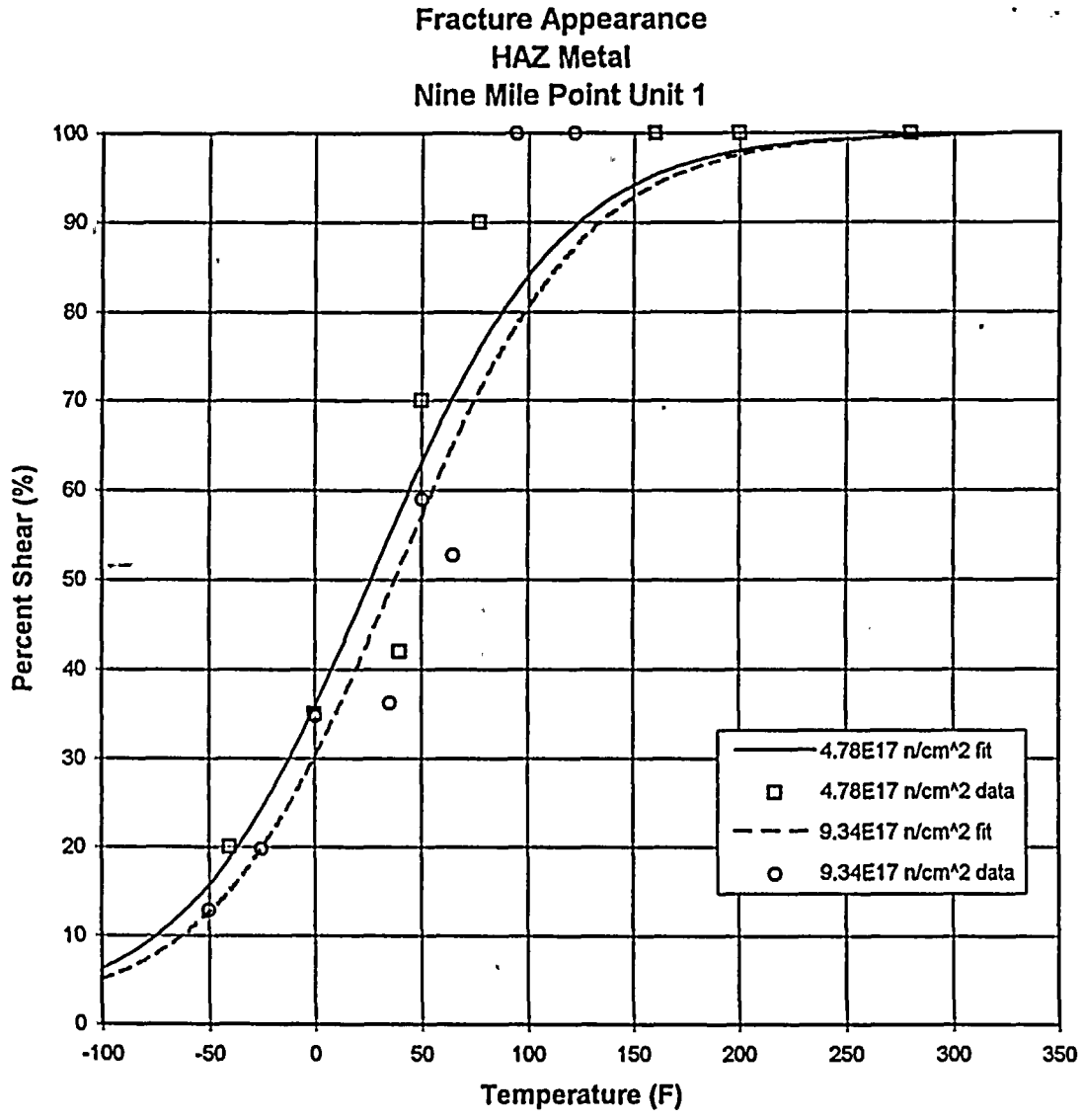

Figure 7-14 Fracture Appearance Data and Curve Fits for HAZ Metal

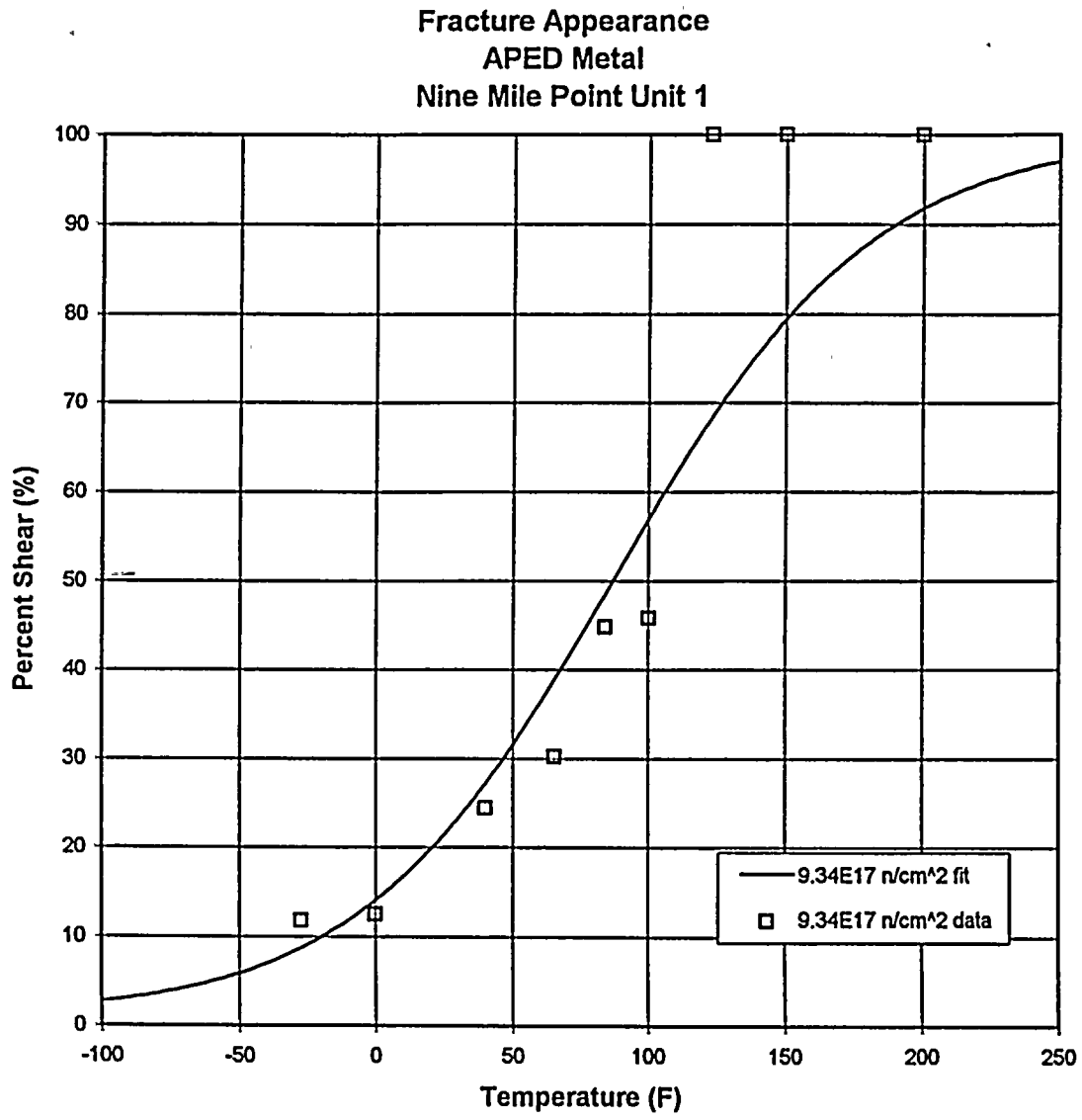

Figure 7-15 Fracture Appearance Data and Curve Fits for APED Metal

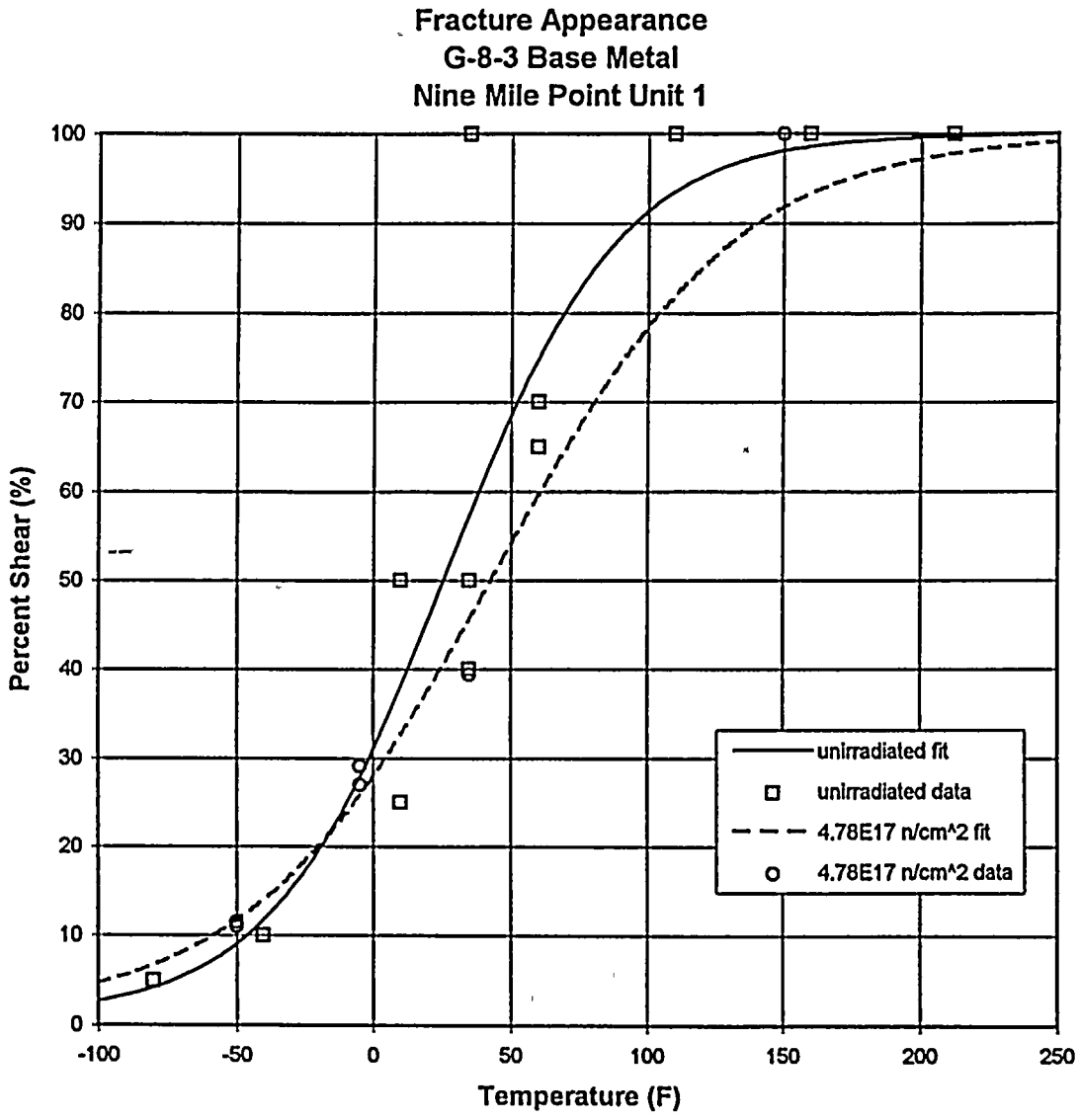

Figure 7-16 Fracture Appearance Data and Curve Fits for G-8-3/G-8-4 Base Metal

8.0 Summary and Conclusions

8.1 Key Results

Testing of the NMP-1 210 degree surveillance capsule and evaluation of the data has led to the following conclusions:

- The neutron induced plate G-8-1 embrittlement is moderate and the Charpy shift is within the expected range. At a fluence of 9.34 x 10^{17} n/cm^2, the Capsule B measured shift in the 30 ft-lb transition temperature is 77.7 F. The measured USE drop was only 0.8 ft-lb which is not statistically significant. Therefore, there was no measurable drop in USE and this result is in agreement with the 300 degree capsule data.

- Similarly moderate surveillance weld embrittlement results were obtained. The Capsule B measured weld metal shift in the 30 ft-lb transition temperature, relative to the 300 degree capsule, is 23.9 F. The surveillance weld 30 ft-lb transition temperature shift and weld USE drop from initial startup to the end of exposure of Capsule B cannot be reported since an unirradiated Charpy curve is not available. However, the 30 ft-lb transition temperature is - 15.2 F after a fluence of 9.34 x 10^{17} n/cm^2. These capsule results, in conjunction with the analyses reported in [8-1], confirm that the plate material is the limiting beltline material. Similarly, the weld USE at a fluence of 9.34 x 10^{17} n/cm^2 is 97.2 ft-lb, and the drop in USE from the time the 300 degree capsule was pulled (fluence = 4.78 x 10^{17} n/cm^2) to March, 1997, was only 12.4 ft-lb. These data confirm the conclusions of [8-2] that the NMP-1 vessel is safe in terms of ductile fracture.

- A fluence of 9.34 x 10^{17} n/cm^2 has been estimated for the Capsule B exposure using the capsule copper dosimetry data and the 300 degree capsule neutron transport analysis results. An evaluation of all of the Capsule B dosimetry data and evaluation of the changes in fuel cycle core designs indicates that fuel cycle effects have affected the accuracy of the previous neutron transport results. Accordingly, MPM is currently performing a neutron transport analysis for resolution of the dosimetry variation. These results will be used in future P-T curve revision. The data indicate that the fuel loading changes which have been implemented over the past few cycles have resulted in a fast flux reduction to the vessel. Based on analysis of the copper dosimetry data, the best estimate average flux for Capsule B is 1.76 x 10^{9} n/cm^2/s.

- Chemical measurements made on the capsule Charpy and tensile specimens have verified that the base metal specimens were fabricated from plate G-8-1 material. The weld and HAZ specimens were fabricated from welded prolongations cut from beltline plate G-8-3 during vessel fabrication.

- Analysis of the G-8-1 plate shift has indicated that the impact on the current P-T curves is not significant. Using the plate chemistry adjustment given in NMEL 90001 [8-1], the Capsule B shift was corrected from the measured value of 77.7 F to 85.7 F. Using the adjusted data in NMEL 90001, the RG 1.99(2) [8-3] Position 2 chemistry factor is 208.2 F. This is very close to the chemistry factor of 205.1 F which was used to calculate the current P-T curves in 1991. The differences in chemistry factors corresponds to ~ 1.5 F increase in the leak/hydro test temperature at 18 EFPY. Since this temperature is very small, well within the experimental uncertainty, and since the measured shift is within 3 F of the RG1.99(2) Position 2 trend curve, immediate revision of the P-T curves is not required. However, the P-T curves must be revised before the next refueling outage because they are only valid to 18 EFPY.

8.2 Chapter 8 References

[8-1] Manahan, M.P., "Nine Mile Point Unit 1 Surveillance Capsule Program", NMEL-90001, dated January 4, 1991

[8-2] NRC Letter dated April 20, 1994, "Elastic-Plastic Fracture Mechanics Assessment of Nine Mile Point Nuclear Station Unit No. 1 Reactor Vessel Beltline Plates"

[8-3] Regulatory Guide 1.99, Revision 2, "Radiation Embrittlement of Reactor Vessel Materials"

9.0 Nomenclature

ASME	-	American Society of Mechanical Engineers
ASTM	-	American Society for Testing and Materials
ASAXS	-	Anomalous Small Angle X-Ray Scattering
ART_{NDT}	-	Adjusted Nil-Ductility Reference Temperature
BWR	-	Boiling Water Reactor
DBTT	-	Ductile-Brittle Transition Temperature
CF	-	Chemistry Factor Specified in RG 1.99(2)
CFR	-	Code of Federal Regulations
EOL	-	End-of-License
F, °F	-	Degrees Farenheit
Ge(Li)	-	Germanium-Lithium gamma ray detector
GRSS	-	Gamma Ray Spectrometer System
HPGe	-	HyperPure Germanium gamma ray detector
ICP-OE	-	Inductively-Coupled Plasma Optical Emission spectroscopy
ID	-	Inner Diameter
KeV	-	Kiloelectron Volt (unit of gamma ray emission energy)
LT	-	Longitudinal-Transverse
LEFM	-	Linear-Elastic Fracture Mechanics
LWR	-	Light Water Reactor
NMP-1	-	Nine Mile Point Unit 1
NMPC	-	Niagara Mohawk Power Corporation
NRC	-	Nuclear Regulatory Commission
NIST	-	National Institute of Standards and Technology
OSQ	-	On-Screen Quantification software package
OSU-NRL	-	The Ohio State University Nuclear Reactor Laboratory
P-T	-	Pressure-Temperature
PWR	-	Pressurized Water Reactor
RG1.99(2)	-	Regulatory Guide 1.99 (Revision 2)
RPV	-	Reactor Pressure Vessel
RT_{NDT}	-	Nil-Ductility Reference Temperature
$\Delta RT_{NDT}, \Delta T_{30}$	-	Neutron Induced Shift in Nil-Ductility Reference Temperature Indexed at 30 ft-lbs of absorbed energy
T	-	Vessel Wall Thickness
TL	-	Transverse-Longitudinal
USE	-	Upper Shelf Energy
ΔUSE	-	Charpy Upper Shelf Energy Drop
USE_o	-	Unirradiated USE
UTS	-	Ultimate Tensile Strength
YS	-	Yield Strength

Appendices

Appendix A Capsule B Tensile Flow Curves

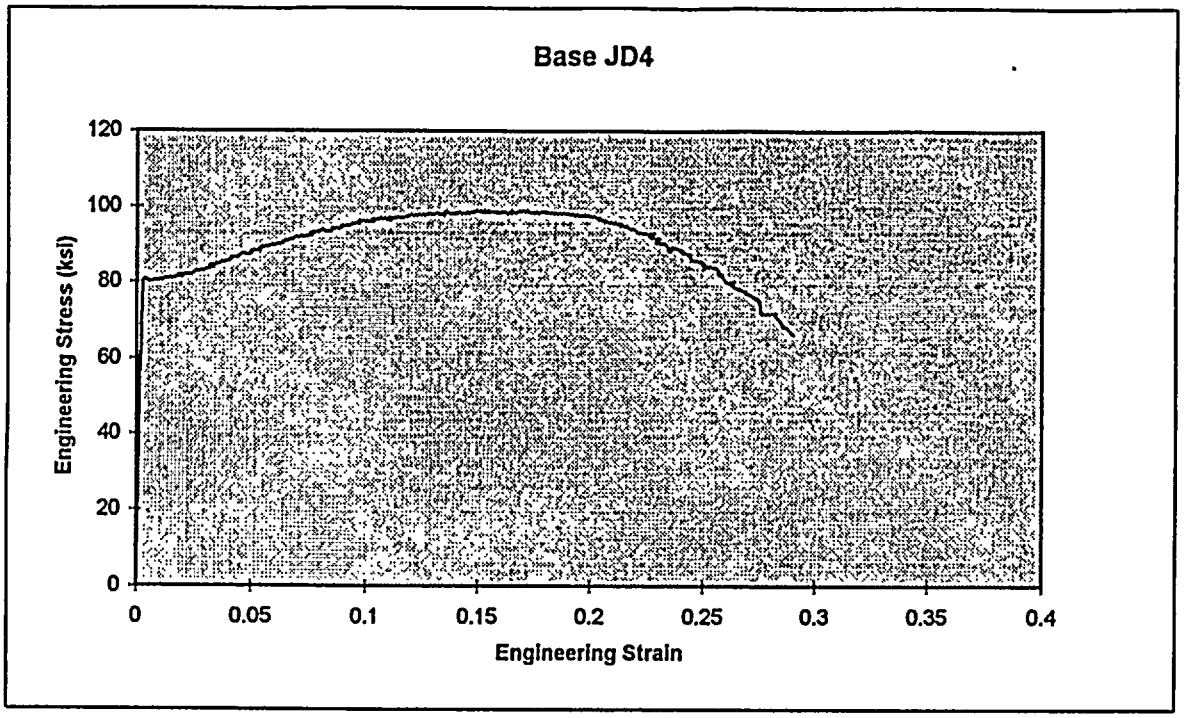

Figure A-1 Stress-Strain Curve for Base Metal Specimen JD4

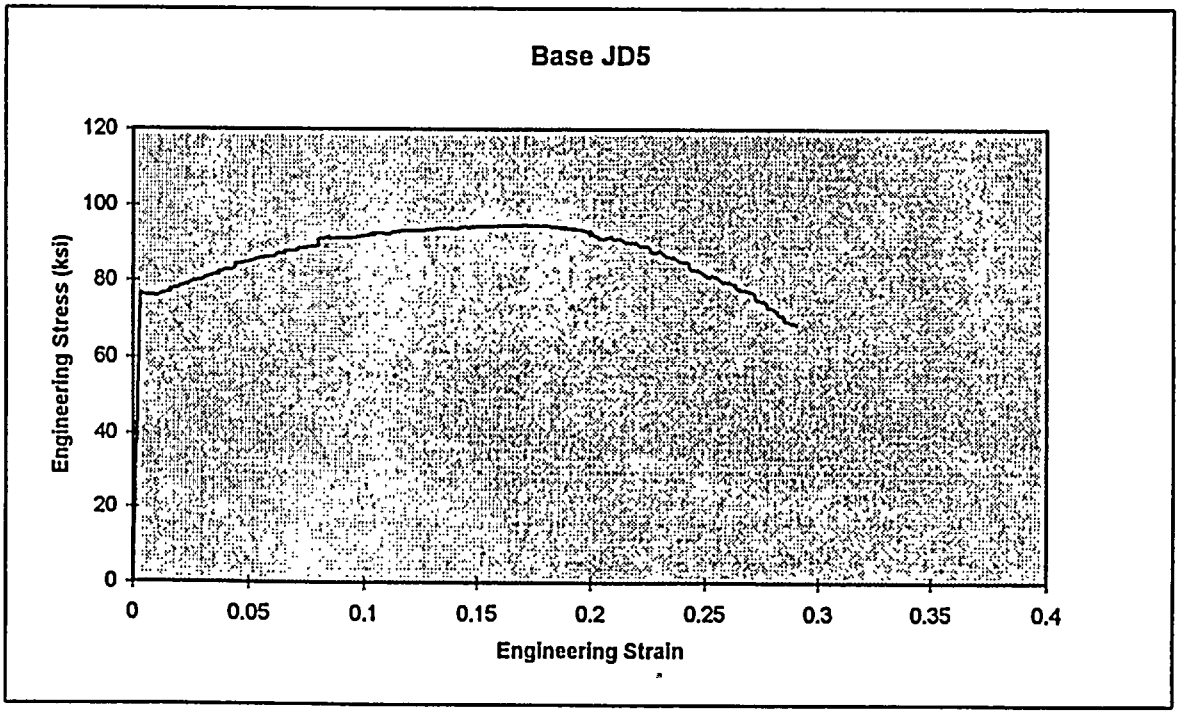

Figure A-2 Stress-Strain Curve for Base Metal Specimen JD5

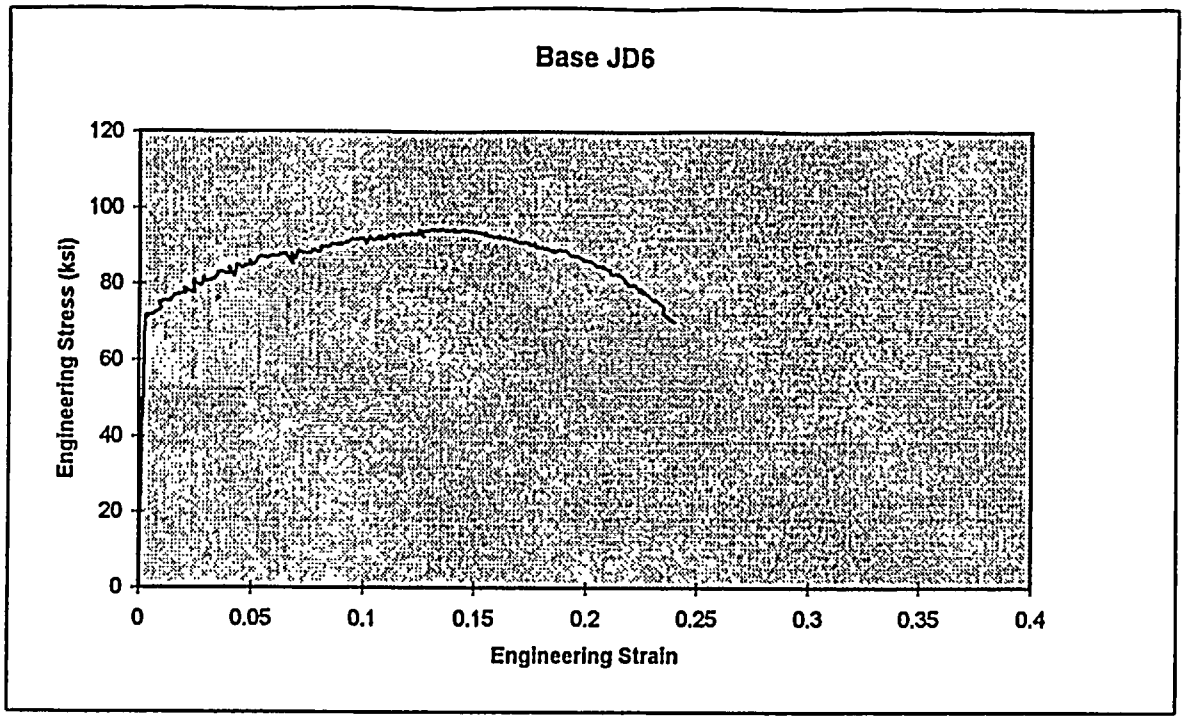

Figure A-3 Stress-Strain Curve for Base Metal Specimen JD6

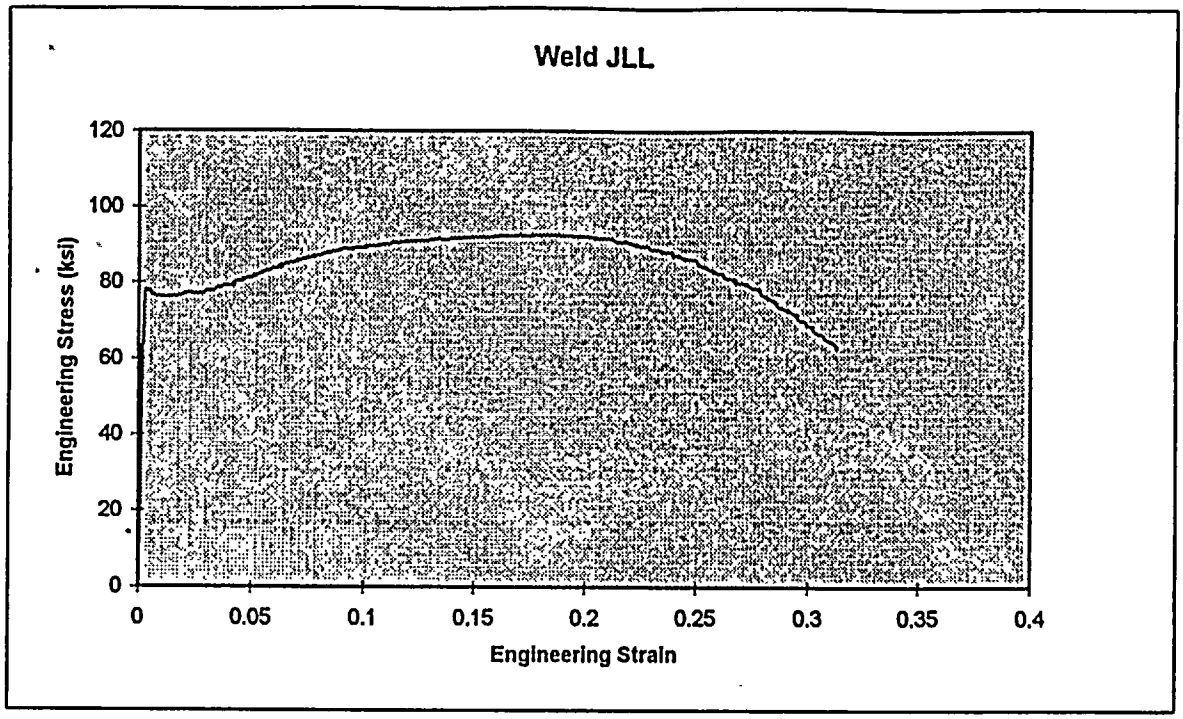

Figure A-4 Stress-Strain Curve for Weld Specimen JLL

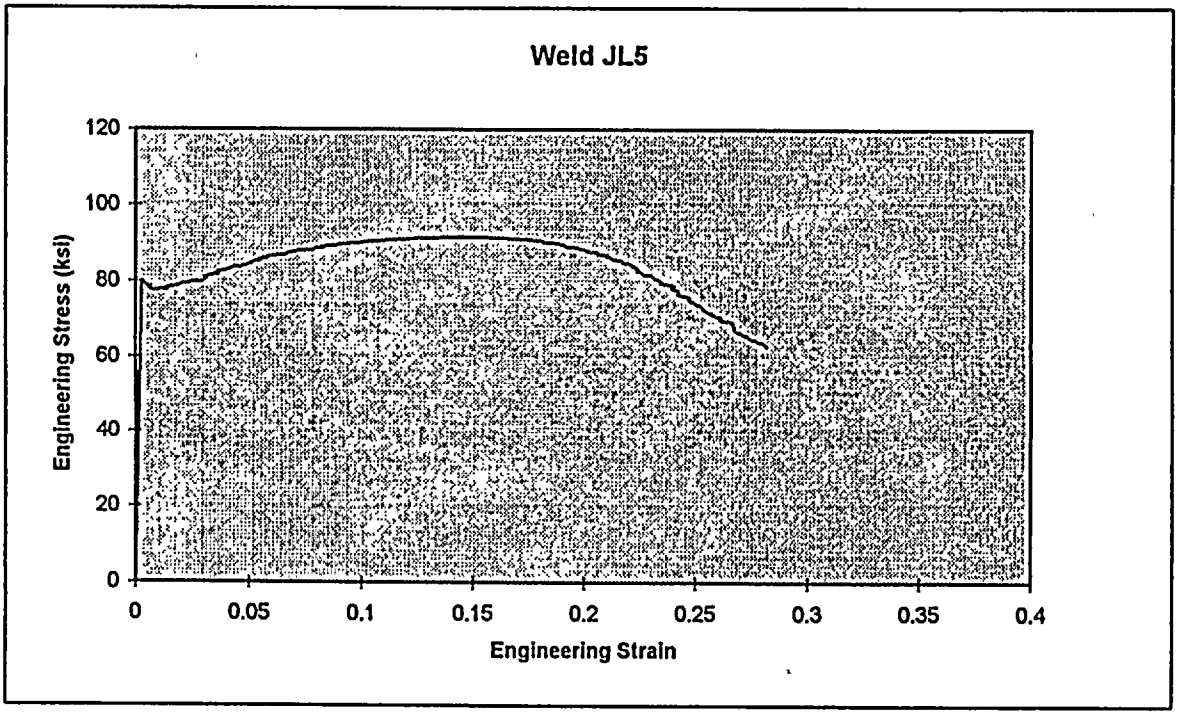

Figure A-5 Stress-Strain Curve for Weld Specimen JL5

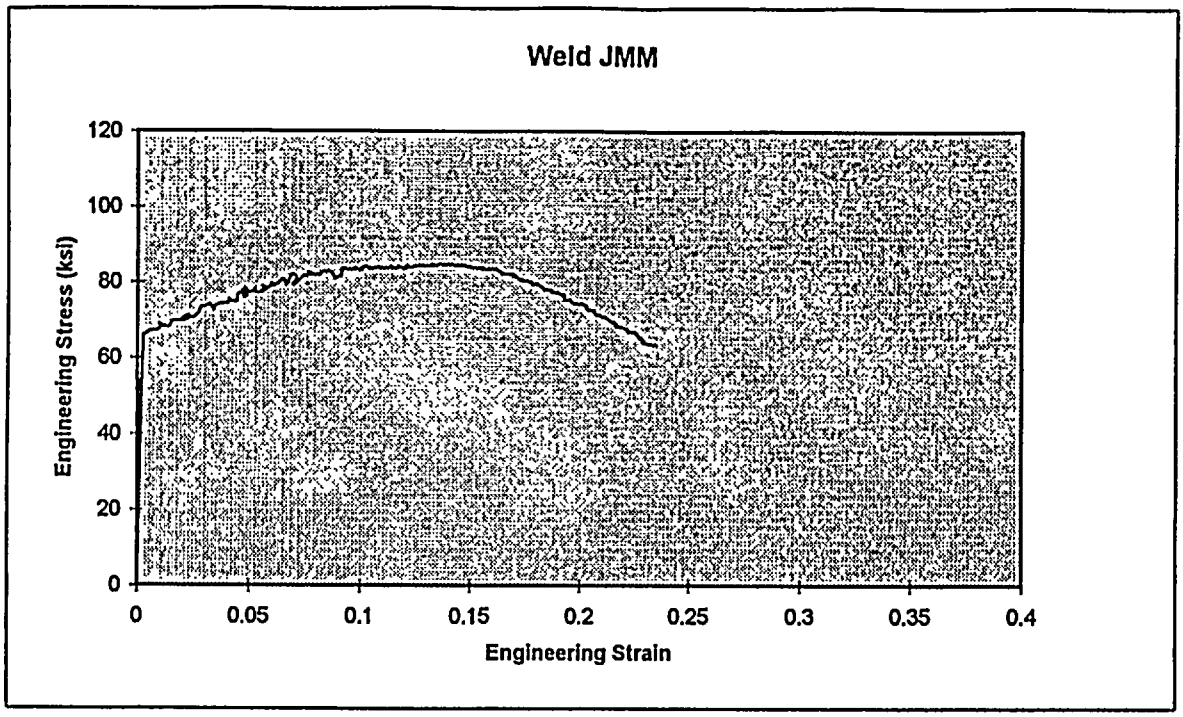

Figure A-5 Stress-Strain Curve for Weld Specimen JMM

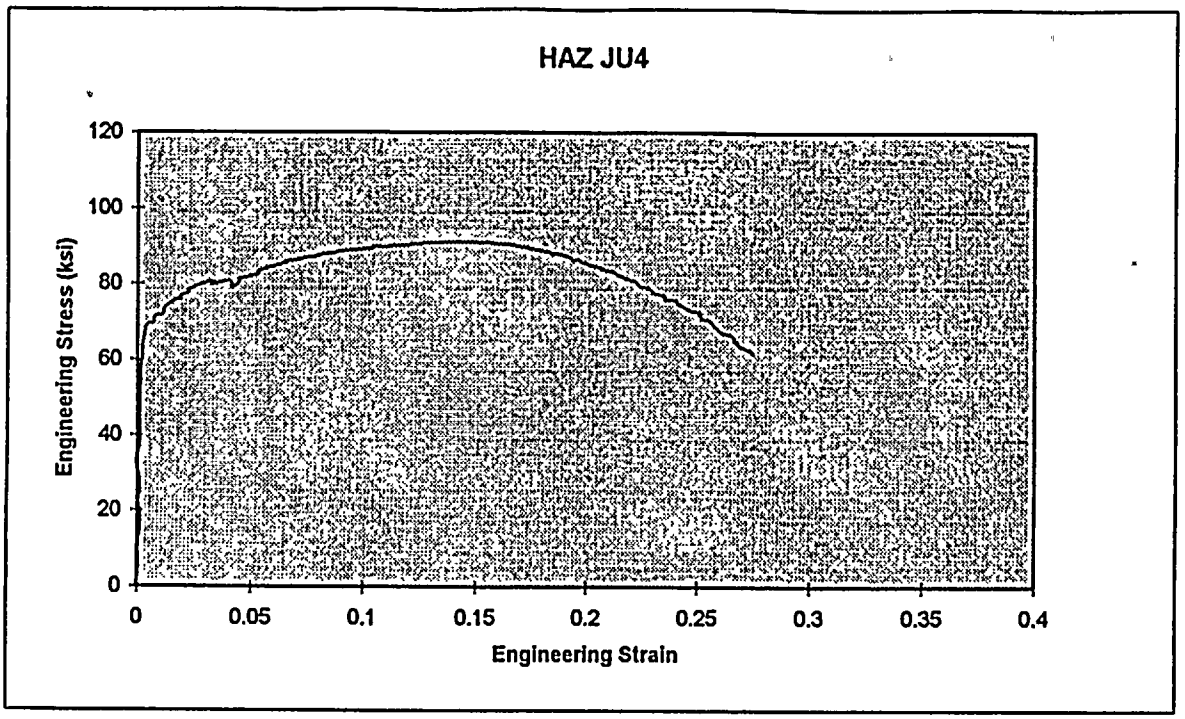

Figure A-7 Stress-Strain Curve for HAZ Specimen JU4

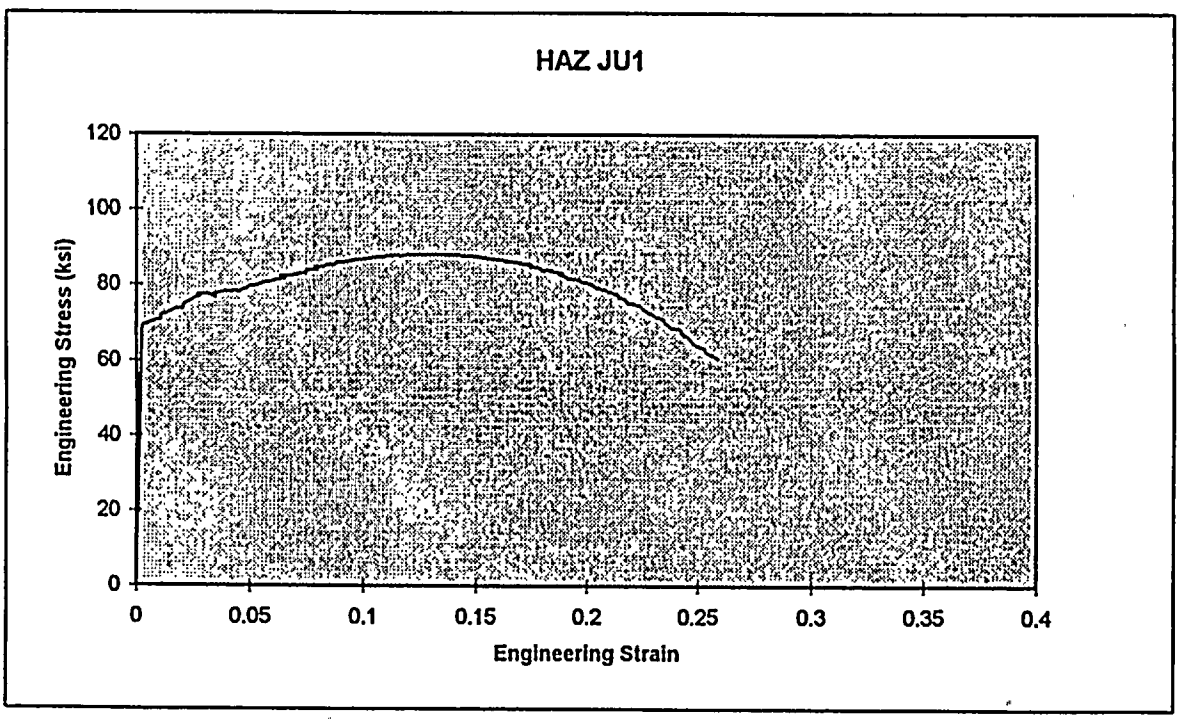

Figure A-8 Stress-Strain Curve for HAZ Specimen JU1

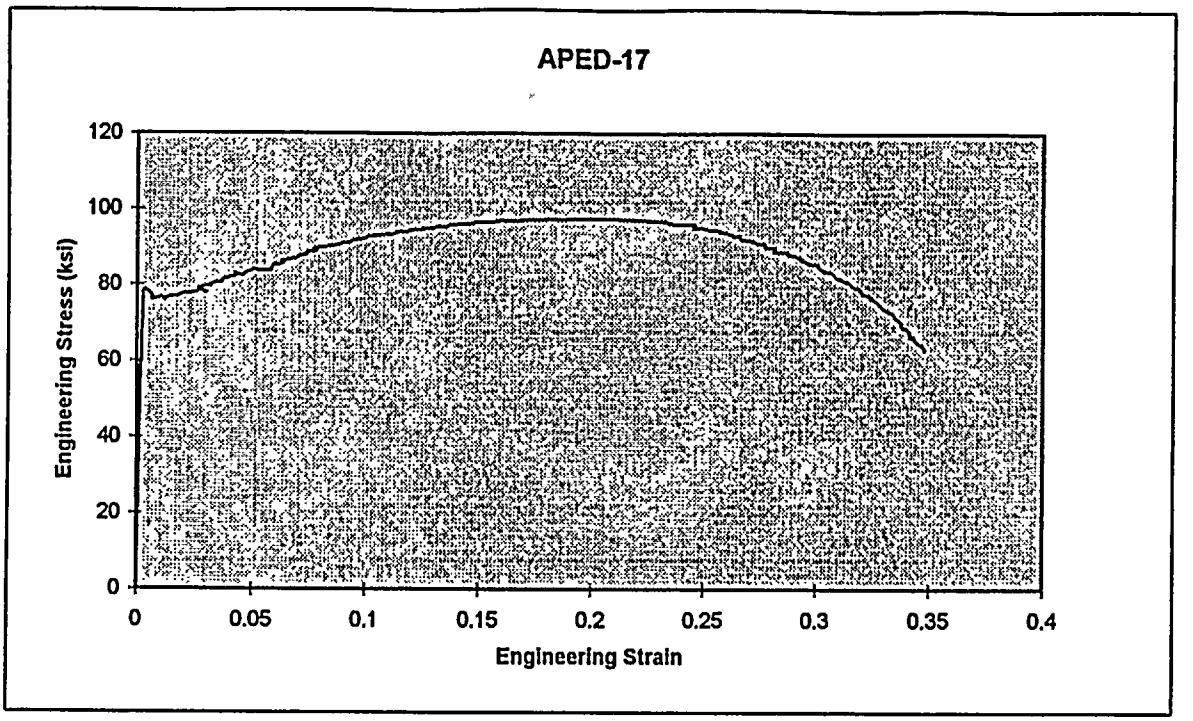

Figure A-9 Stress-Strain Curve for APED Specimen 17

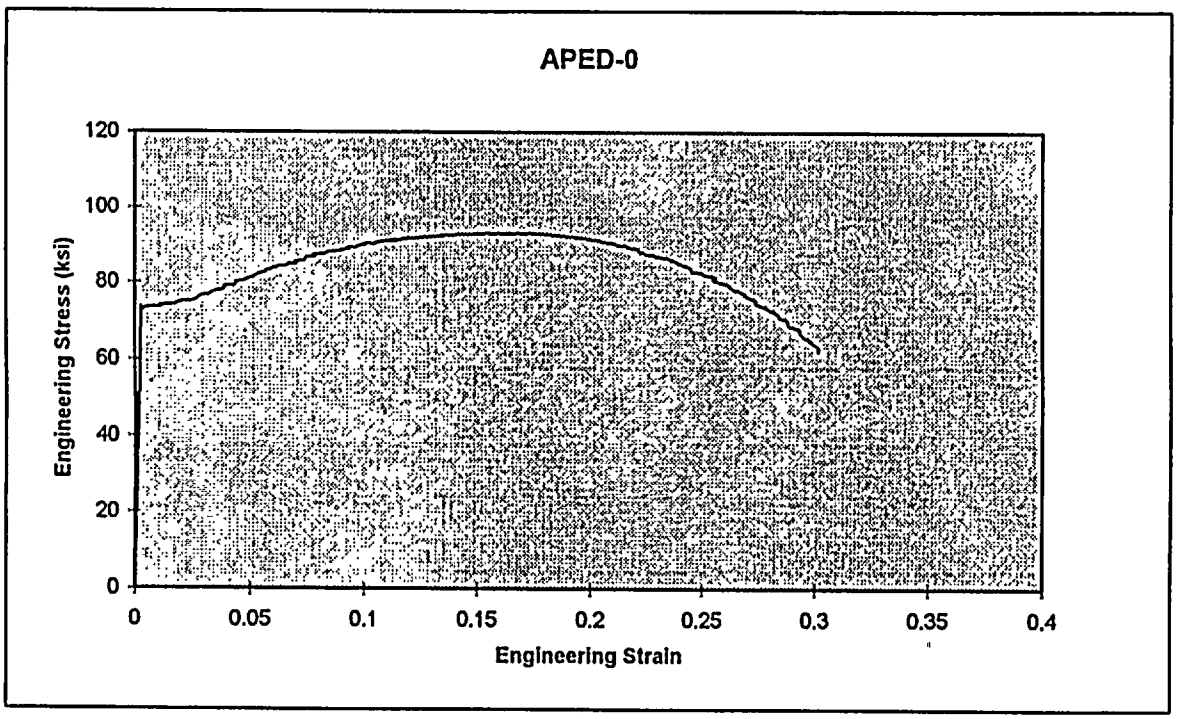

Figure A-10 Stress-Strain Curve for APED Specimen 0

Appendix B Instrumented Impact Data

Appendix B-1 Base Metal Plate G-8-1 Data

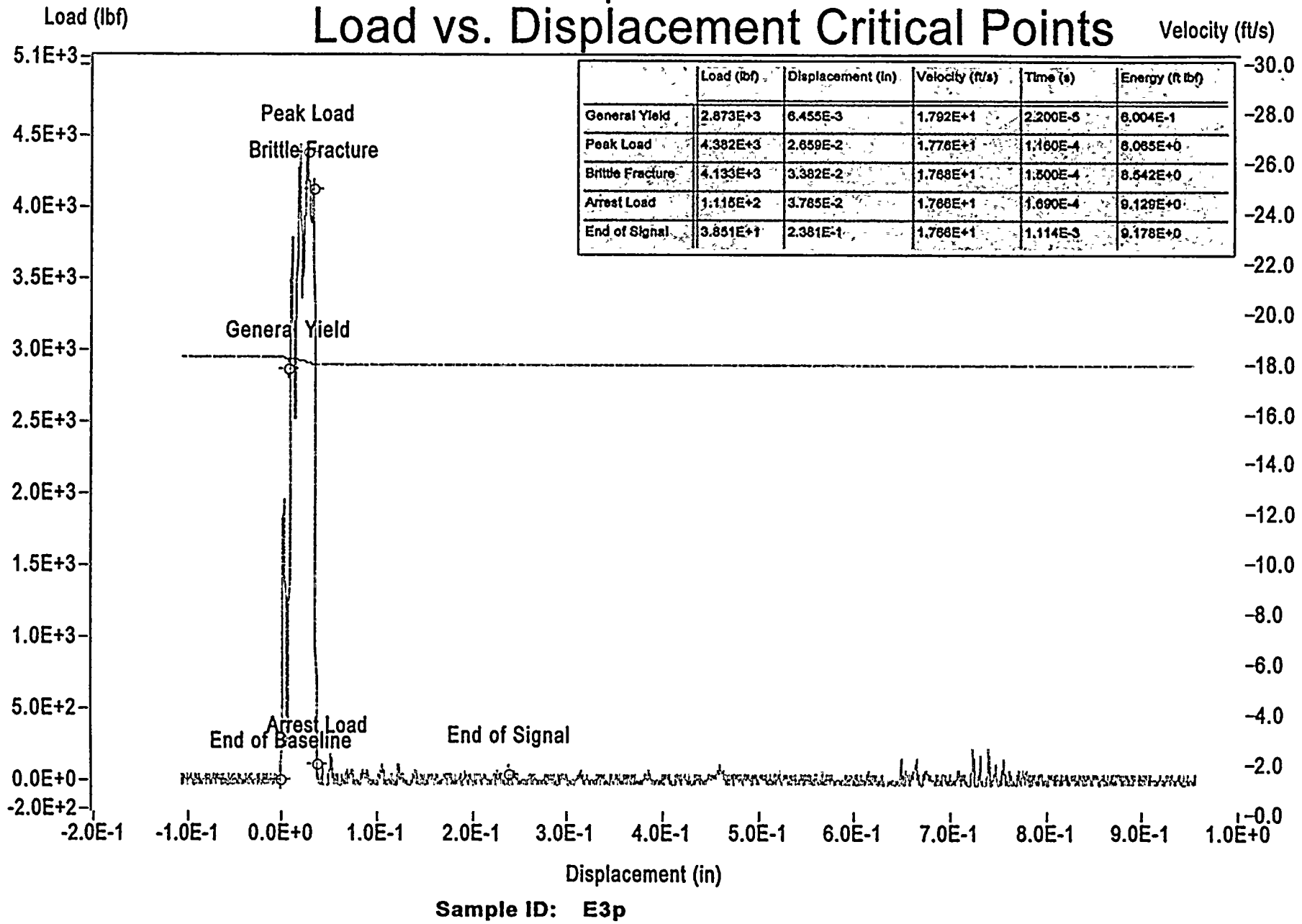

	Load (lbf)	Displacement (in)	Velocity (ft/s)	Time (s)	Energy (ft lbf)
General Yield	2.873E+3	6.455E-3	1.792E+1	2.200E-5	6.004E-1
Peak Load	4.382E+3	2.659E-2	1.776E+1	1.160E-4	6.085E+0
Brittle Fracture	4.133E+3	3.382E-2	1.768E+1	1.500E-4	8.542E+0
Arrest Load	1.115E+2	3.785E-2	1.766E+1	1.690E-4	9.129E+0
End of Signal	3.851E+1	2.381E-1	1.766E+1	1.114E-3	9.178E+0

Figure B-1 Plate G-8-1 Specimen E3p Tested at 10.0 F

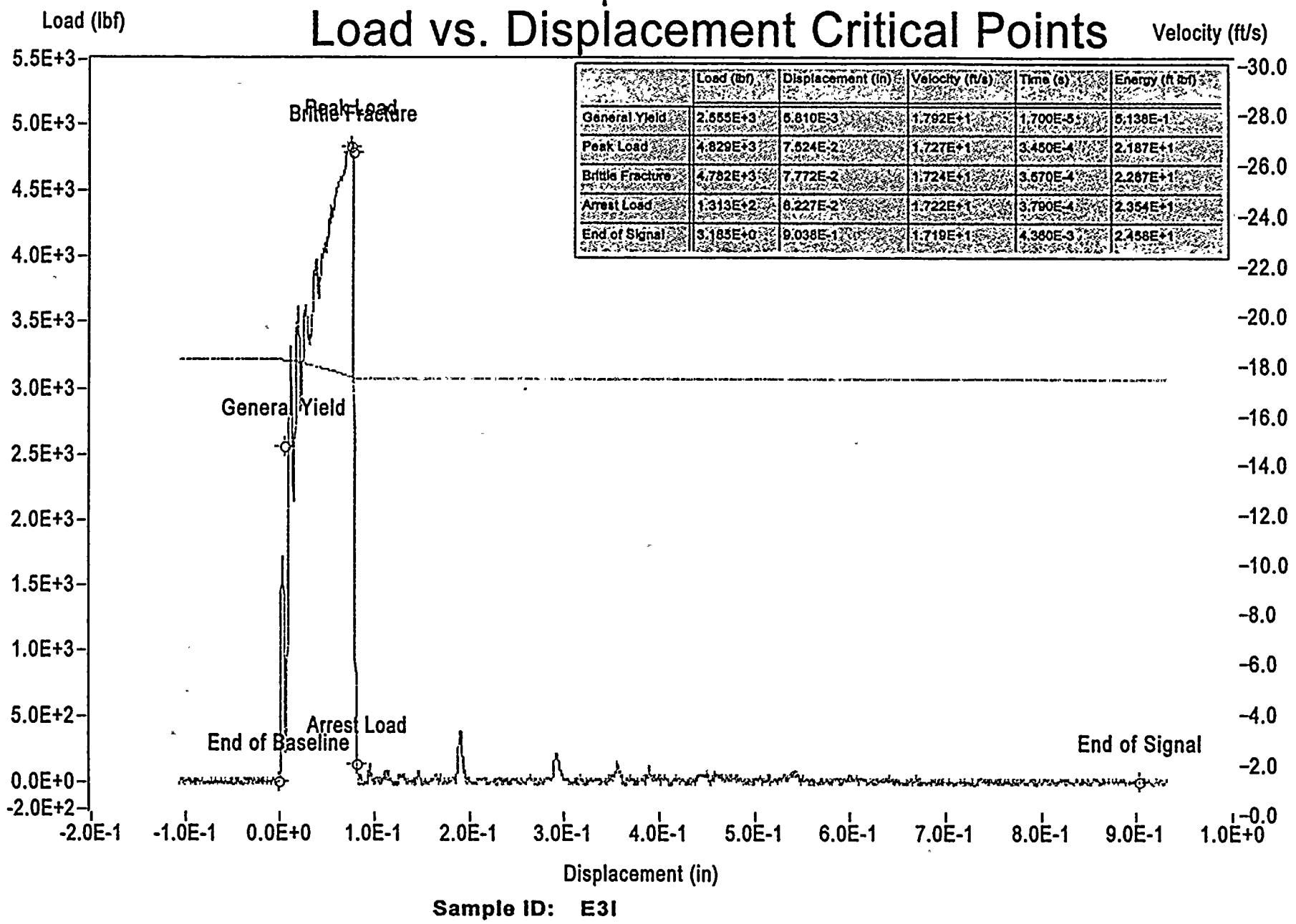

	Load (lbf)	Displacement (in)	Velocity (ft/s)	Time (s)	Energy (ft lbf)
General Yield	2.555E+3	5.810E-3	1.792E+1	1.700E-5	5.138E-1
Peak Load	4.829E+3	7.624E-2	1.727E+1	3.450E-4	2.187E+1
Brittle Fracture	4.782E+3	7.772E-2	1.724E+1	3.570E-4	2.287E+1
Arrest Load	1.313E+2	8.227E-2	1.722E+1	3.790E-4	2.354E+1
End of Signal	3.185E+0	9.038E-1	1.719E+1	4.360E-3	2.458E+1

Figure B-2 Plate G-8-1 Specimen E3I Tested at 66.5 F

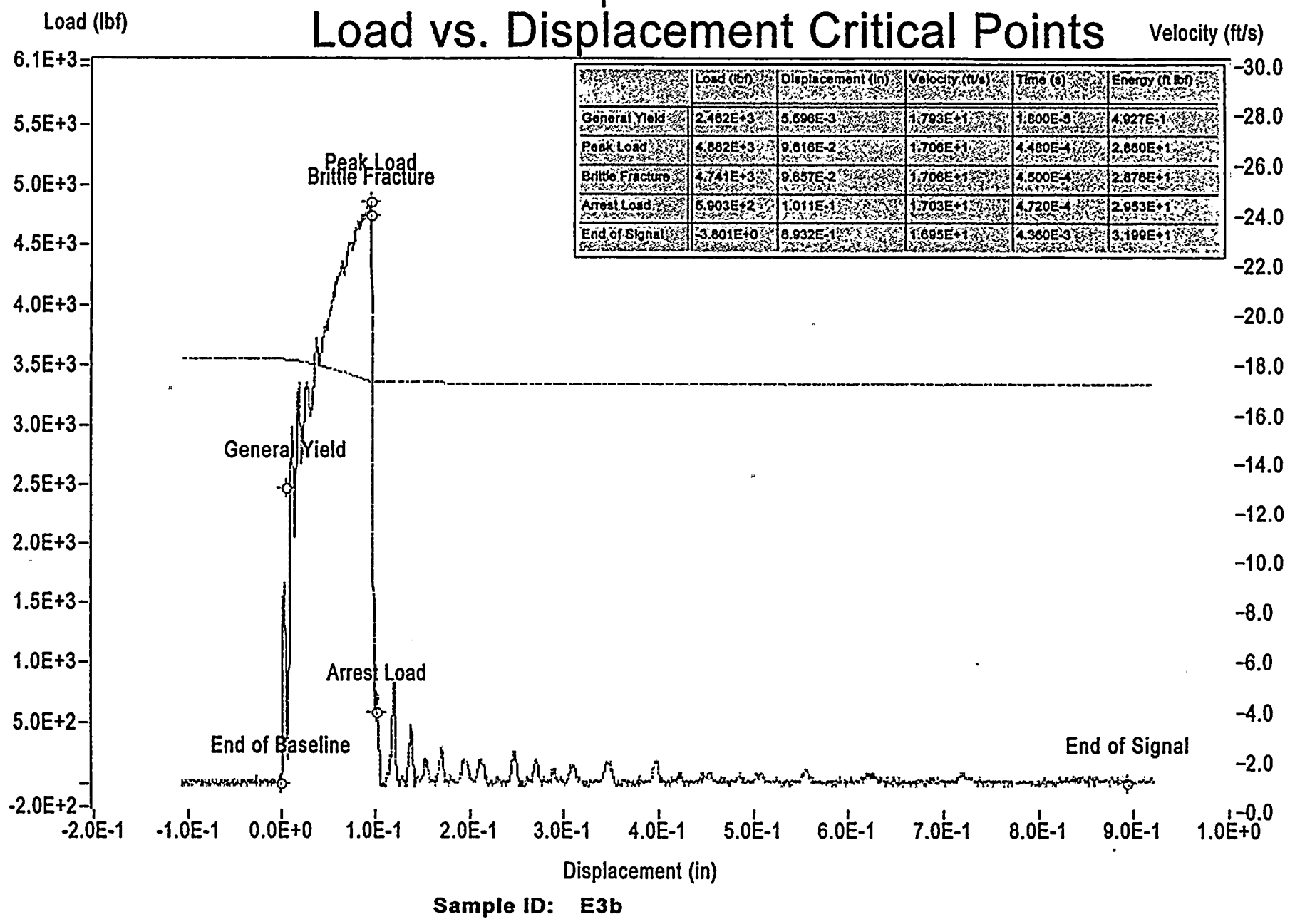

	Load (lbf)	Displacement (in)	Velocity (ft/s)	Time (s)	Energy (ft lbf)
General Yield	2.462E+3	5.696E-3	1.793E+1	1.800E-3	4.927E-1
Peak Load	4.862E+3	9.616E-2	1.706E+1	4.480E-4	2.660E+1
Brittle Fracture	4.741E+3	9.657E-2	1.706E+1	4.500E-4	2.676E+1
Arrest Load	5.903E+2	1.011E-1	1.703E+1	4.720E-4	2.953E+1
End of Signal	-3.601E+0	8.932E-1	1.695E+1	4.360E-3	3.199E+1

Figure B-3 Plate G-8-1 Specimen E3b Tested at 91.0 F

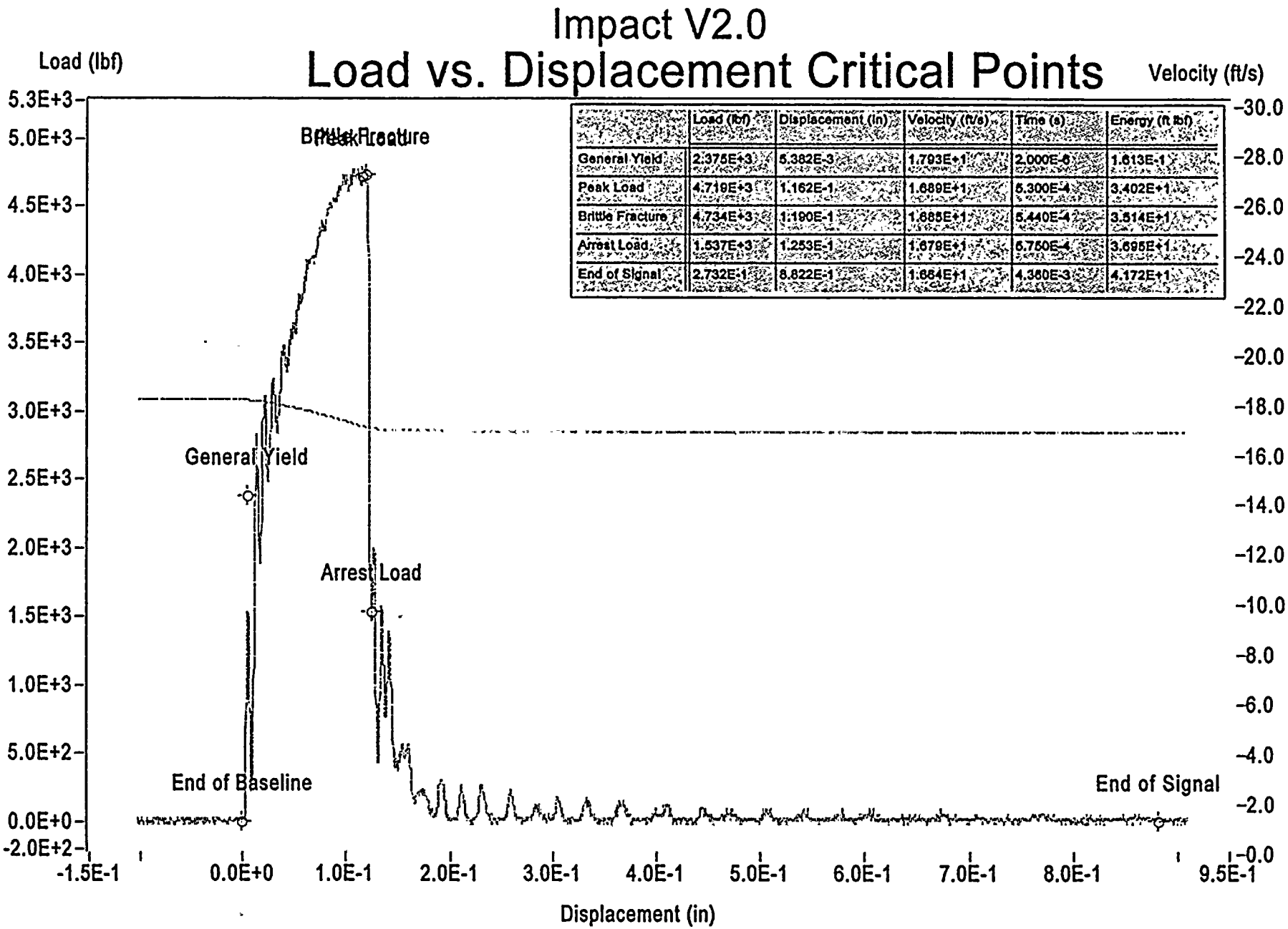

	Load (lbf)	Displacement (in)	Velocity (ft/s)	Time (s)	Energy (ft lbf)
General Yield	2.375E+3	5.382E-3	1.793E+1	2.000E-6	1.613E-1
Peak Load	4.719E+3	1.162E-1	1.689E+1	5.300E-4	3.402E+1
Brittle Fracture	4.734E+3	1.190E-1	1.685E+1	5.440E-4	3.514E+1
Arrest Load	1.537E+3	1.253E-1	1.679E+1	5.750E-4	3.695E+1
End of Signal	2.732E-1	8.822E-1	1.664E+1	4.360E-3	4.172E+1

Figure B-4 Plate G-8-1 Specimen E2a Tested at 116.0 F

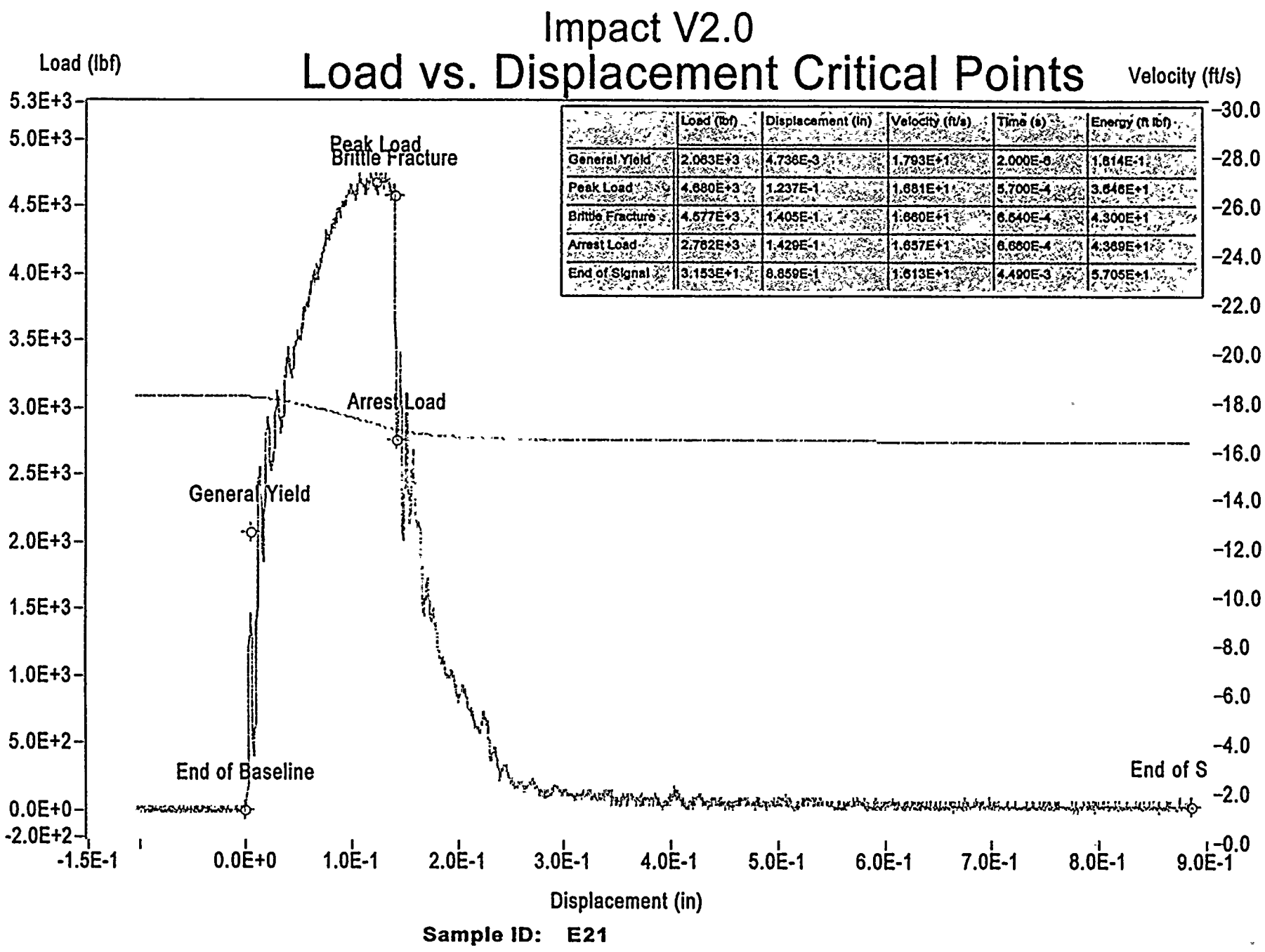

	Load (lbf)	Displacement (in)	Velocity (ft/s)	Time (s)	Energy (ft lbf)
General Yield	2.063E+3	4.736E-3	1.793E+1	2.000E-6	1.614E-1
Peak Load	4.680E+3	1.237E-1	1.681E+1	5.700E-4	3.646E+1
Brittle Fracture	4.577E+3	1.405E-1	1.660E+1	6.640E-4	4.300E+1
Arrest Load	2.782E+3	1.429E-1	1.657E+1	6.660E-4	4.369E+1
End of Signal	3.153E+1	8.859E-1	1.613E+1	4.490E-3	5.705E+1

Figure B-5 Plate G-8-1 Specimen E21 Tested at 165.0 F

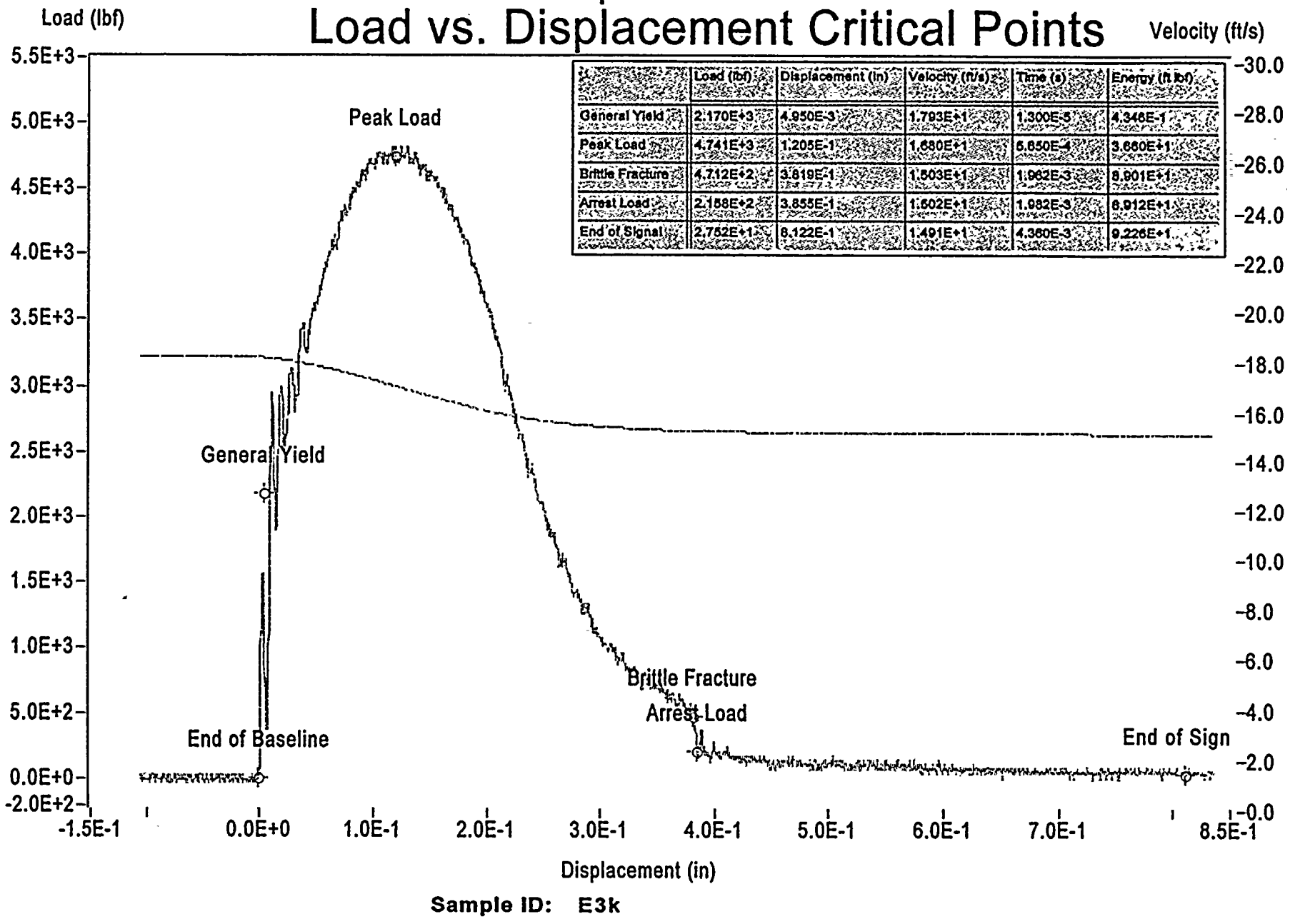

	Load (lbf)	Displacement (in)	Velocity (ft/s)	Time (s)	Energy (ft-lbf)
General Yield	2.170E+3	4.950E-3	1.793E+1	1.300E-3	4.346E-1
Peak Load	4.741E+3	1.205E-1	1.680E+1	5.650E-3	3.660E+1
Brittle Fracture	4.712E+2	3.819E-1	1.503E+1	1.962E-3	8.901E+1
Arrest Load	2.188E+2	3.855E-1	1.502E+1	1.982E-3	8.912E+1
End of Signal	2.752E+1	8.122E-1	1.491E+1	4.360E-3	9.226E+1

Figure B-6 Plate G-8-1 Specimen E3k Tested at 225.0 F

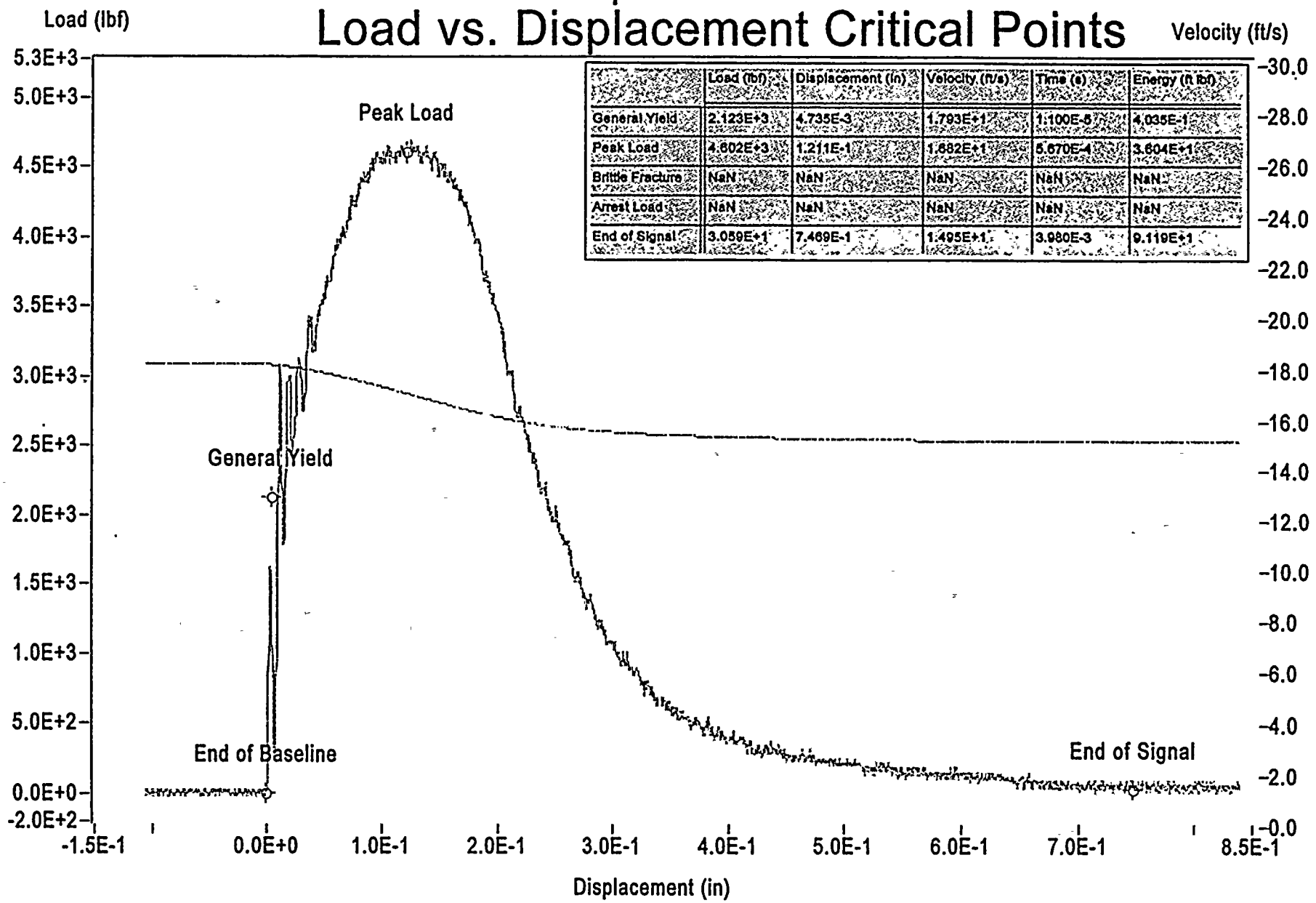

	Load (lbf)	Displacement (in)	Velocity (ft/s)	Time (s)	Energy (ft lbf)
General Yield	2.123E+3	4.735E-3	1.793E+1	1.100E-6	4.035E-1
Peak Load	4.602E+3	1.211E-1	1.682E+1	5.670E-4	3.604E+1
Brittle Fracture	NaN	NaN	NaN	NaN	NaN
Arrest Load	NaN	NaN	NaN	NaN	NaN
End of Signal	3.059E+1	7.469E-1	1.495E+1	3.980E-3	9.119E+1

Figure B-7 Plate G-8-1 Specimen E3d Tested at 275.0 F

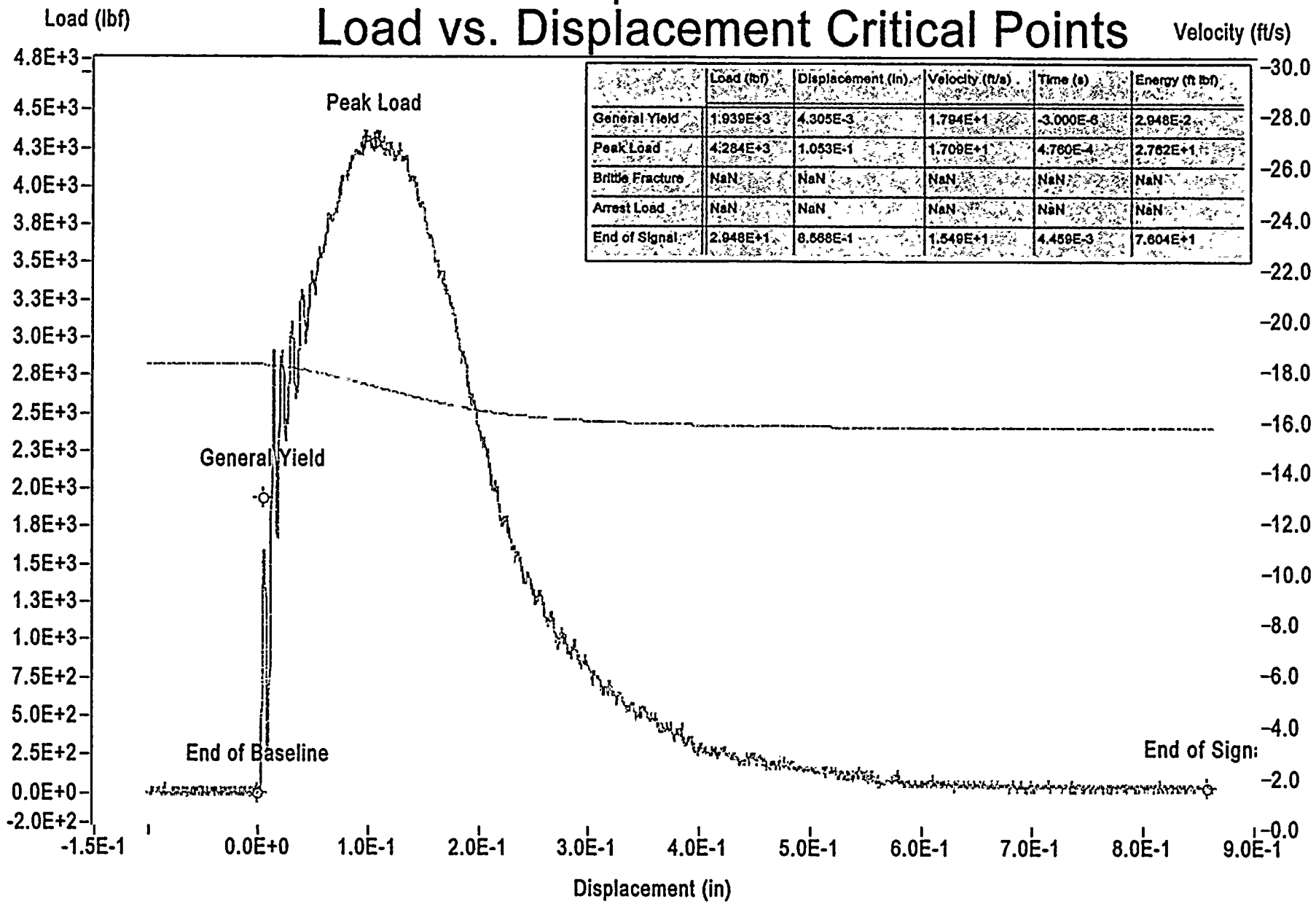

	Load (lbf)	Displacement (in)	Velocity (ft/s)	Time (s)	Energy (ft lbf)
General Yield	1.939E+3	4.305E-3	1.784E+1	-3.000E-6	2.948E-2
Peak Load	4.284E+3	1.053E-1	1.709E+1	4.760E-4	2.762E+1
Brittle Fracture	NaN	NaN	NaN	NaN	NaN
Arrest Load	NaN	NaN	NaN	NaN	NaN
End of Signal	2.948E+1	8.568E-1	1.549E+1	4.459E-3	7.604E+1

Sample ID: Eam

Figure B-8 Plate G-8-1 Specimen Eam Tested at 300.0 F

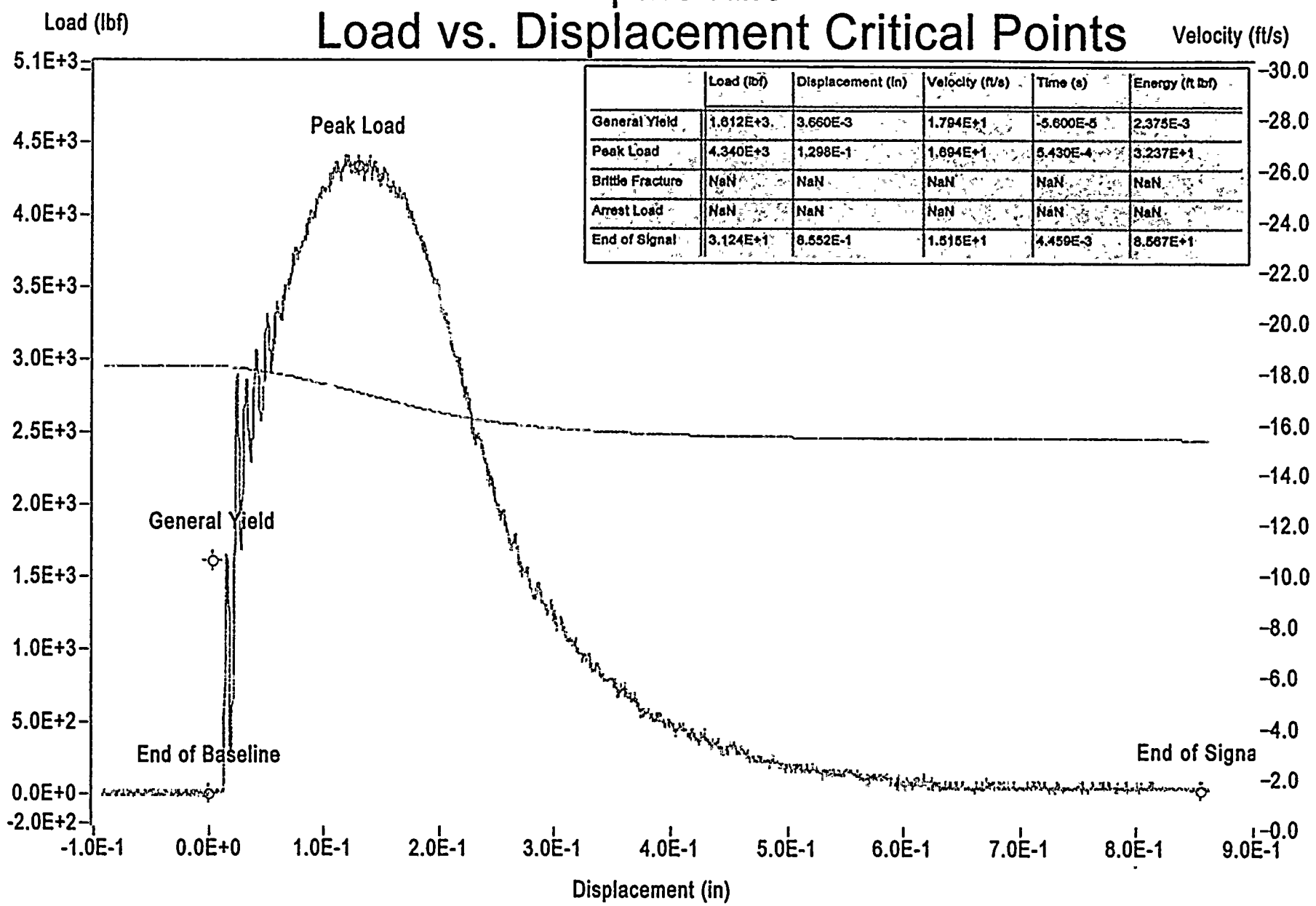

	Load (lbf)	Displacement (in)	Velocity (ft/s)	Time (s)	Energy (ft lbf)
General Yield	1.612E+3	3.660E-3	1.794E+1	-5.600E-5	2.375E-3
Peak Load	4.340E+3	1.298E-1	1.694E+1	5.430E-4	3.237E+1
Brittle Fracture	NaN	NaN	NaN	NaN	NaN
Arrest Load	NaN	NaN	NaN	NaN	NaN
End of Signal	3.124E+1	8.552E-1	1.515E+1	4.459E-3	8.567E+1

Figure B-9 Plate G-8-1 Specimen E25 Tested at 325.0 F

Appendix B-2 Weld Metal Data

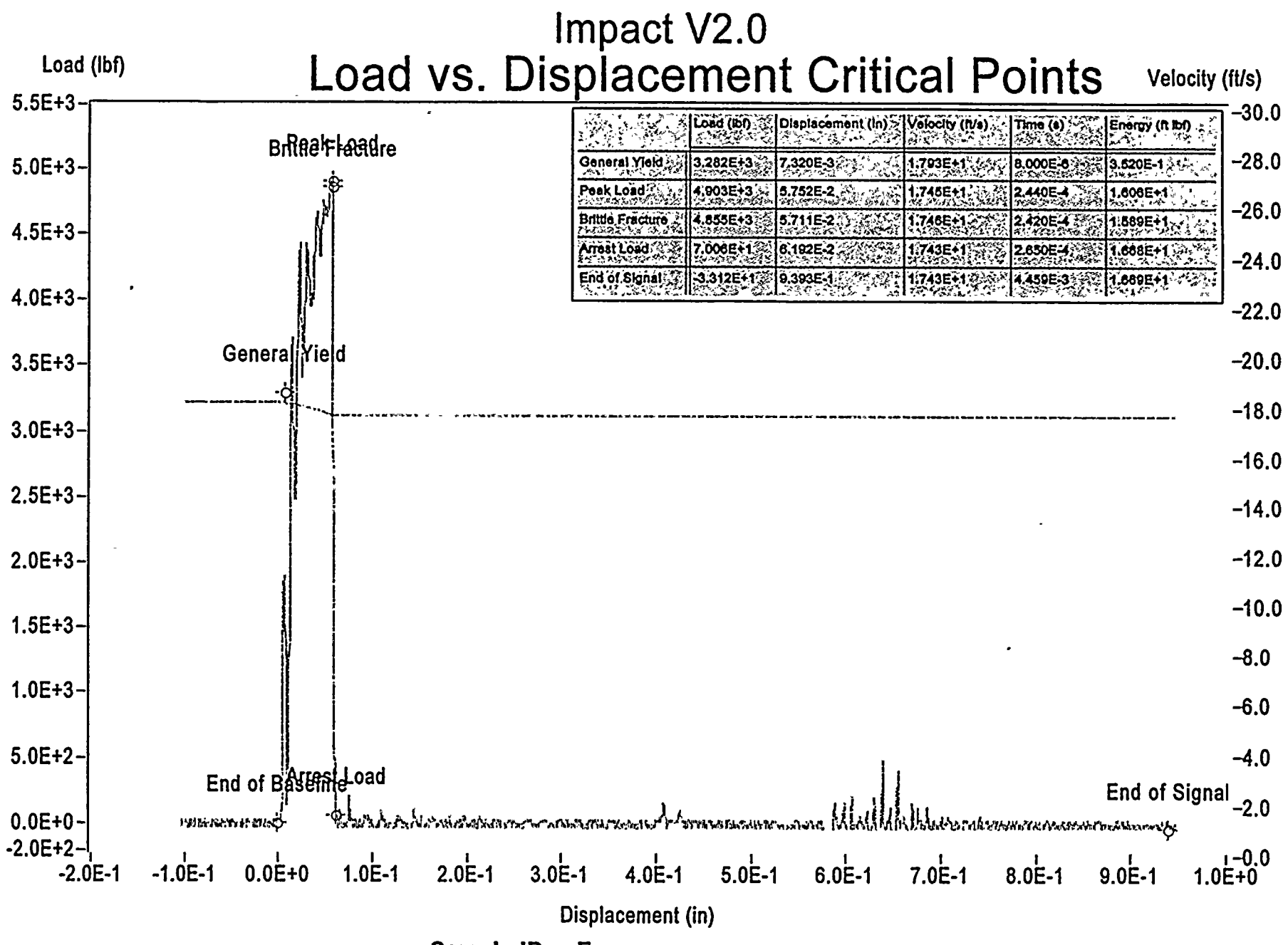

	Load (lbf)	Displacement (in)	Velocity (ft/s)	Time (s)	Energy (ft lbf)
General Yield	3.282E+3	7.320E-3	1.793E+1	8.000E-6	3.520E-1
Peak Load	4.903E+3	5.752E-2	1.745E+1	2.440E-4	1.606E+1
Brittle Fracture	4.855E+3	5.711E-2	1.746E+1	2.420E-4	1.589E+1
Arrest Load	7.006E+1	6.192E-2	1.743E+1	2.650E-4	1.668E+1
End of Signal	-3.312E+1	9.393E-1	1.743E+1	4.459E-3	1.669E+1

Figure B-10 Weld Specimen Eea Tested at -60.0 F

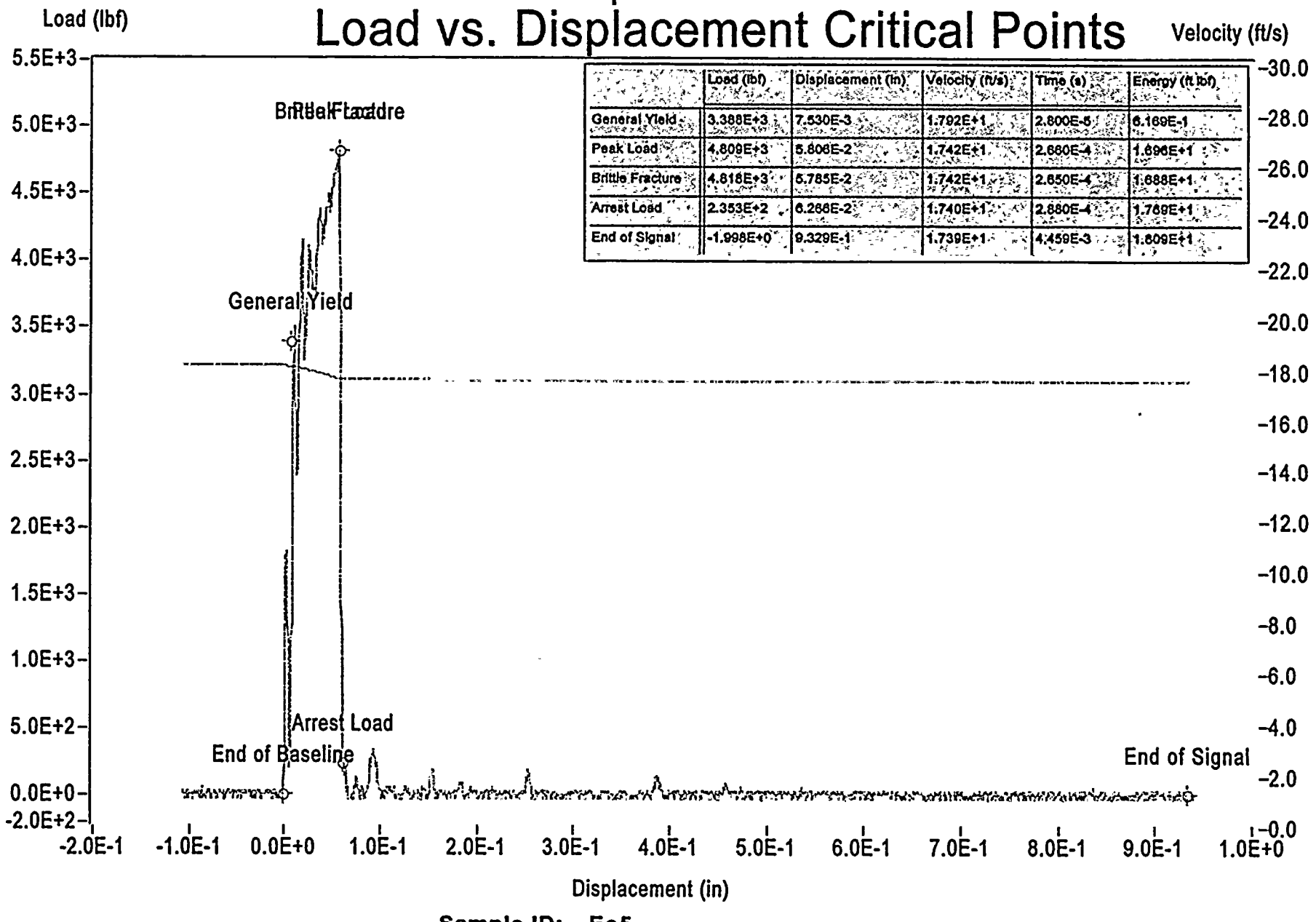

	Load (lbf)	Displacement (in)	Velocity (ft/s)	Time (s)	Energy (ft lbf)
General Yield	3.388E+3	7.530E-3	1.792E+1	2.800E-5	6.169E-1
Peak Load	4.809E+3	5.806E-2	1.742E+1	2.660E-4	1.696E+1
Brittle Fracture	4.818E+3	5.785E-2	1.742E+1	2.650E-4	1.688E+1
Arrest Load	2.353E+2	6.266E-2	1.740E+1	2.880E-4	1.769E+1
End of Signal	-1.998E+0	9.329E-1	1.739E+1	4.459E-3	1.609E+1

Figure B-11 Weld Specimen Ee5 Tested at -30.0 F

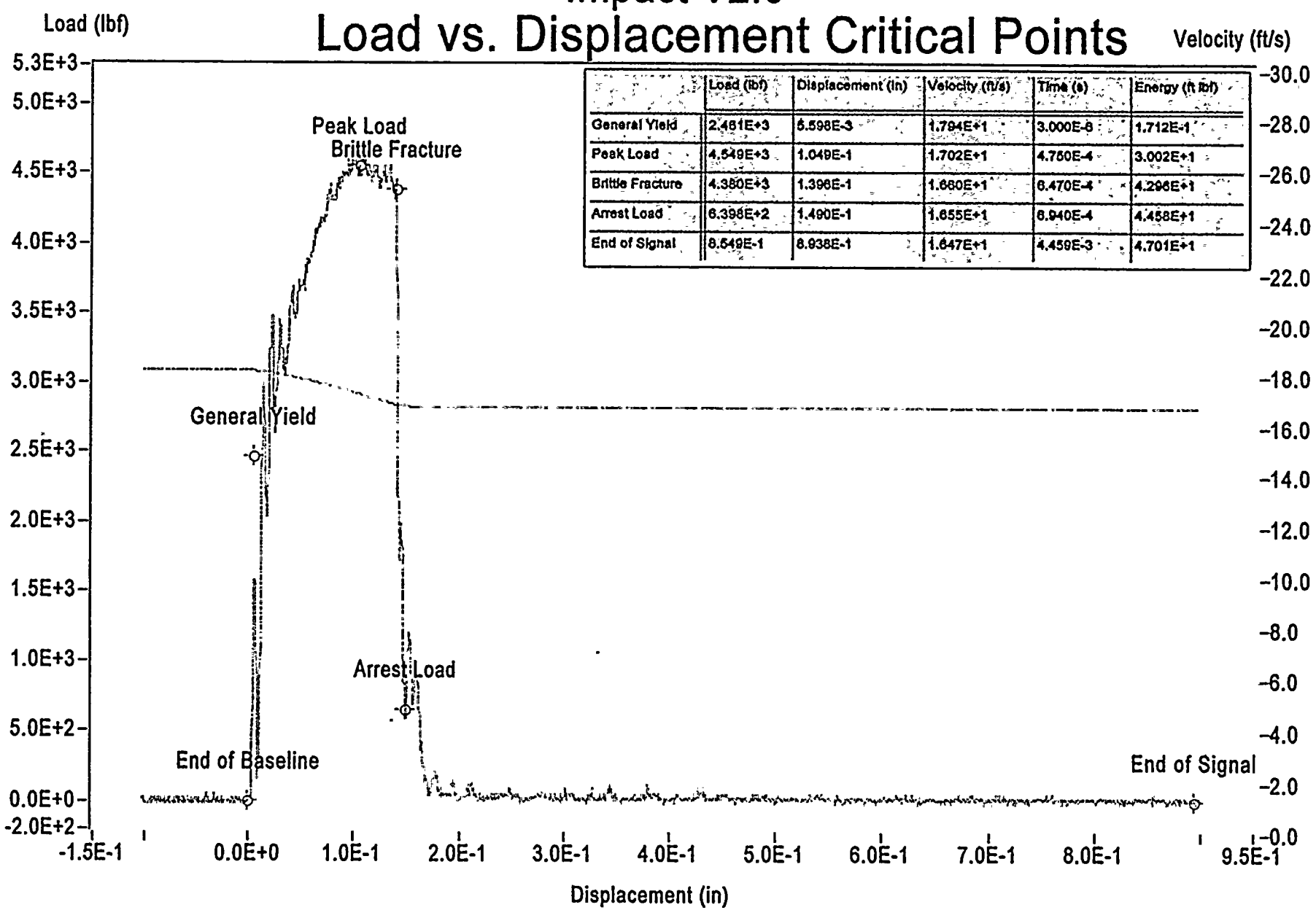

	Load (lbf)	Displacement (in)	Velocity (ft/s)	Time (s)	Energy (ft lbf)
General Yield	2.481E+3	5.598E-3	1.794E+1	3.000E-6	1.712E-1
Peak Load	4.549E+3	1.049E-1	1.702E+1	4.750E-4	3.002E+1
Brittle Fracture	4.380E+3	1.396E-1	1.660E+1	6.470E-4	4.296E+1
Arrest Load	6.398E+2	1.490E-1	1.655E+1	6.940E-4	4.458E+1
End of Signal	8.549E-1	8.938E-1	1.647E+1	4.459E-3	4.701E+1

Figure B-12 Weld Specimen Eeb Tested at 5.0 F

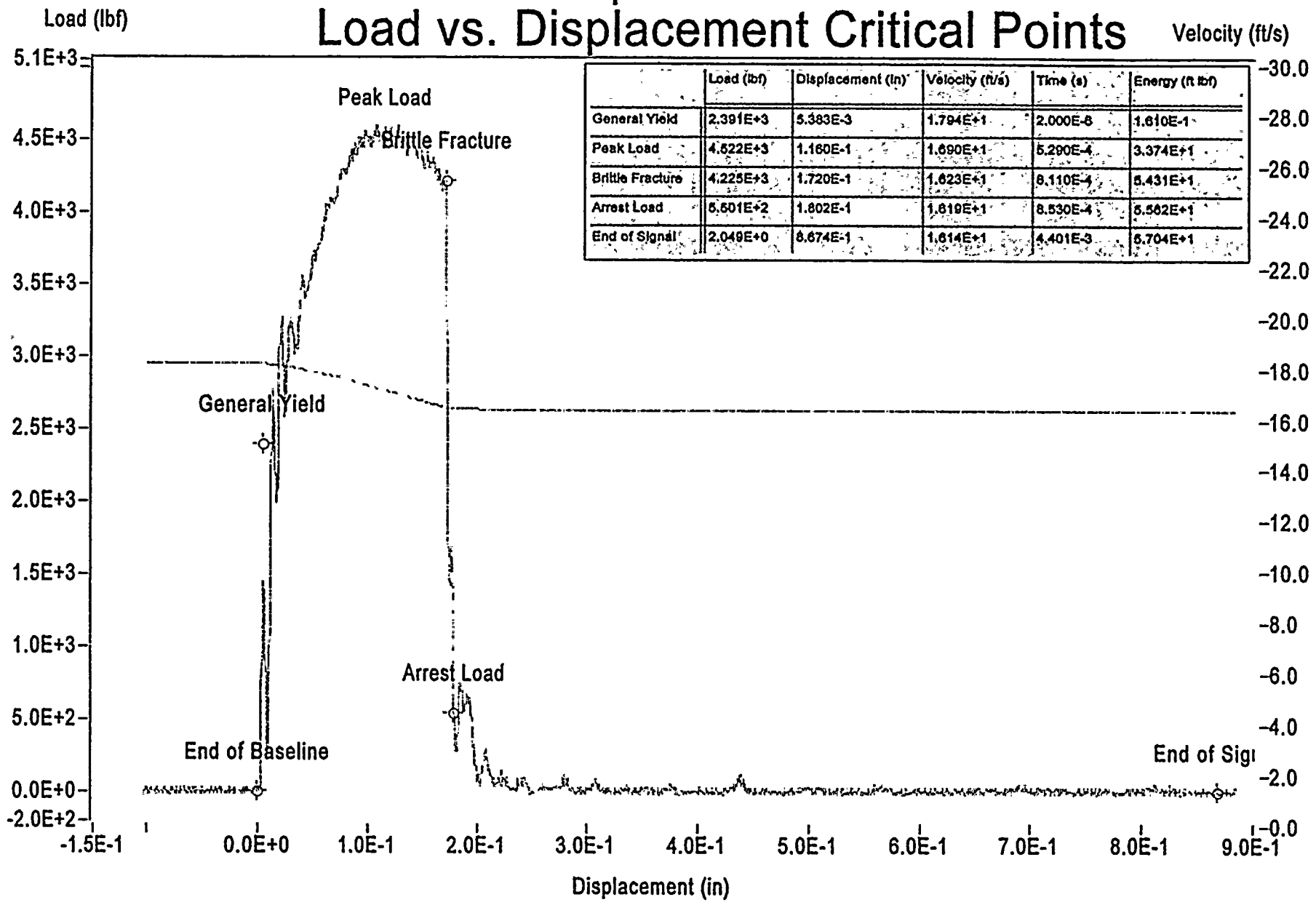

	Load (lbf)	Displacement (in)	Velocity (ft/s)	Time (s)	Energy (ft lbf)
General Yield	2.391E+3	5.383E-3	1.794E+1	2.000E-6	1.610E-1
Peak Load	4.522E+3	1.160E-1	1.690E+1	5.290E-4	3.374E+1
Brittle Fracture	4.225E+3	1.720E-1	1.623E+1	8.110E-4	5.431E+1
Arrest Load	5.501E+2	1.802E-1	1.619E+1	8.530E-4	5.562E+1
End of Signal	2.049E+0	8.674E-1	1.614E+1	4.401E-3	5.704E+1

Figure B-13 Weld Specimen Ee4 Tested at 35.0 F

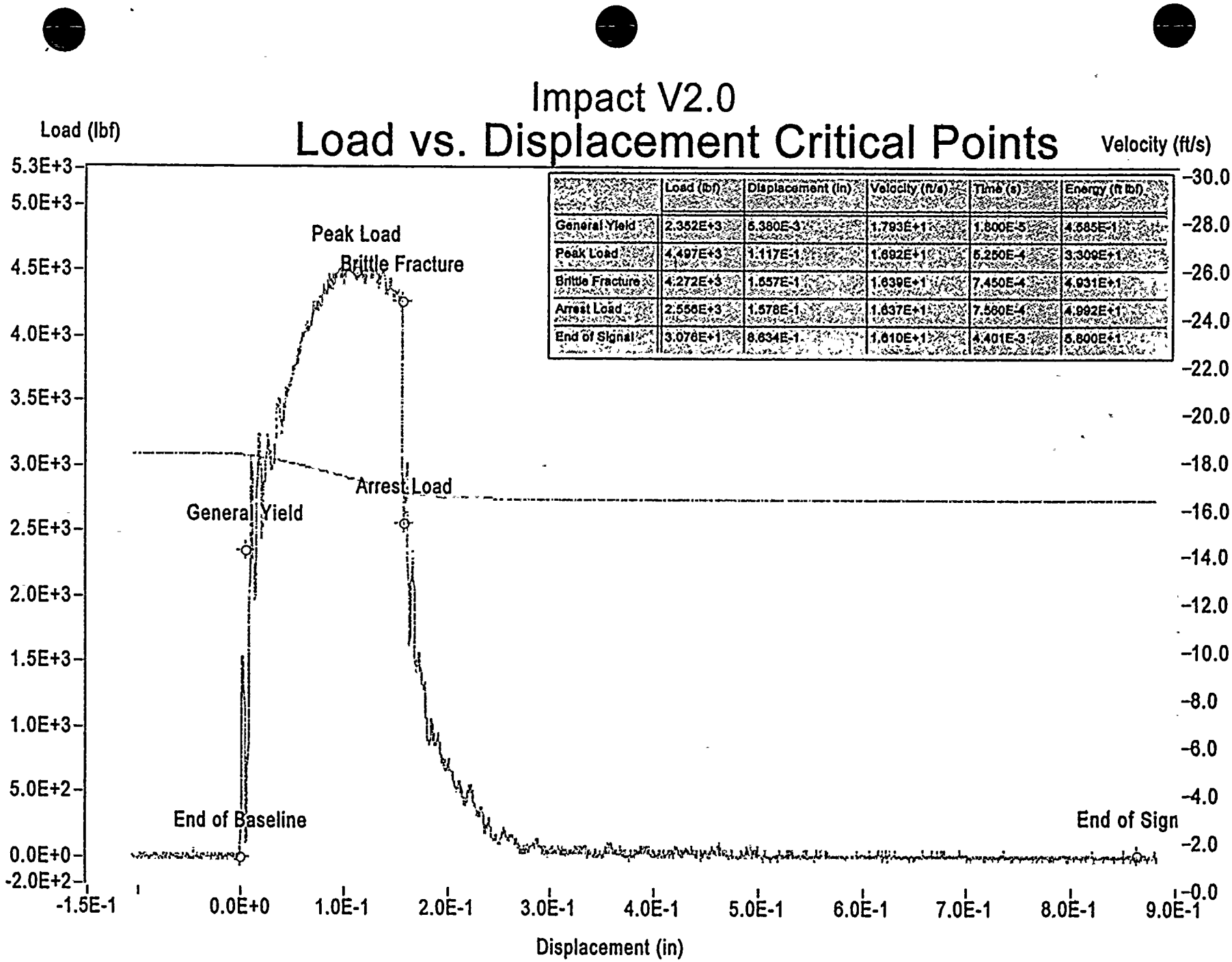

	Load (lbf)	Displacement (in)	Velocity (ft/s)	Time (s)	Energy (ft lbf)
General Yield	2.352E+3	6.380E-3	1.793E+1	1.800E-5	4.685E-1
Peak Load	4.497E+3	1.117E-1	1.692E+1	5.250E-4	3.309E+1
Brittle Fracture	4.272E+3	1.557E-1	1.639E+1	7.450E-4	4.931E+1
Arrest Load	2.556E+3	1.578E-1	1.637E+1	7.560E-4	4.992E+1
End of Signal	3.076E+1	8.634E-1	1.610E+1	4.401E-3	5.800E+1

Figure B-14 Weld Specimen Ee7 Tested at 66.5.0 F

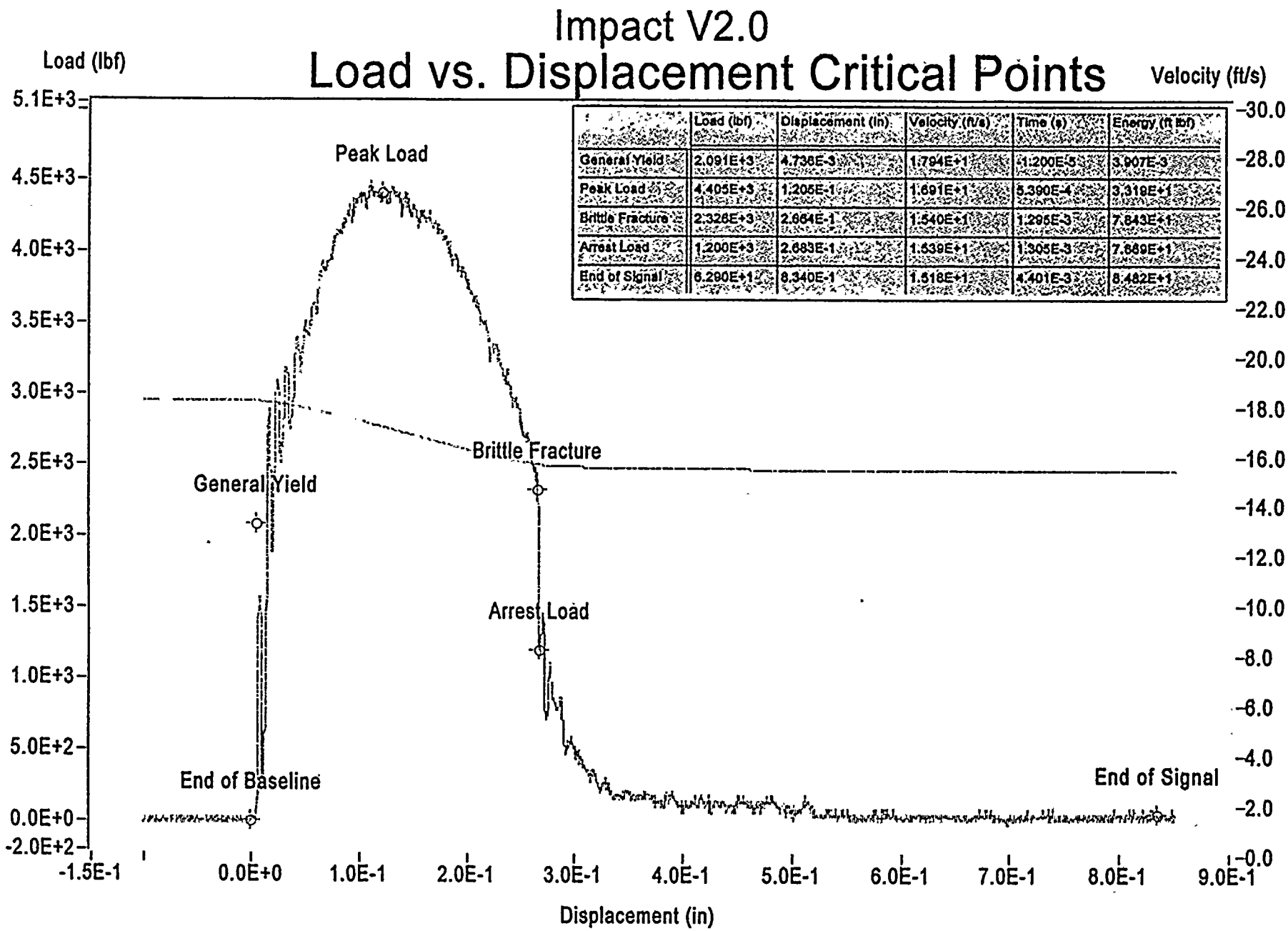

	Load (lbf)	Displacement (in)	Velocity (ft/s)	Time (s)	Energy (ft lbf)
General Yield	2.091E+3	4.736E-3	1.794E+1	1.200E-5	3.907E-3
Peak Load	4.405E+3	1.205E-1	1.691E+1	5.390E-4	3.319E+1
Brittle Fracture	2.326E+3	2.664E-1	1.540E+1	1.295E-3	7.843E+1
Arrest Load	1.200E+3	2.683E-1	1.539E+1	1.305E-3	7.869E+1
End of Signal	6.290E+1	8.340E-1	1.518E+1	4.401E-3	8.482E+1

Figure B-15 Weld Specimen Edp Tested at 114.5.0 F

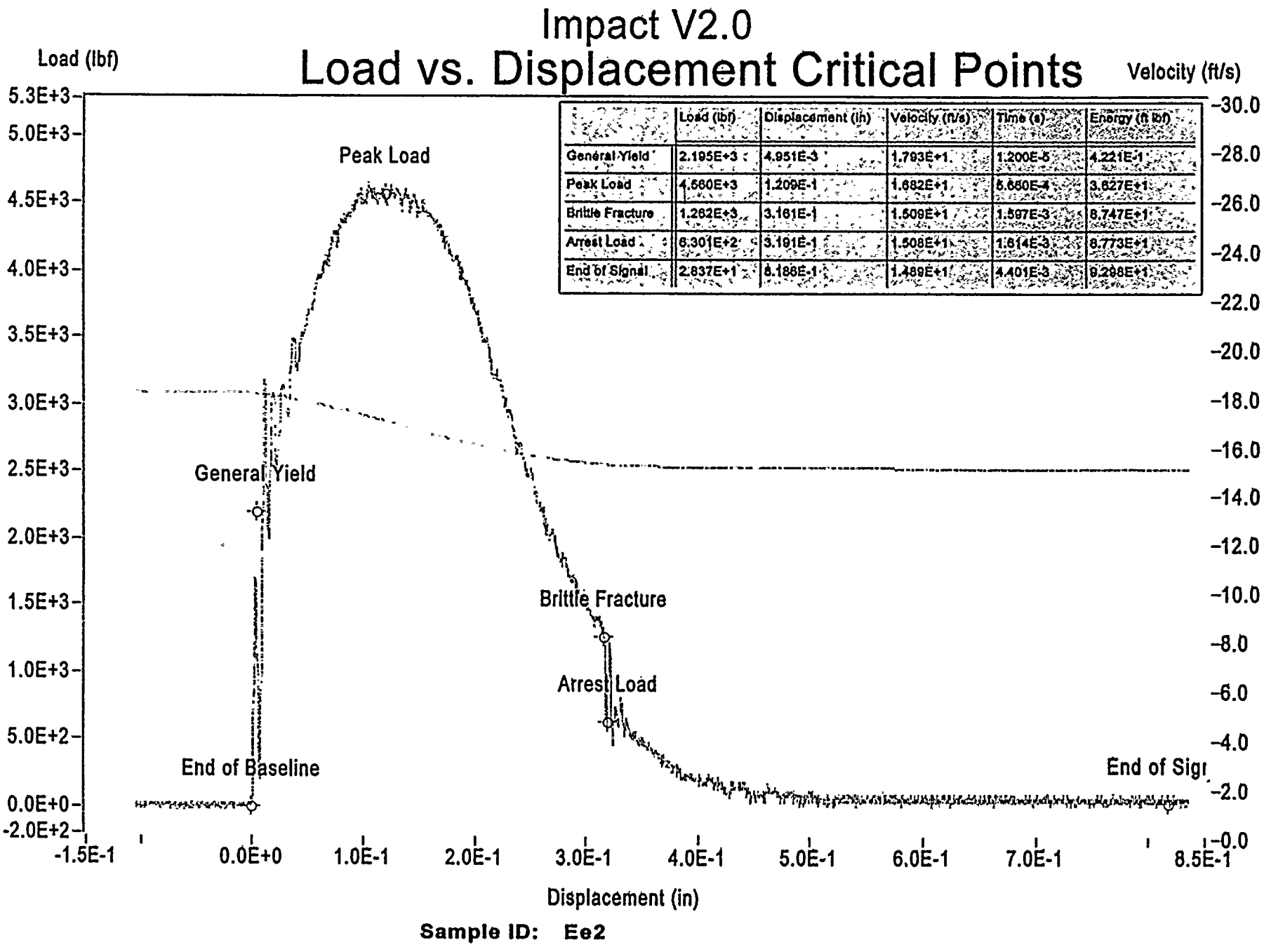

	Load (lbf)	Displacement (in)	Velocity (ft/s)	Time (s)	Energy (ft lbf)
General Yield	2.195E+3	4.951E-3	1.793E+1	1.200E-5	4.221E-1
Peak Load	4.560E+3	1.209E-1	1.682E+1	5.660E-4	3.627E+1
Brittle Fracture	1.262E+3	3.161E-1	1.509E+1	1.597E-3	8.747E+1
Arrest Load	6.301E+2	3.191E-1	1.508E+1	1.614E-3	8.773E+1
End of Signal	2.837E+1	8.188E-1	1.489E+1	4.401E-3	9.208E+1

Figure B-16 Weld Specimen Ee2 Tested at 165.0 F

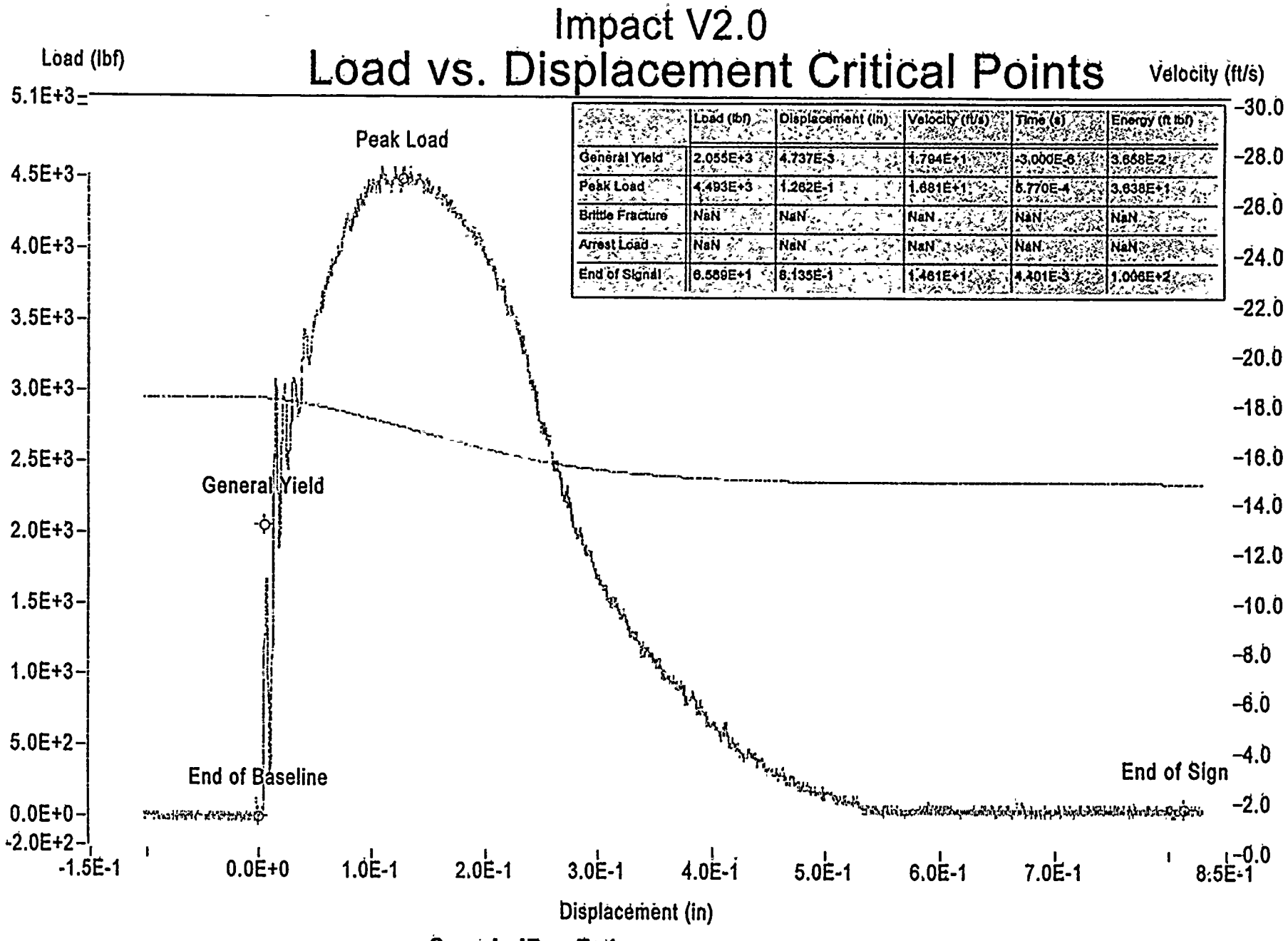

Figure B-17 Weld Specimen Ee1 Tested at 215.0 F

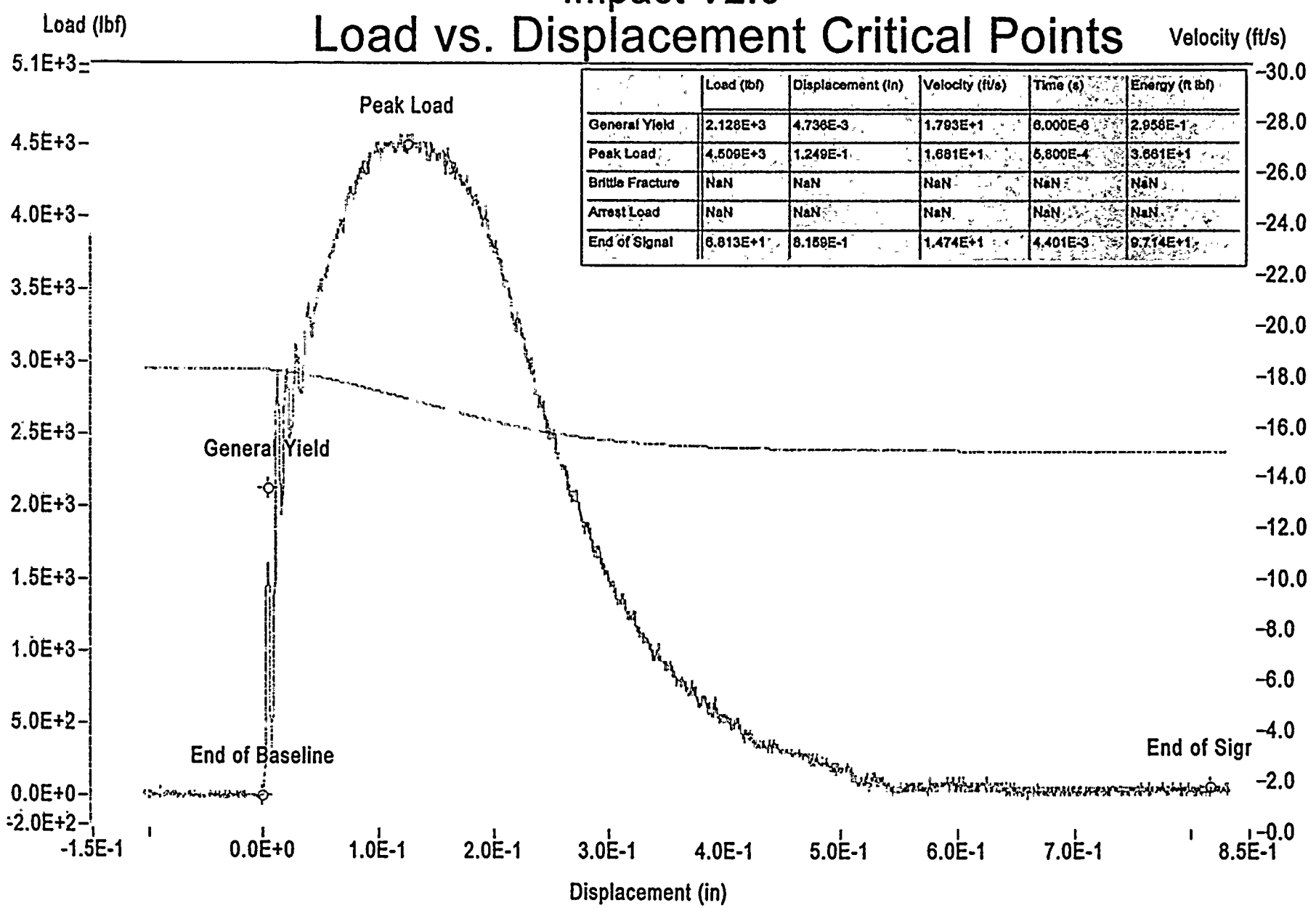

	Load (lbf)	Displacement (in)	Velocity (ft/s)	Time (s)	Energy (ft lbf)
General Yield	2.128E+3	4.736E-3	1.793E+1	6.000E-6	2.958E-1
Peak Load	4.509E+3	1.249E-1	1.681E+1	5.800E-4	3.661E+1
Brittle Fracture	NaN	NaN	NaN	NaN	NaN
Arrest Load	NaN	NaN	NaN	NaN	NaN
End of Signal	6.813E+1	8.159E-1	1.474E+1	4.401E-3	9.714E+1

Figure B-18 Weld Specimen Ee6 Tested at 260.0 F

Appendix B-3 HAZ Data

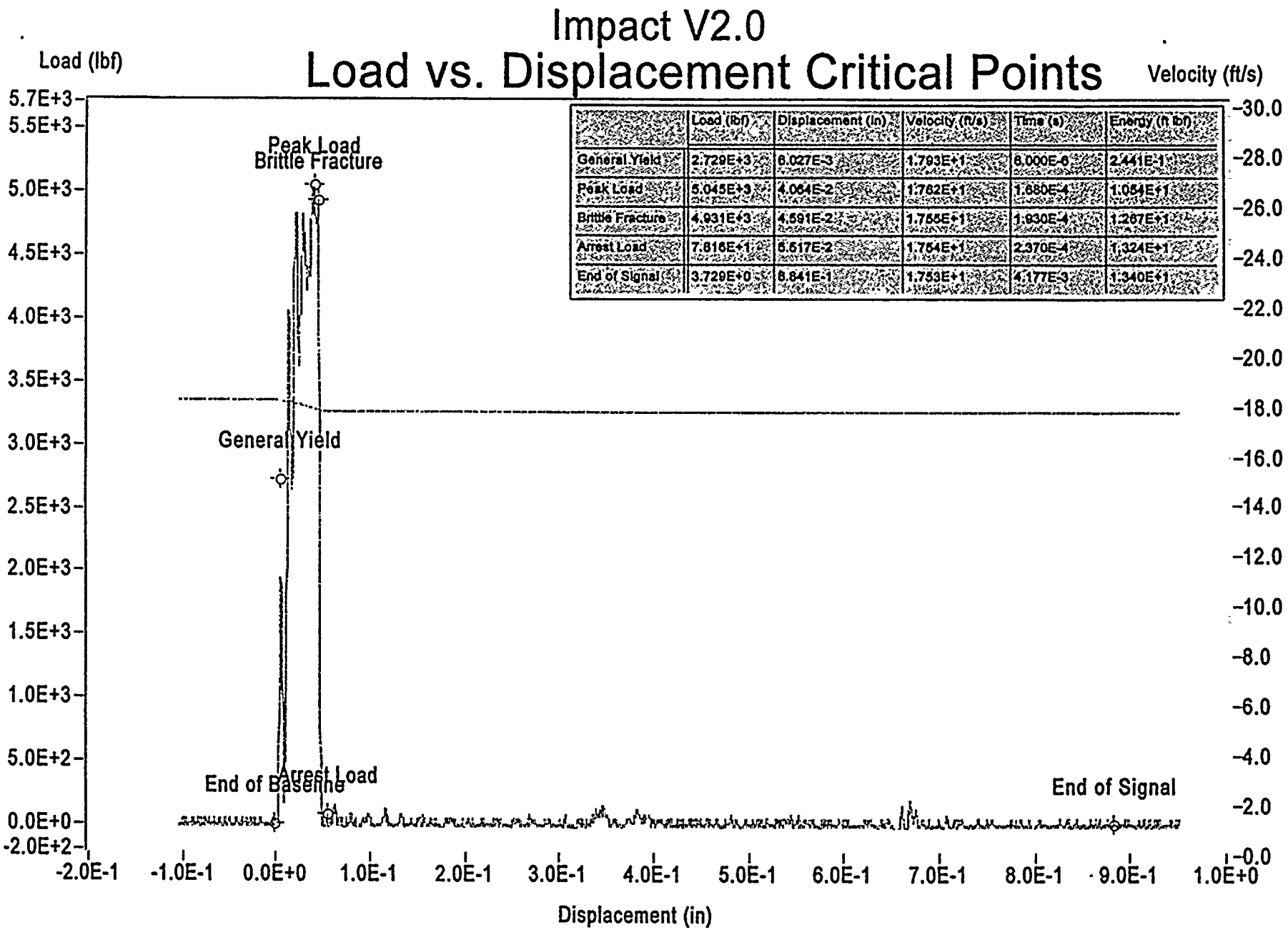

	Load (lbf)	Displacement (in)	Velocity (ft/s)	Time (s)	Energy (ft lbf)
General Yield	2.729E+3	6.027E-3	1.793E+1	6.000E-6	2.441E-1
Peak Load	5.045E+3	4.064E-2	1.782E+1	1.680E-4	1.054E+1
Brittle Fracture	4.931E+3	4.591E-2	1.755E+1	1.930E-4	1.267E+1
Arrest Load	7.816E+1	5.617E-2	1.754E+1	2.370E-4	1.324E+1
End of Signal	3.729E+0	8.641E-1	1.753E+1	4.177E-3	1.340E+1

Figure B-19 HAZ Specimen J21 Tested at -50.0 F

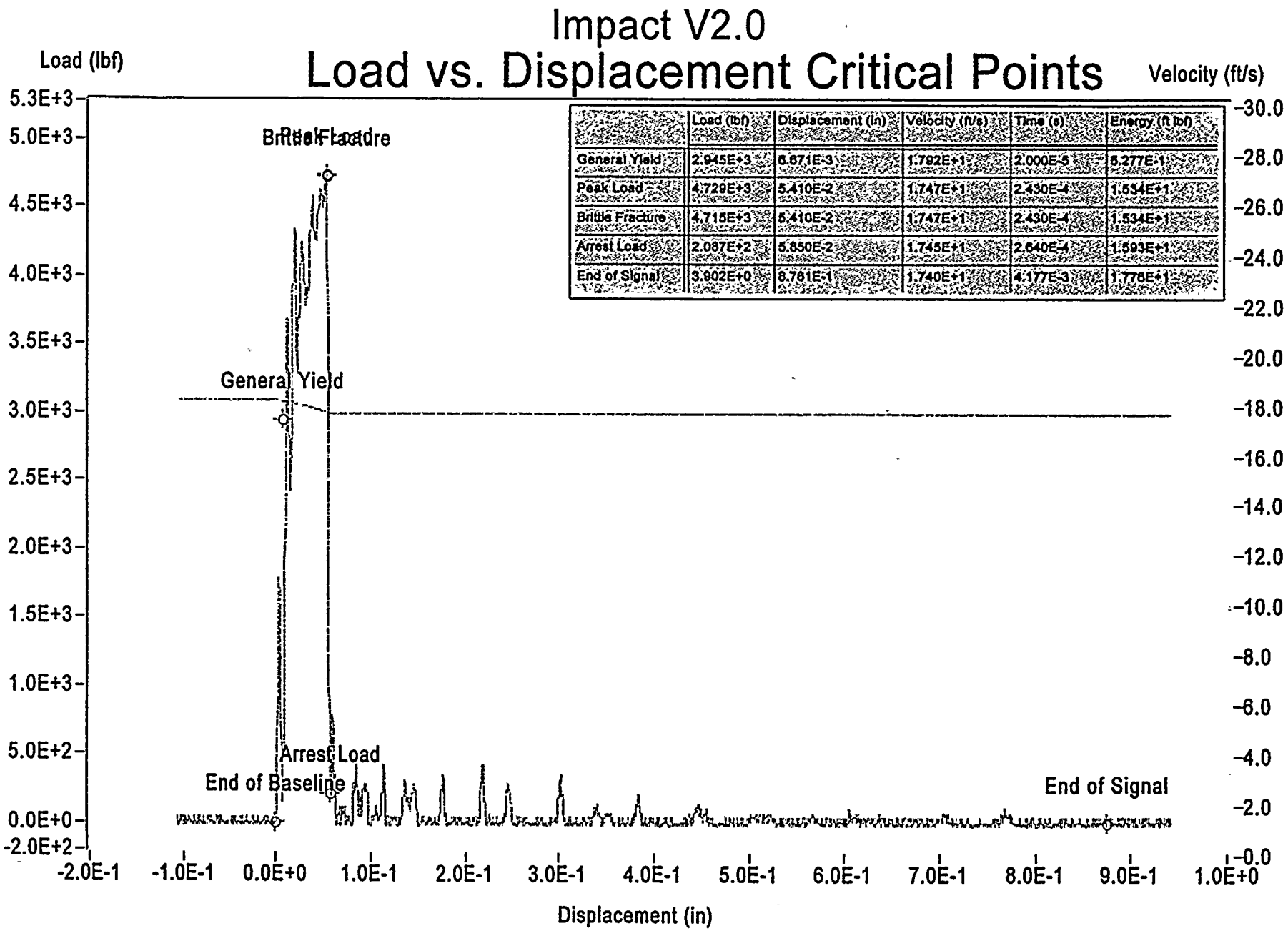

	Load (lbf)	Displacement (in)	Velocity (ft/s)	Time (s)	Energy (ft lbf)
General Yield	2.945E+3	6.671E-3	1.792E+1	2.000E-5	8.277E-1
Peak Load	4.729E+3	5.410E-2	1.747E+1	2.430E-4	1.534E+1
Brittle Fracture	4.715E+3	5.410E-2	1.747E+1	2.430E-4	1.534E+1
Arrest Load	2.087E+2	5.850E-2	1.745E+1	2.640E-4	1.593E+1
End of Signal	3.902E+0	8.761E-1	1.740E+1	4.177E-3	1.778E+1

Sample ID: J27

Figure B-20 HAZ Specimen J27 Tested at -25.0 F

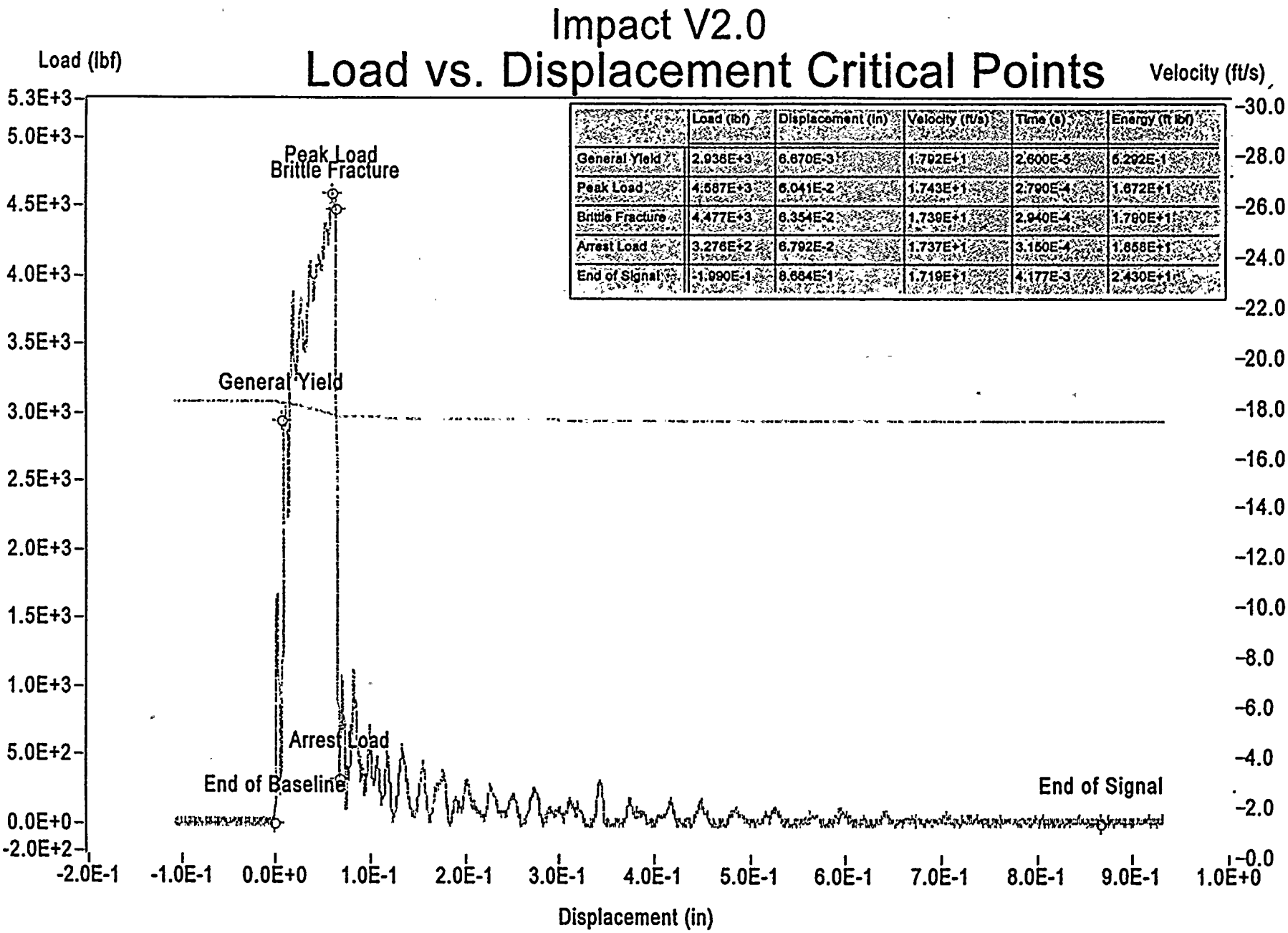

	Load (lbf)	Displacement (in)	Velocity (ft/s)	Time (s)	Energy (ft lbf)
General Yield	2.936E+3	6.670E-3	1.792E+1	2.600E-5	6.292E-1
Peak Load	4.587E+3	6.041E-2	1.743E+1	2.790E-4	1.672E+1
Brittle Fracture	4.477E+3	6.354E-2	1.739E+1	2.940E-4	1.790E+1
Arrest Load	3.276E+2	6.792E-2	1.737E+1	3.150E-4	1.858E+1
End of Signal	-1.990E-1	8.684E-1	1.719E+1	4.177E-3	2.430E+1

Sample ID: J2b

Figure B-21 HAZ Specimen J2b Tested at 0.0 F

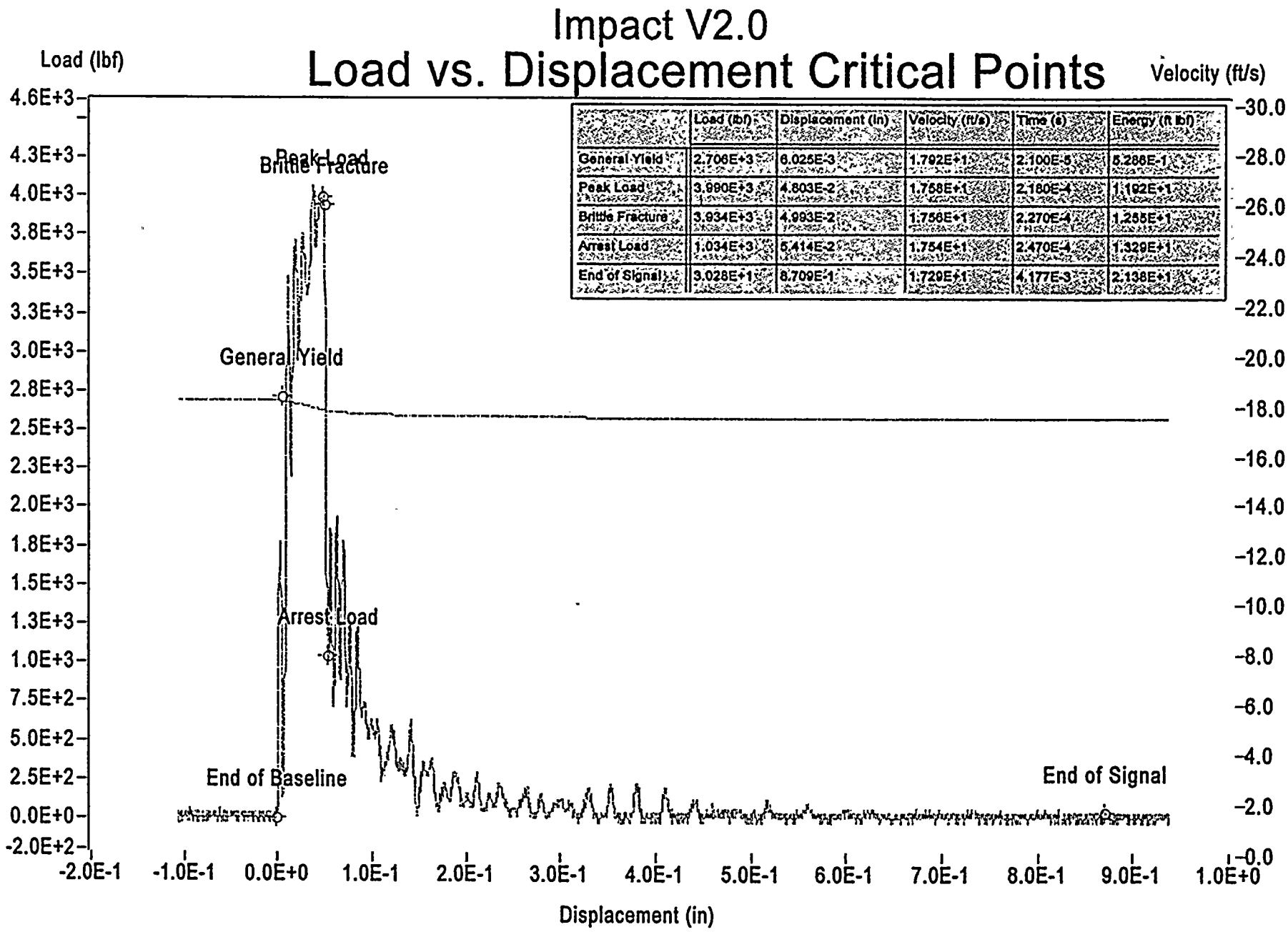

Figure B-22 HAZ Specimen J2a Tested at 35.5 F

This page is intentionally blank. The instrumented signal was not acquired.

Figure B-23 HAZ Specimen J24 Tested at 50.5 F

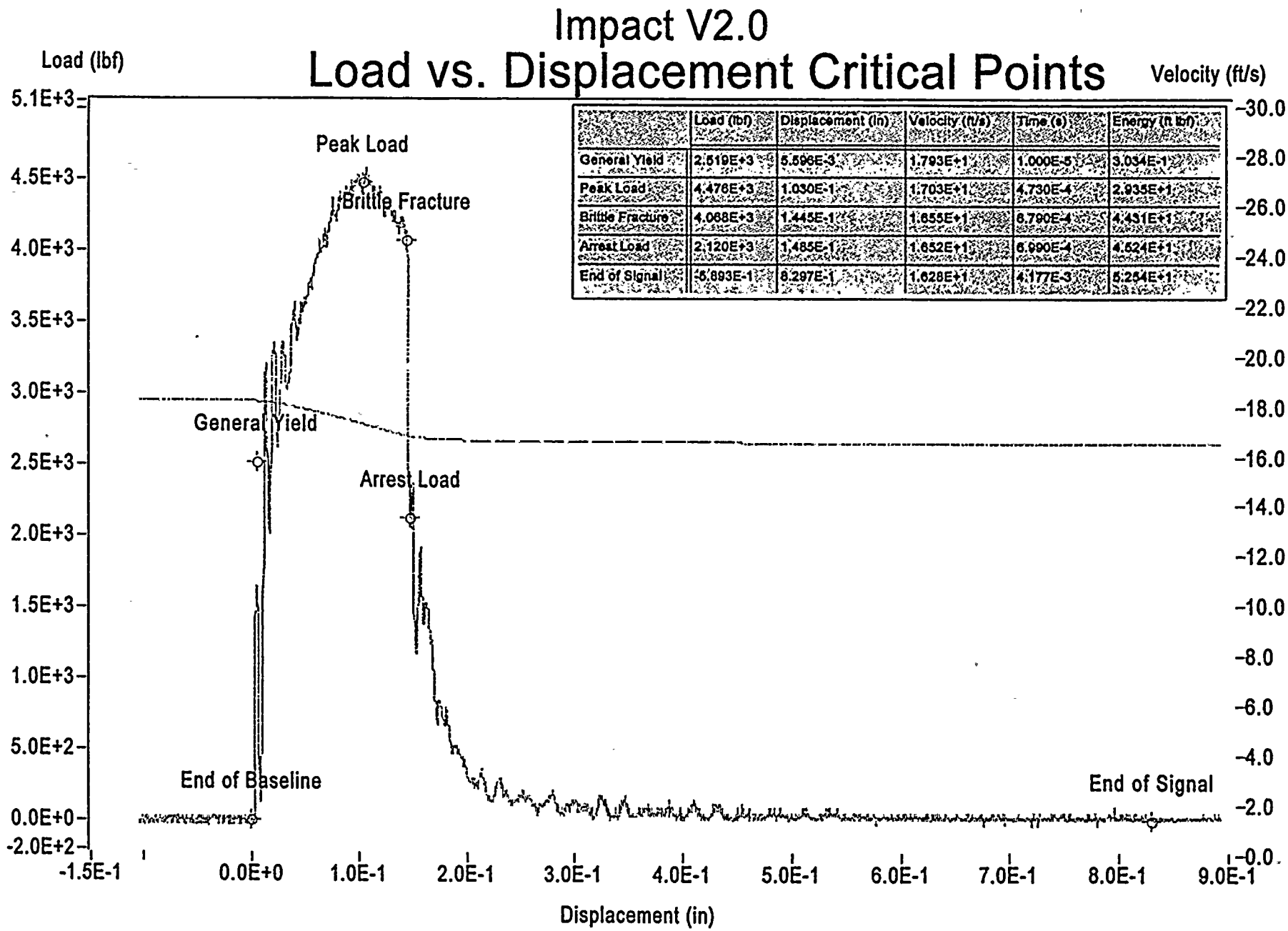

	Load (lbf)	Displacement (in)	Velocity (ft/s)	Time (s)	Energy (ft lbf)
General Yield	2.519E+3	5.596E-3	1.793E+1	1.000E-5	3.034E-1
Peak Load	4.476E+3	1.030E-1	1.703E+1	4.730E-4	2.935E+1
Brittle Fracture	4.068E+3	1.445E-1	1.655E+1	6.790E-4	4.431E+1
Arrest Load	2.120E+3	1.485E-1	1.652E+1	6.990E-4	4.624E+1
End of Signal	-5.893E-1	8.297E-1	1.628E+1	4.177E-3	5.254E+1

Figure B-24 HAZ Specimen J26 Tested at 65.1 F

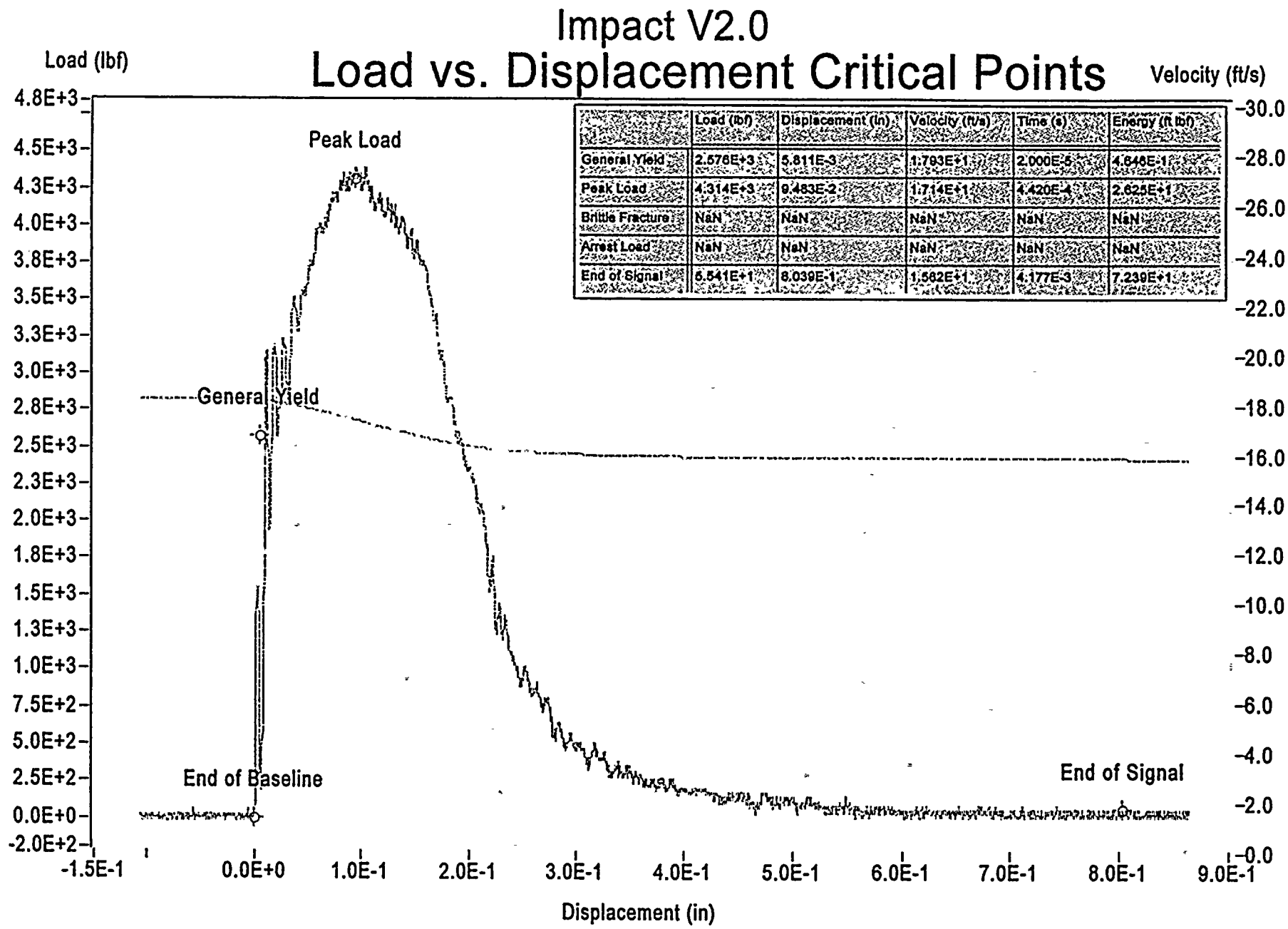

	Load (lbf)	Displacement (in)	Velocity (ft/s)	Time (s)	Energy (ft lbf)
General Yield	2.576E+3	5.811E-3	1.793E+1	2.000E-5	4.646E-1
Peak Load	4.314E+3	9.483E-2	1.714E+1	4.420E-4	2.625E+1
Brittle Fracture	NaN	NaN	NaN	NaN	NaN
Arrest Load	NaN	NaN	NaN	NaN	NaN
End of Signal	6.541E+1	8.039E-1	1.582E+1	4.177E-3	7.239E+1

Sample ID: J23

Figure B-25 HAZ Specimen J23 Tested at 94.5 F

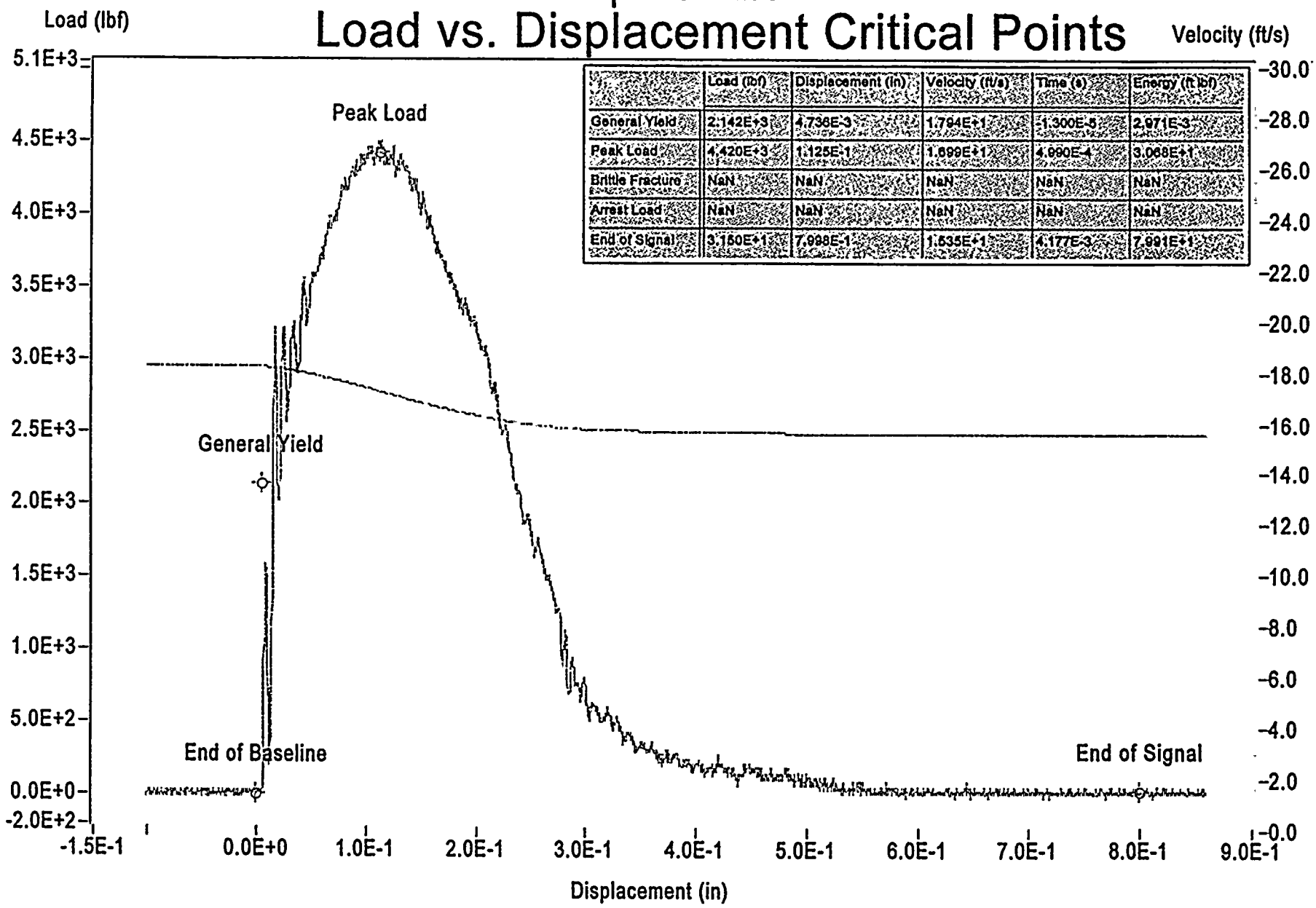

	Load (lbf)	Displacement (in)	Velocity (ft/s)	Time (s)	Energy (ft lbf)
General Yield	2.142E+3	4.736E-3	1.784E+1	1.300E-5	2.971E-3
Peak Load	4.420E+3	1.125E-1	1.699E+1	4.690E-4	3.068E+1
Brittle Fracture	NaN	NaN	NaN	NaN	NaN
Arrest Load	NaN	NaN	NaN	NaN	NaN
End of Signal	3.150E+1	7.998E-1	1.535E+1	4.177E-3	7.991E+1

Figure B-26 HAZ Specimen J25 Tested at 122.0 F

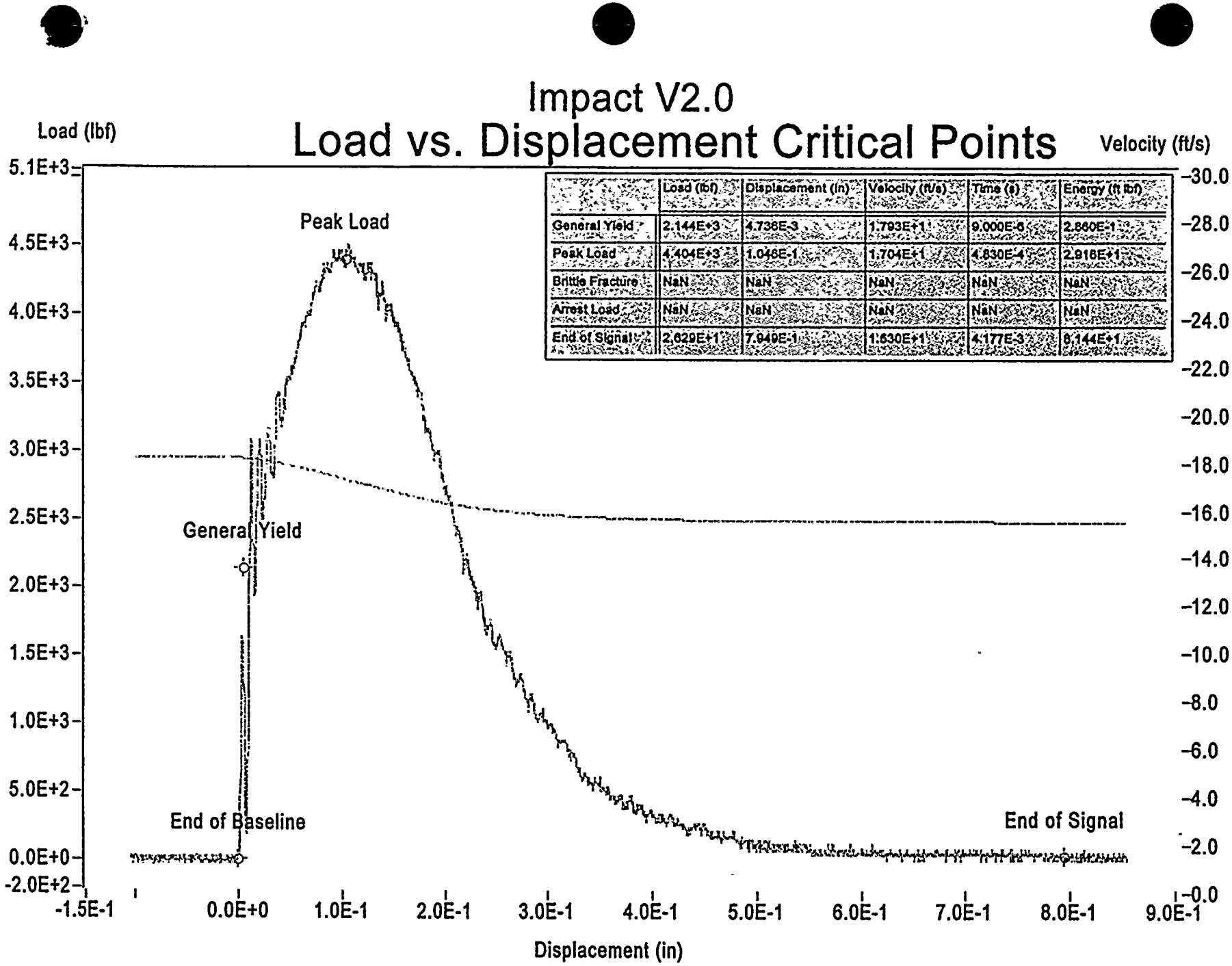

Sample ID: J22

Figure B-27 HAZ Specimen J22 Tested at 160.0 F

Appendix B-4 APED Data

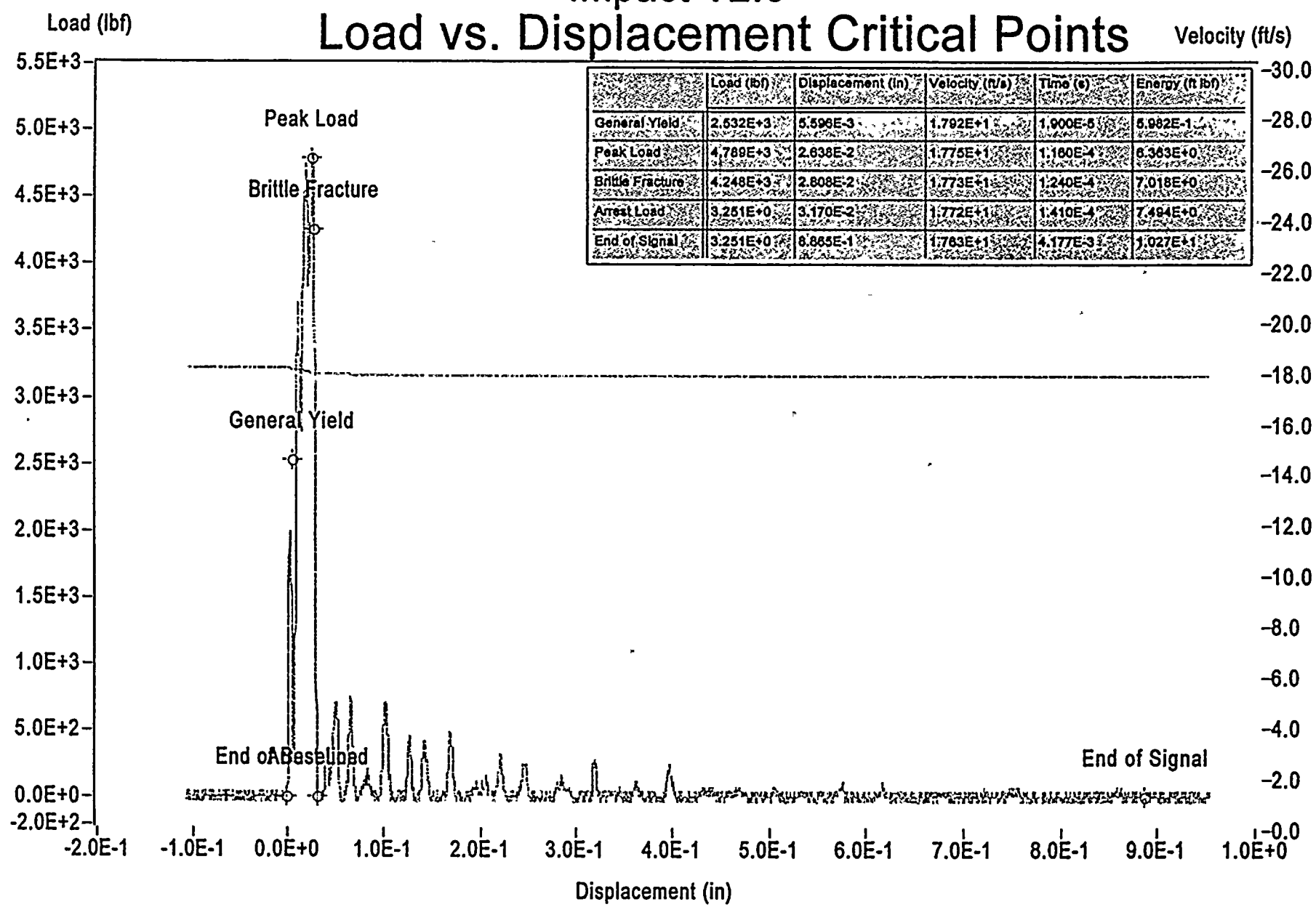

Sample ID: Aped-001

Figure B-28 APED Specimen Aped-001 Tested at -27.0 F

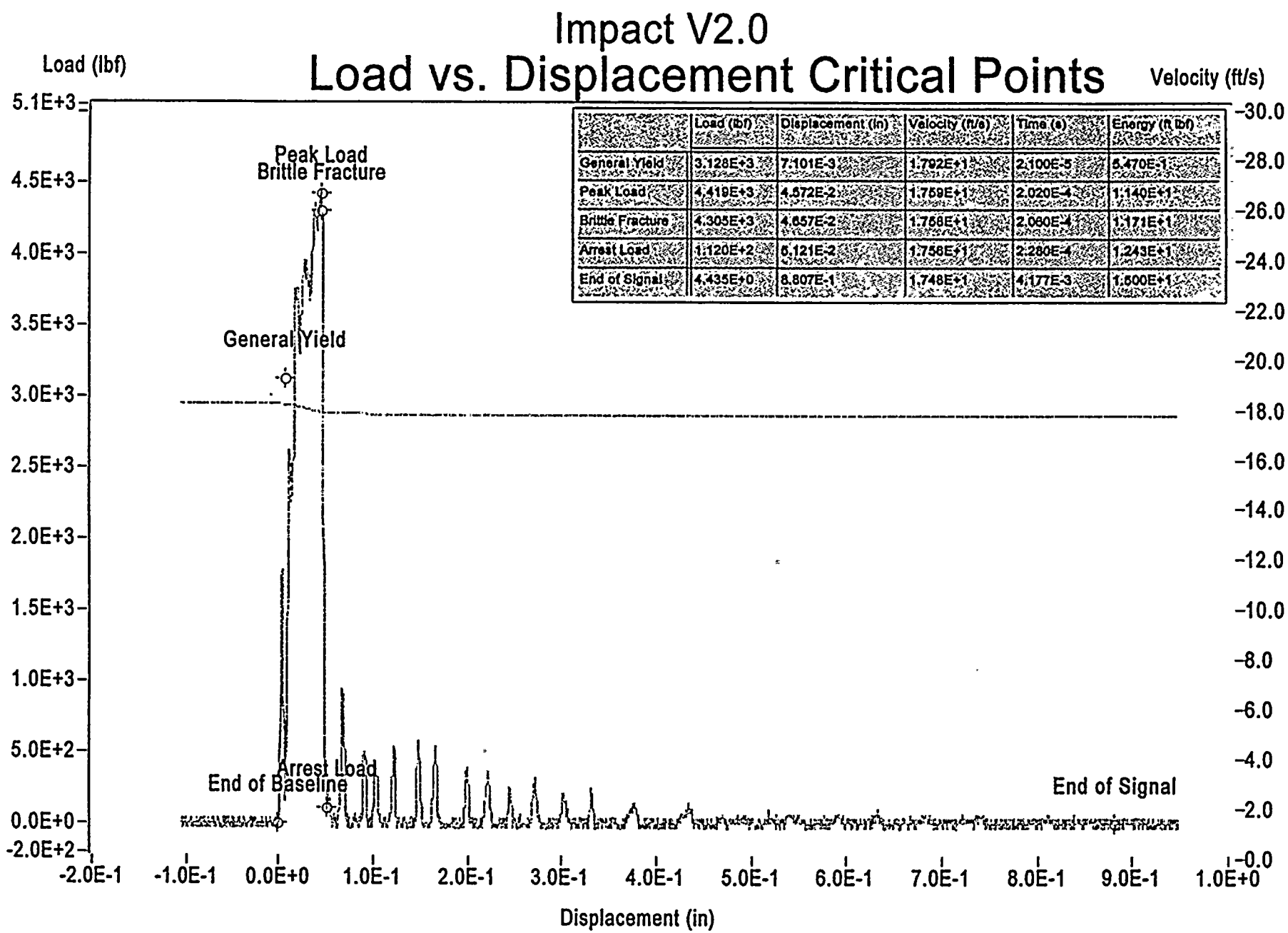

	Load (lbf)	Displacement (in)	Velocity (ft/s)	Time (s)	Energy (ft lbf)
General Yield	3.128E+3	7.101E-3	1.792E+1	2.100E-5	5.470E-1
Peak Load	4.419E+3	4.572E-2	1.769E+1	2.020E-4	1.140E+1
Brittle Fracture	4.305E+3	4.657E-2	1.768E+1	2.060E-4	1.171E+1
Arrest Load	1.120E+2	5.121E-2	1.758E+1	2.280E-4	1.243E+1
End of Signal	4.435E+0	8.807E-1	1.748E+1	4.177E-3	1.500E+1

Sample ID: Aped-002

Figure B-29 APED Specimen Aped-002 Tested at 0.0 F

This page is intentionally blank. The instrumented signal was not acquired.

Figure B-30 APED Specimen Aped-007 Tested at 40.0 F

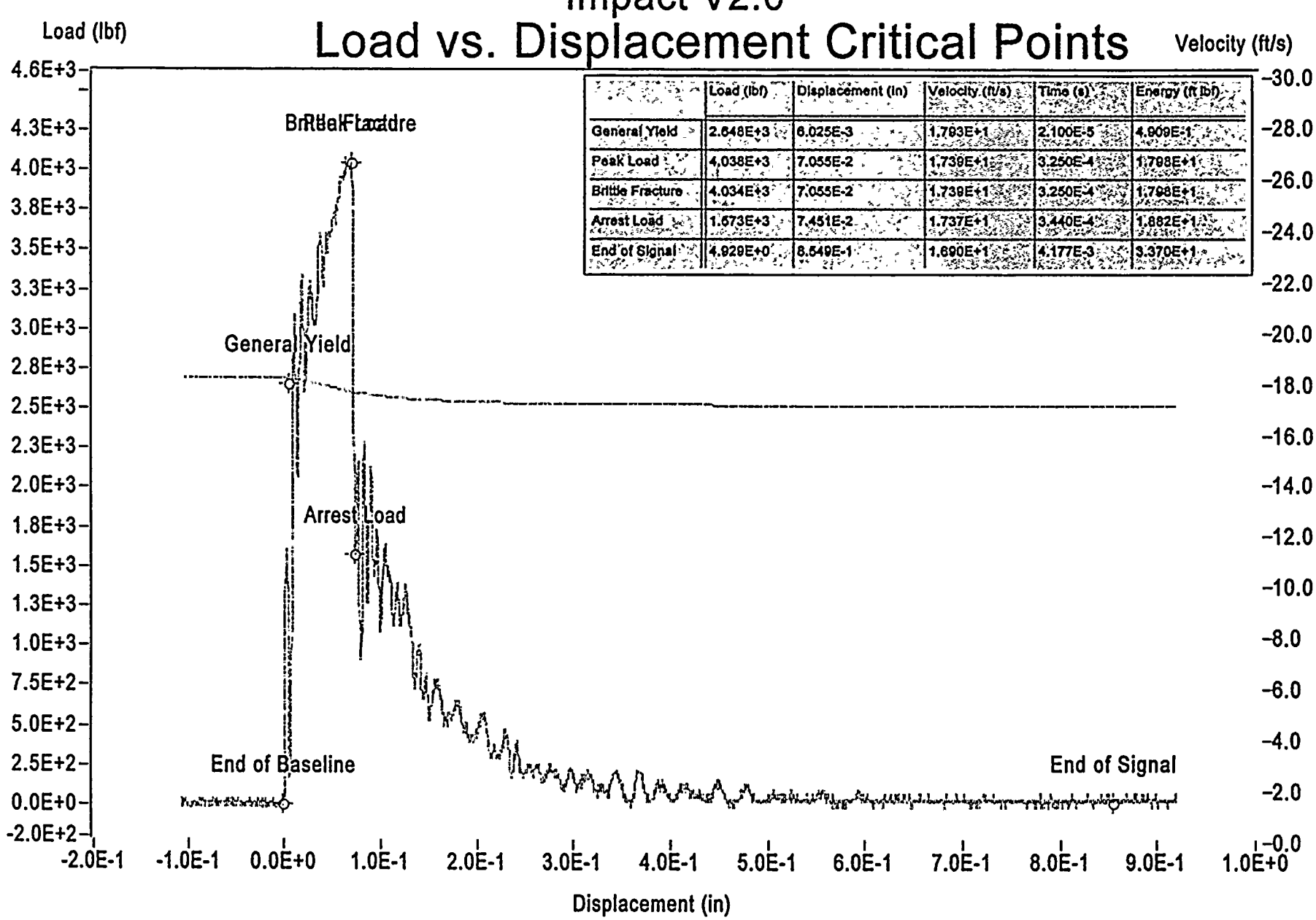

Figure B-31 APED Specimen Aped-008 Tested at 65.5 F

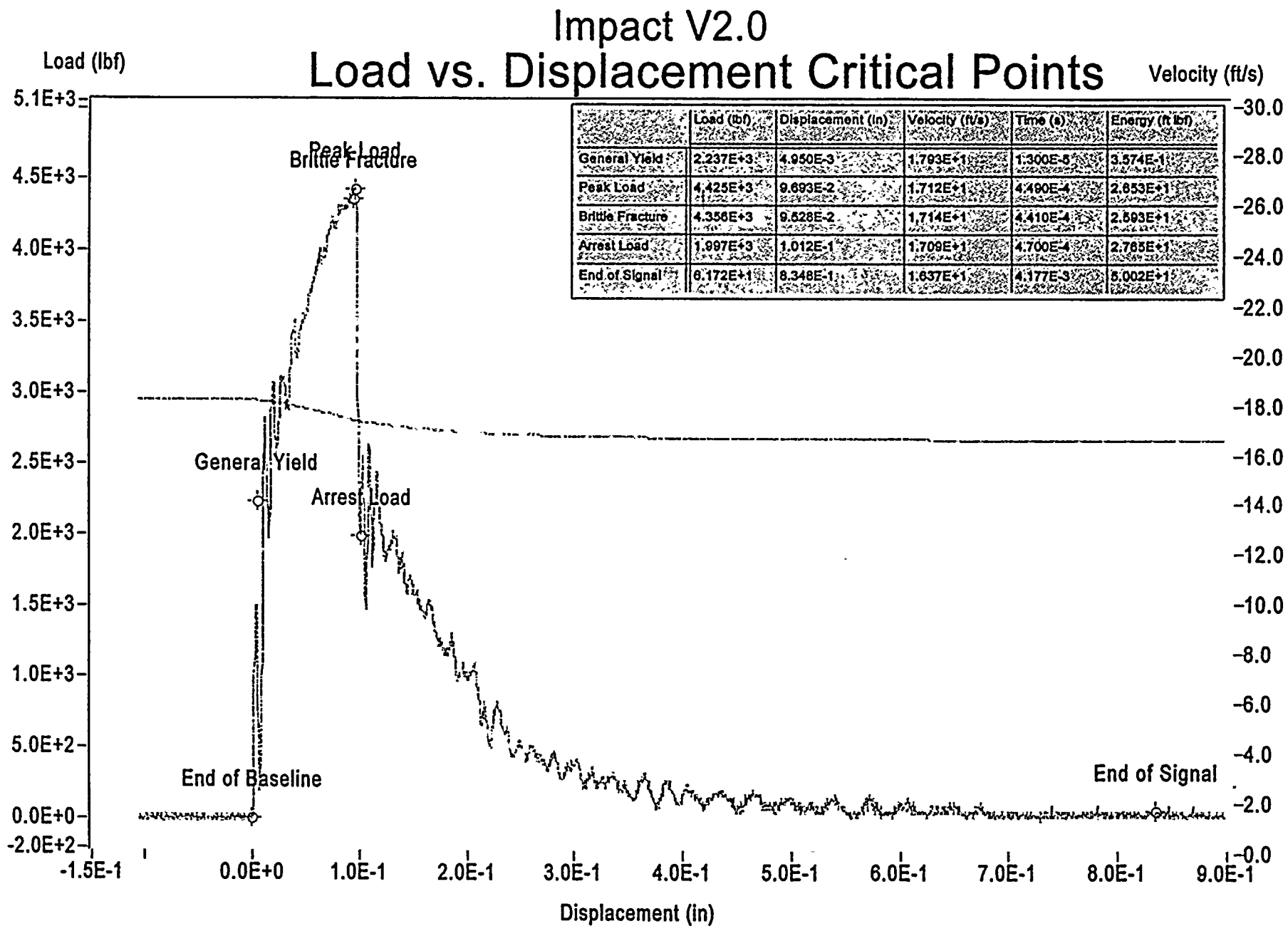

	Load (lbf)	Displacement (in)	Velocity (ft/s)	Time (s)	Energy (ft lbf)
General Yield	2.237E+3	4.950E-3	1.793E+1	1.300E-5	3.574E-1
Peak Load	4.425E+3	9.693E-2	1.712E+1	4.490E-4	2.853E+1
Brittle Fracture	4.356E+3	9.528E-2	1.714E+1	4.410E-4	2.593E+1
Arrest Load	1.997E+3	1.012E-1	1.709E+1	4.700E-4	2.765E+1
End of Signal	6.172E+1	8.348E-1	1.637E+1	4.177E-3	5.002E+1

Figure B-32 APED Specimen Aped-006 Tested at 84.2 F

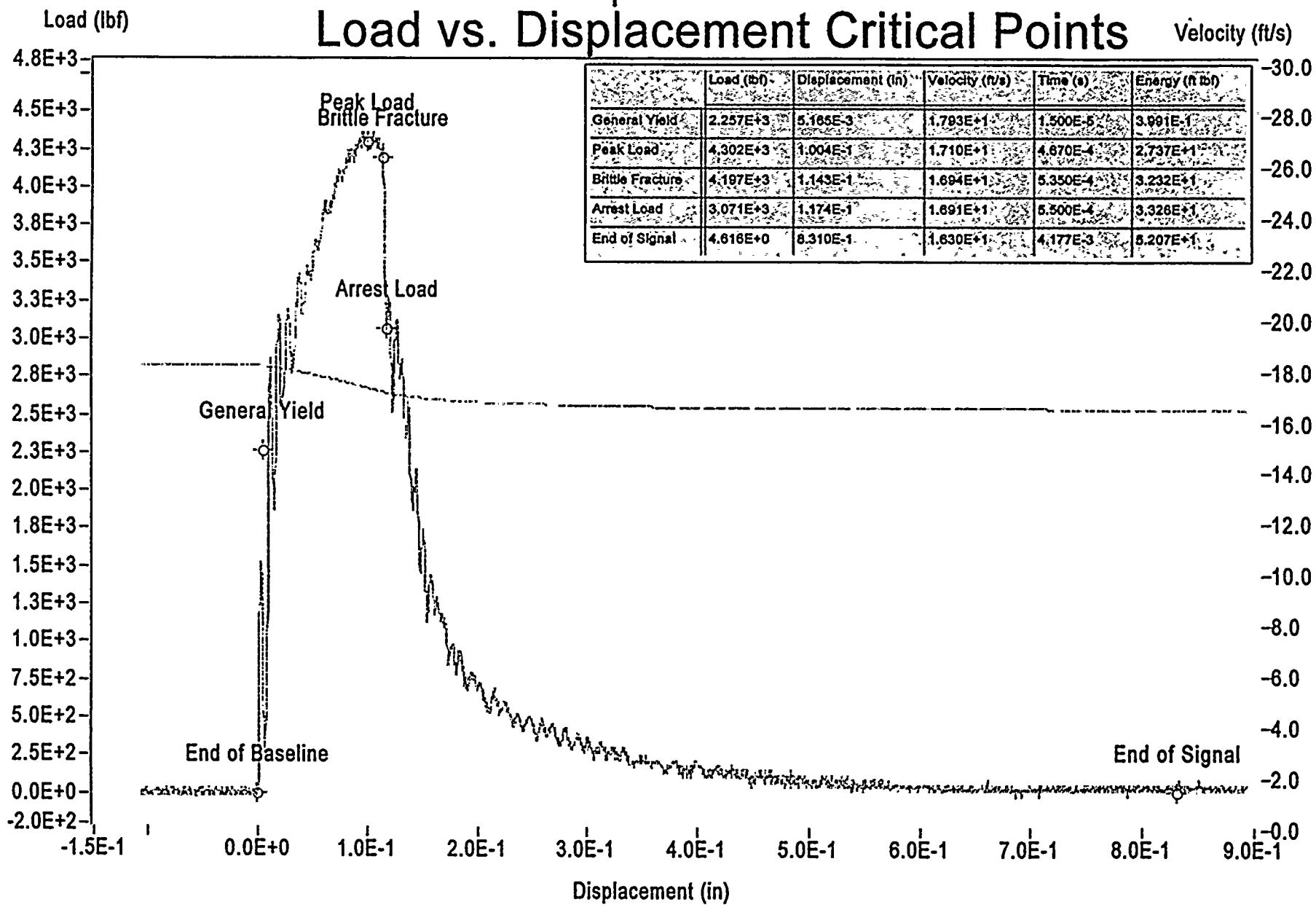

Figure B-33 APED Specimen Aped-005 Tested at 100.2 F

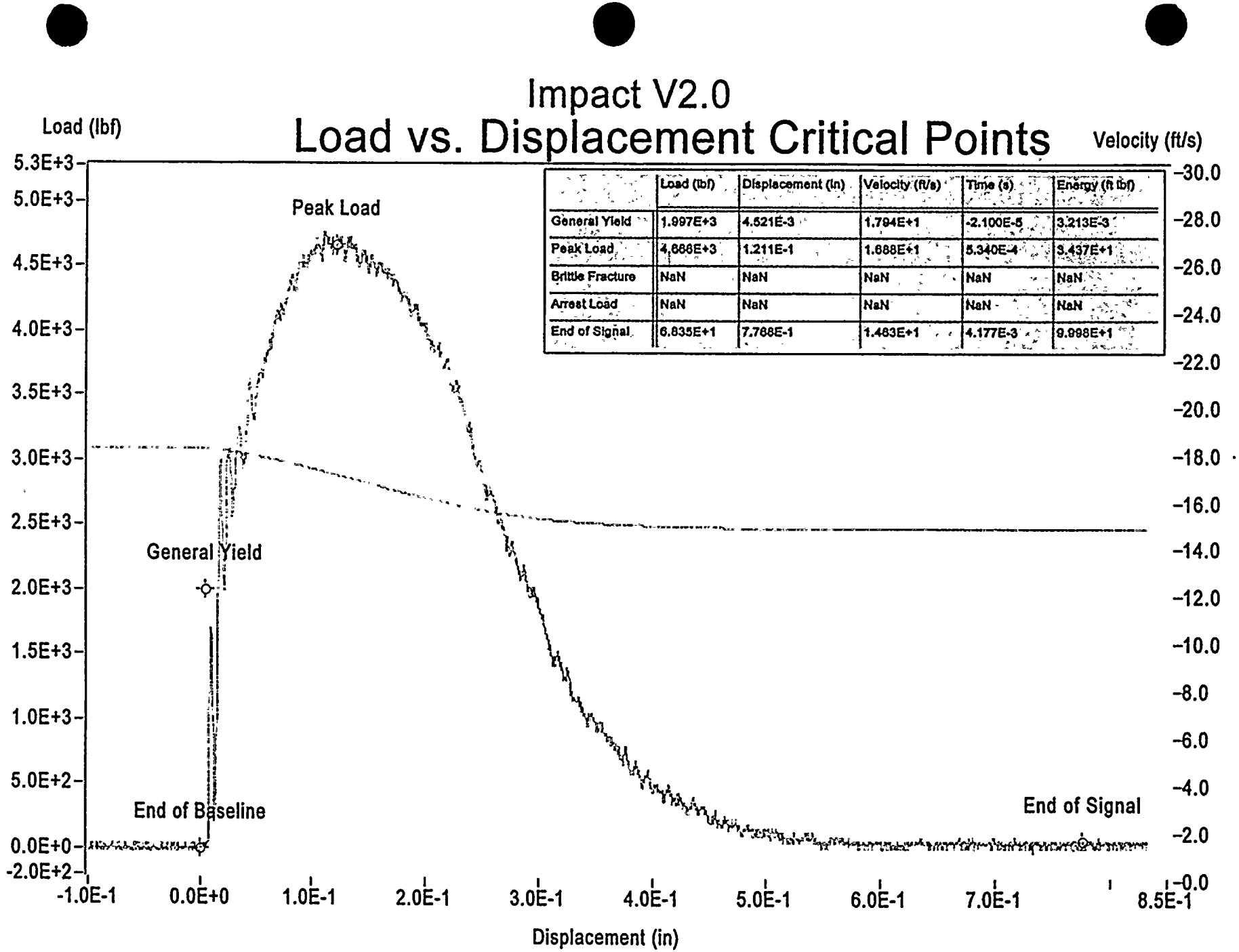

	Load (lbf)	Displacement (in)	Velocity (ft/s)	Time (s)	Energy (ft lbf)
General Yield	1.997E+3	4.521E-3	1.794E+1	-2.100E-5	3.213E-3
Peak Load	4.666E+3	1.211E-1	1.688E+1	5.340E-4	3.437E+1
Brittle Fracture	NaN	NaN	NaN	NaN	NaN
Arrest Load	NaN	NaN	NaN	NaN	NaN
End of Signal	6.835E+1	7.768E-1	1.463E+1	4.177E-3	9.998E+1

Sample ID: Aped-009

Figure B-34 APED Specimen Aped-009 Tested at 122.9 F

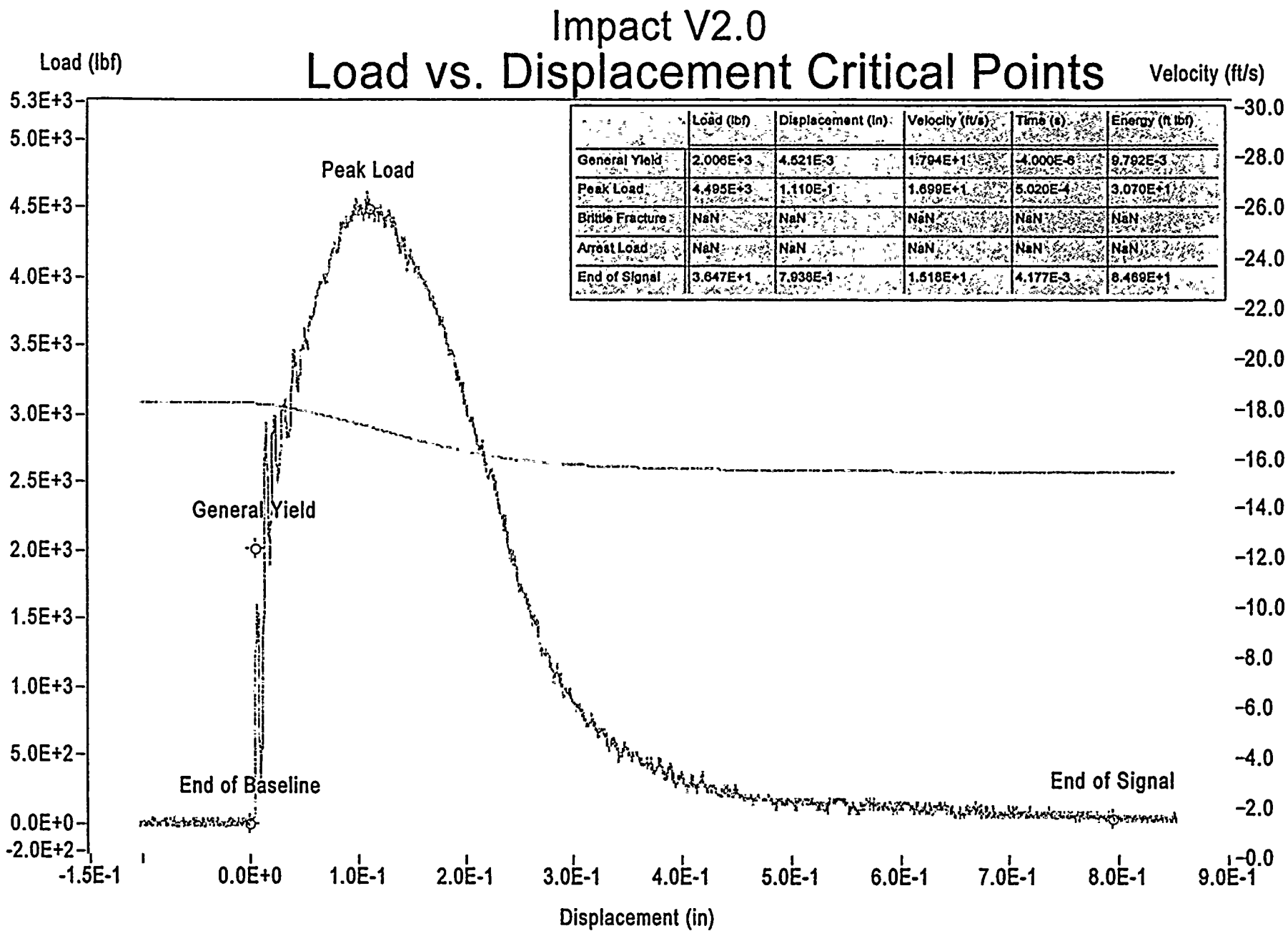

	Load (lbf)	Displacement (in)	Velocity (ft/s)	Time (s)	Energy (ft lbf)
General Yield	2.006E+3	4.521E-3	1.794E+1	4.000E-6	9.792E-3
Peak Load	4.495E+3	1.110E-1	1.699E+1	5.020E-4	3.070E+1
Brittle Fracture	NaN	NaN	NaN	NaN	NaN
Arrest Load	NaN	NaN	NaN	NaN	NaN
End of Signal	3.647E+1	7.938E-1	1.518E+1	4.177E-3	8.469E+1

Sample ID: Aped-004

Figure B-35 APED Specimen Aped-004 Tested at 150.0 F

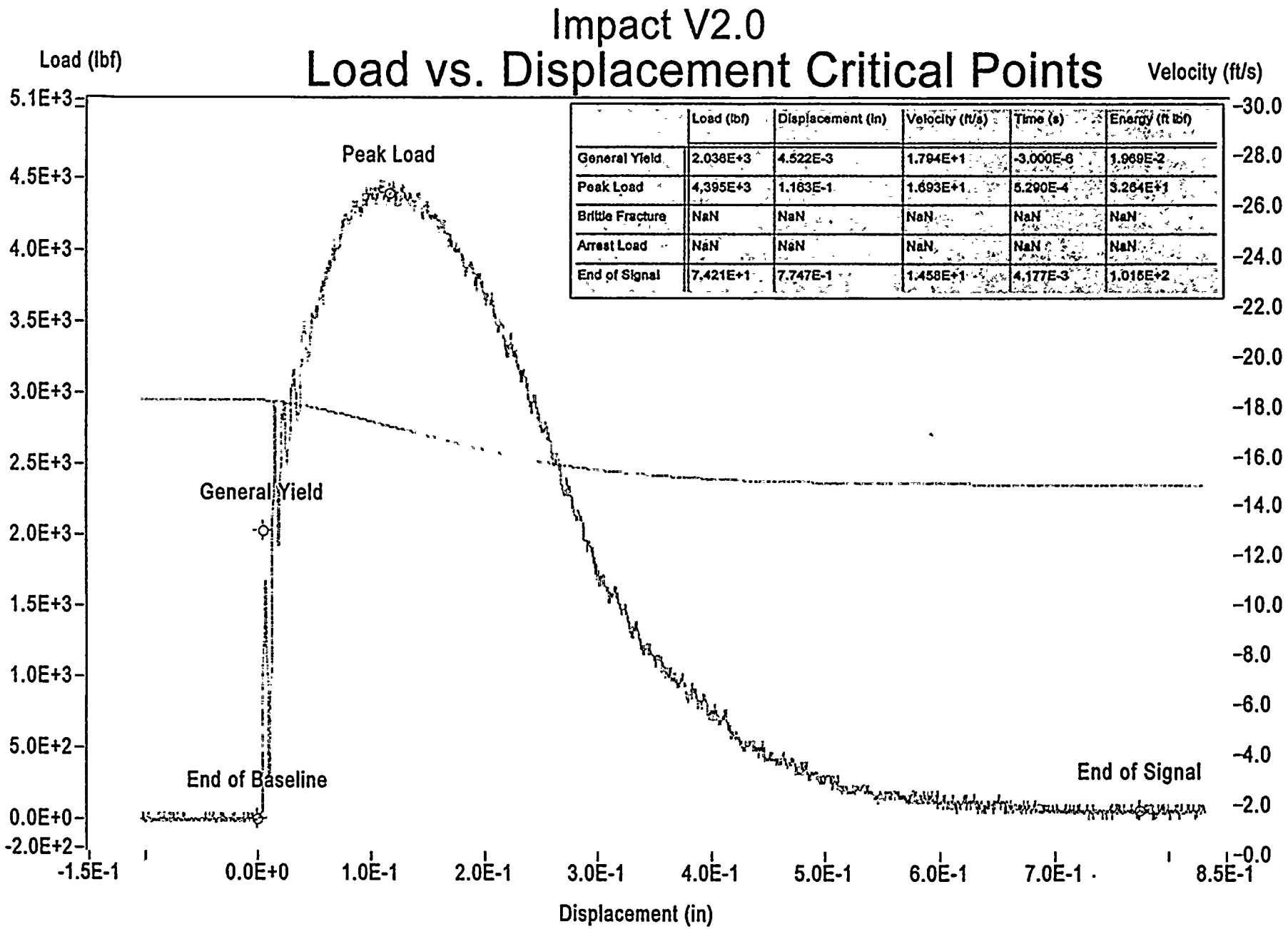

	Load (lbf)	Displacement (in)	Velocity (ft/s)	Time (s)	Energy (ft lbf)
General Yield	2.036E+3	4.522E-3	1.794E+1	-3.000E-6	1.969E-2
Peak Load	4.395E+3	1.163E-1	1.693E+1	5.290E-4	3.264E+1
Brittle Fracture	NaN	NaN	NaN	NaN	NaN
Arrest Load	NaN	NaN	NaN	NaN	NaN
End of Signal	7.421E+1	7.747E-1	1.458E+1	4.177E-3	1.016E+2

Figure B-36 APED Specimen Aped-003 Tested at 200.0 F

Copyright Notice

MPM Technologies, Inc.

M. P. Manahan, Sr.
President

NIAGARA MOHAWK

NINE MILE POINT NUCLEAR STATION
P.O. BOX 63, LYCOMING, NEW YORK 13093

FAX COVER LETTER

NINE MILE POINT UNIT 2

FROM:

FAX TELEPHONE NUMBER: (315) 349-1400

NAME: Tom EGAN

DEPARTMENT: LICENSING/ENVIRONMENTAL

TELEPHONE NUMBER: (315) 349-7683

FAX #

TO: Doris Hoover (301) 415-3707

TOTAL NUMBER OF PAGES FAXED (INCLUDING COVER LETTER): 2

DATE: 4-17-98 TIME: 1445

MESSAGE: Attached is Copyright Release Authorization per Darl Hood's request

Tom Egan